# *THE ONYCHOPHORAN PROTOCEREBRUM WAS ANCESTRALLY BIPARTITE: Developmental evidence from a phosphatised early Cambrian lobopodian*

EMMA JAYNE LONG

# THE ONYCHOPHORAN PROTOCEREBRUM WAS ANCESTRALLY BIPARTITE

*Developmental evidence from a phosphatised early Cambrian lobopodian*

Thesis submitted in fulfilment

of the requirements for the degree

of

Master of Science by Research in Geological Sciences

at

Durham University

By Emma Jayne Long

Durham University

Supervisors: Dr Martin Smith, Dr Kate Dobson

December 2019

# ACKNOWLEDGEMENTS

I would like to take this opportunity to acknowledge Ms. H.-Q. Zhang, the technician who discovered the remarkable fossil without which this project would not have been possible. Secondly, I wish to acknowledge Xi-Guang Zhang's role in the project's conception, and for his work in producing the scanning electron micrographs of the fossil's external anatomy. I would also like to acknowledge Yang Jie, and all those at Yunnan University who contributed to this research. I am grateful to my friend and colleague, Stella Felsinger, whose critical guidance and skill in the field of phylogenetics I have relied upon throughout this project. I would also like to thank Kate Dobson for producing the volume dataset of the fossil's internal anatomy, and for her expertise and support in Avizo. Finally, I would like to thank Martin Smith for his patient guidance and unwavering enthusiasm. Acknowledgements

# CONTENTS



## CHAPTER 1 - INTRODUCTION



# CHAPTER 2 - MATERIAL & METHODS



# CHAPTER 3 - DESCRIPTION

# CHAPTER 4 – INTERPRETATION



# CHAPTER 5 – DISCUSSION



# ABSTRACT

The panarthropods (euarthropods, tardigrades, and onychophorans) are the most diverse and successful group of animals on the planet. The 'heads' of these animals are evolutionarily and morphologically plastic regions comprising modified appendage-bearing segments. Despite decades of genetic, embryological, and palaeontological research, the segmental homologies of these appendages remain disputed. Illuminating the evolutionary origins of the first protocerebral segment may hold the key to understanding the panarthropod head.

The protocerebral segments of extant onychophorans and euarthropods are genetically subdivided into an apical antennal / labral domain and an ocular domain by expression of the genes *optix* and *orthodenticle (otd)*. Unlike the segmental *otd* element, the antennal *optix* region lacks the *engrailed (en)* segment boundary indicator gene and is thus considered asegmental. The presence of two protocerebral genetic domains suggests that this region was ancestrally bipartite, composed of morphologically discrete asegmental and segmental components. Until now, the hypothetical ancestral division of these domains has been based principally on modern developmental studies, supplemented with macrofossils of adult euarthropods and onychophorans. Here I provide the first palaeodevelopmental data, from a phosphatised Cambrian (stage 3) stem-group onychophoran embryo from China's Yu'anshan Formation.

This specimen provides the first fossil evidence for an ancestrally bipartite protocerebrum. The protocerebrum is made up of an apical asegmental domain containing a dorsal brain, which innervates antenniform frontal appendages, and a subsequent ocular domain in the first true body segment, homologous with the ocular *otd* element. The onychophoran antennae are thus asegmental, and not homologous with segmental appendages. The configuration of the specimen's eyes provides morphological support for their appendicular origins, suggesting that eyes, rather than antennae, are the protocerebral appendages of onychophorans. The pre-oral raptorial-like appendages and labral complexes of euarthropods are therefore asegmental, and homologous to the onychophoran antennae.

The loss of the ancestral nerve ring, the incorporation of the second trunk appendage into the head, and the fusion of the asegmental and segmental protocerebral domains into a single element occurred independently in Euarthropoda and Onychophora – weakening the case that these phyla form a clade, consistent with fossil, musculoskeletal, and neurological evidence that tardigrades are the sister-group to the euarthropods (the Tactopoda hypothesis).

# CHAPTER 1

# INTRODUCTION

## 1.1. THE CAMBRIAN EXPLOSION

The dramatic diversification and radiation of body plans between the late Neoproterozoic and the early Cambrian lasted for less than 2% of the duration of the fossil record of animals, and yet it gave rise to almost all modern animal phyla (Marshall, 2006; Valentine, Jablonski, & Erwin, 1999). Fossils that date to this radical era thus act as windows to the start of life as we know it, from which almost "endless forms most beautiful and most wonderful have been, and are being, evolved" (Darwin, 1859). The study of this 'Cambrian Explosion' therefore allows for a greater understanding of the emergence of today's taxa.

Explanations for the Cambrian Explosion vary from developmental plasticity enabling more non-lethal experimentation than was observed in the developmentally 'hardened' Phanerozoic, to the expansion of animal life as a result of a vast ocean of opportunity and 'empty ecospace' (Budd & Jensen, 2000; Valentine, 1995). Alternatively, Budd and Jensen (2000) dismiss this popularised 'explosive' evolutionary episode as a misinterpretation of the fossil record and a caveat to systematic taxonomy. Nevertheless, when it comes to

understanding the origins of animal diversity and complexity, the Cambrian is an excellent place to start.

## 1.2. ECDYSOZOA

Like most life on earth, the evolutionary origins of the Annelida, a phylum comprising polychaetes, oligochaetes, and leeches, and the Panarthropoda, a group containing euarthropods, onychophorans and tardigrades, can be traced back to the Cambrian (Conway Morris, 1979; Liu & Dunlop, 2014).

On account of their segmented body plans, Georges Cuvier (1817) grouped the Panarthropoda and the Annelida into a common taxon, the 'Articulés', or Articulata, a group descended from a segmented spiral-cleaving ancestor (Scholtz, 1998; Nielsen 2001). Cuvier's 200-year-old hypothesis was only recently dismantled in the past two decades by technological advances in confocal microscopy and molecular biology, which exposed key differences in the embryonic cleavage patterns and ribosomal RNA sequencing of annelids and panarthropods, leading to the rival Ecdysozoa hypothesis (Figure 1.1; for more on the Ecdysozoa hypothesis, see Aguinaldo et al., 1997; Baguñà et al., 2008; Balavoine, de Rosa & Adouette, 2002; Bourlat

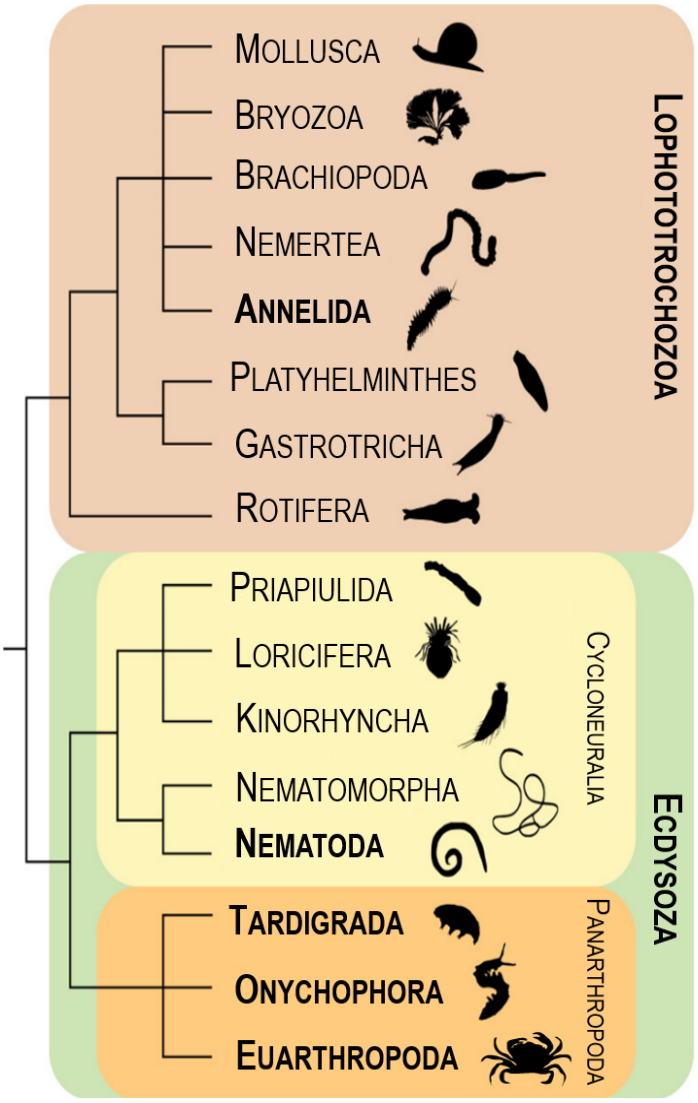


**FIGURE 1.1.** *Phylogenetic tree of the Ecdysozoa, a group comprising the panarthropods and cyclonerualians, and the Lophotrochozoa, a group containing the distantly related annelids. Modified from Schumann et al. (2018). Ecdysozoa phylogeny based on Giribet and Edgecombe (2017), Lophotrochozoa phylogeny based on Kocot (2016).*

et al., 2008; de Rosa et al., 1999; Edgecombe, 2009; Giribet, 2003; Hejnol & Schnabel, 2006; Helmkampf, Bruchhaus & Hausdorf, 2008; Kusche et al., 2005; Mallatt et al., 2004; Mallatt & Giribet, 2006; Petrov & Vladychenskaya, 2005; Philippe, Lartillot & Brinkmann, 2005; Podsiadlowksi, Braband & Mayer, 2008 Ruiz-Trillo et al., 2002; Sempere et al., 2007).

Members of the Ecdysozoa are unified by the presence of a protective cuticle that is shed in a complex process known as ecdysis, after which the group is named (Brusca & Brusca, 2002).

## 1.3. PANARTHROPODA

Panarthropoda is a major animal group containing euarthropods, onychophorans, and tardigrades (Figure 1.2). Together with the Cycloneuralia, these animals comprise the Ecdysozoa (Figure 1.1). Panarthropods are the most speciose, abundant, and successful group of animals on the planet. Since their origins in the Cambrian, the panarthropods have flourished and diversified for over 500 million years, occupying every life mode, including parasitism, and colonising almost every known habitat, from Himalayan glaciers to deep sea volcanic vents (Fortey & Thomas, 1998; Strausfeld, Ma & Edgecombe, 2016; Zhang 2011 & 2013). However, the evolutionary relationships within Panarthropoda remain contested (Ortega-Hernández, Janssen & Budd, 2017).

The prevailing hypotheses place Euarthropoda either as the sister taxon to (1) Onychophora, forming the ‘Arthropoda’ (Figure 1.2 a; Lankester, 1904), or to (2) Tardigrada, forming the ‘Tactopoda’ (Figure 1.2 b; Budd, 2001). A third, little remarked hypothesis that suggests a sister-group relationship between Onychophora and Tardigrada, forming the ‘Protarthropoda’, is not discussed further due to the notable lack of recent supporting molecular or morphological evidence (for more on the Protarthropoda hypothesis, see: Nielsen, 1995; Ortega-Hernández, 2014; Wägele et al., 1999; Waggoner, 1996).

A little over a century ago, Sir Edwin Ray Lankester (1904) proposed the putative clade comprising onychophorans and euarthropods (the Arthropoda hypothesis) based on three synapomorphies: an open haemocoelic circulatory system, segmental nephridia, and a dorsal heart with segmentally paired ostiae (Edgecombe, 2010; Lankester, 1904; Weygoldt, 1986).

The competing Tactopoda hypothesis, proposed almost two decades ago by Graham Budd (2001), is supported by palaeontological, neurological, and musculoskeletal evidence. The parsasegmental organisation of ganglia within the nerve cords of euarthropods and tardigrades (Mayer et al., 2013a), the tritocerebral innervation pattern of their stomatogastric

ganglia (Mayer et al., 2013b), and the specific segmental arrangement of longitudinal musculature (Marchioro et al., 2013; Schulze & Schmidt-Rhaesa, 2011) are all suggestive of a sister-group relationship between Euarthropoda and Tardigrada.

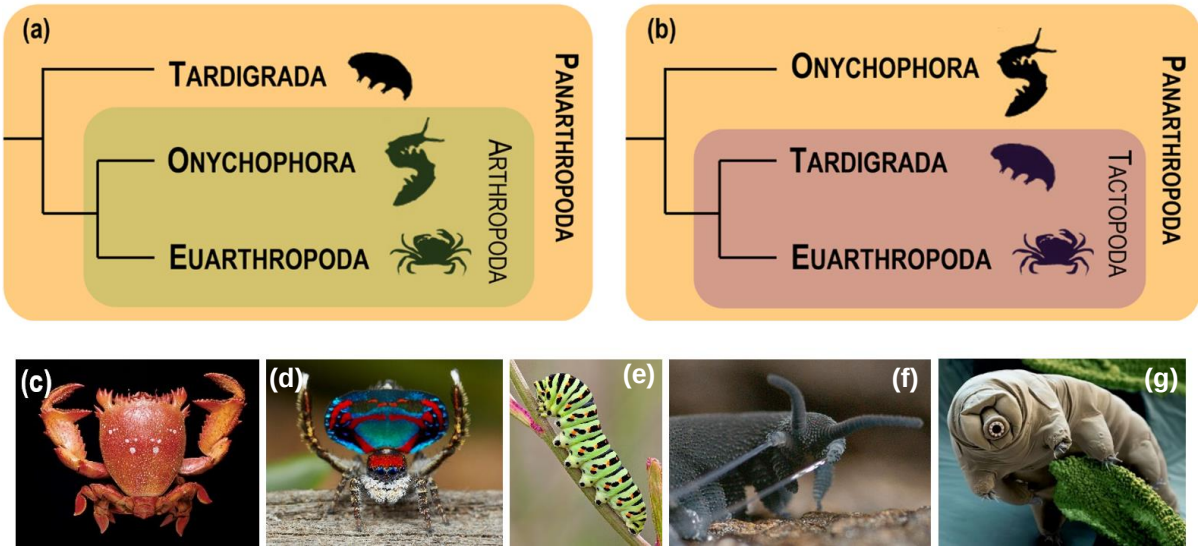


**FIGURE 1.2.** *The prevailing hypotheses for the phylogenetic relationships of panarthropods places Euarthropoda as the sister taxon to* (a) *Onychophora, forming the 'Arthropoda' (Lankester, 1904), or to* (b) *Tardigrada, forming the 'Tactopoda' (Budd, 2001).* (c-e) *Euarthropods.* (c) *Spanner crab (Natural History Museum / Alamy, n.d),* (d) *Peacock spider (Otto, 2015),* (e) *Swallowtail caterpillar (Dowding, n.d.),* (f) *Onychophoran (Baer et al., 2018),* (g) *Tardigrade (Science Photo Library, n.d.).*

## 1.4. THE SEGMENTED BAUPLAN

One suggested reason for the morphological breadth of the panarthropods is their segmented body plans. The classical definition (Goodrich, 1897; Scholtz, 2002) of a segment describes it as a body unit with a specific set of morphological characters, such as ventral ganglia, metanephridia, or appendages that are serially repeated along the anterior-posterior (AP) axis. Under this definition, a body segment can only give rise to a single pair of appendages (Warren and Carroll, 1995; Janssen, Prpic & Damen, 2004).

Panarthropod body segments are also defined by the expression of the *engrailed (en)* gene during development. *Engrailed* is selectively expressed in embryonic neuroblasts demarcating the posterior border of each segment, thereby distinguishing adjacent body regions (Figure 1.3; Browne et al., 2005; Fjose, McGinnis & Gehring, 1985; Kornberg et al., 1985; Patel et al., 1989a; Patel, Kornberg & Goodman, 1989b). The anteriormost segment in

panarthropods is the protocerebrum, which innervates the euarthropod labrum and the serially homologous onychophoran antennae (Eriksson, Tait & Budd, 2003; Ortega-Hernández et al., 2017). When present, the eyes of panarthropods are invariably found in this protocerebral (or ocular) segment (Ortega-Hernández et al., 2017). A patch of *engrailed* expression is observable in the protocerebral region where the optic lobes will develop and has sometimes been interpreted as the indicator of an additional segment boundary. However, this occurs in the daughter cells of the original neuroblasts and is thus found too late in development to be interpreted as a segment margin indicator (Boyan & Williams, 2002). The second and third segments are termed the deuto- and tritocerebral segments respectively (Ortega-Hernández et al., 2017).

In varying the specialisation of segments and their associated appendages, the segmental nature of which is also exploited in Euarthropoda, the function of numerous segments becomes increasingly differentiated, resulting in a multitude of specialised morphologies under the umbrella Euarthropod Bauplan (Brusca & Brusca, 2002; Valentine & Hamilton, 1997). However, the presence of a modular body plan does not confer the same evolutionary success to other segmented animals, such as the distantly related Annelida. Euarthropod diversity can thus be attributed to the additional presence of a hardened exoskeleton enabling a level of diversity that is unattainable to soft-bodied forms (Valentine & Hamilton, 1997).

Panarthropod diversity can also be attributed to tagmosis – the evolution of morphologically distinct body regions, or tagmata, that comprise several adjacent segments. The three tagmata of insects are (1) the abdomen, (2) the thorax, and (3) the head (Figure 1.4; Hughes, 2003; Valentine & Hamilton, 1997).

## 1.5. THE HEAD

The head is a remarkable evolutionary innovation found in almost all complex life on the planet (Figure 1.4; Brusca & Brusca, 2002). The anterior concentration of mechano- and chemosensory organs, nerves, and the mouth into a ‘head’ triggered an extraordinary evolutionary step-change, with huge implications for sensing, moving, and eating. Sophisticated sensory equipment such as compound eyes evolved, whilst the anterior concentration of nerves led to the formation of a complex brain. Nevertheless, the origins of the head remain uncertain (Scholtz, 2016).

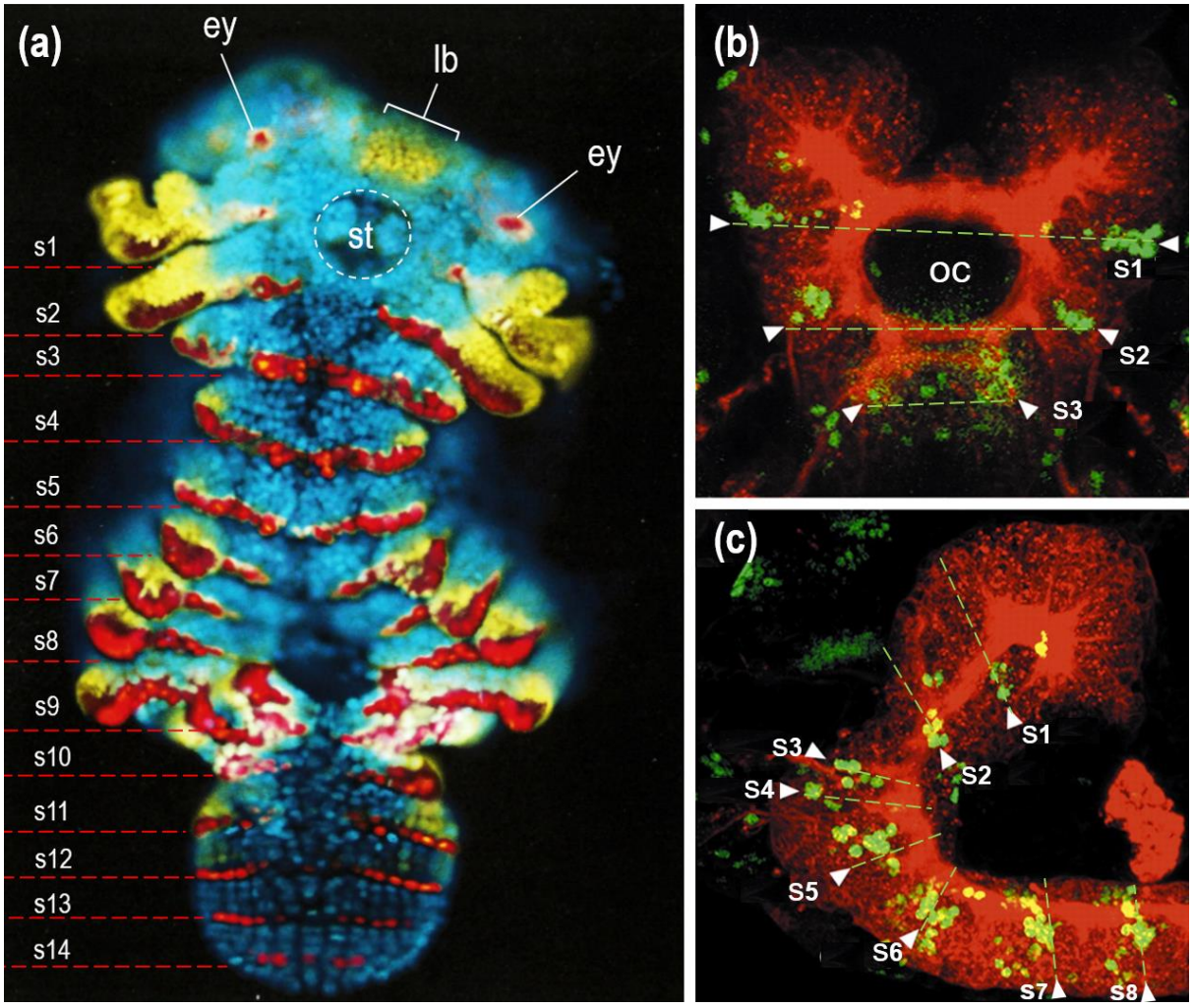


**FIGURE 1.3.** *Embryonic expression of the* engrailed (en) *segment boundary marker gene in* (a) Paryhale hawaiensis *and* (b-c) Drosophila*. Anterior is up.* (a) *Fluorescence microscopy visualisation of gene expression in a 96-hour amphipod crustacean embryo illuminating regions where* engrailed (en) *and* distal-less (Dll)*, genes indicating segment boundaries and appendages respectively, are expressed. Ventral view. The specimen is stained blue using 4',6-diamidino-2-phenylindole (DAPI).* En *is false-coloured red whilst* Dll *is false-coloured yellow. The anteriormost region of the specimen, which contains the developing labrum (lb), expresses* Dll *but not* en, *indicating an asegmental yet appendicular origin for the labrum. The developing eyes (ey) express both* Dll *and* en*, suggesting both an appendicular and a segmental origin for the eyes. The protocerebrum is thus genetically subdivided into an apical asegmental labral domain, and a segmental ocular domain. Modified from Browne et al. (2005).* (b) *Frontal and* (c) *lateral views of laser confocal microscopy of a stage 13/14 wild-type fruit fly embryo. Developing neuropils and neural cells are immunolabelled with horseradish peroxidase (HRP, shown in red). Segment boundaries are indicated in green using antibodies raised against the* en *protein. Modified from Hirth et al., 2003.*

***Abbreviations:*** *ey; developing eye; lb, developing labrum; s, segment; st, stomodeum (developmental precursor of the mouth).*

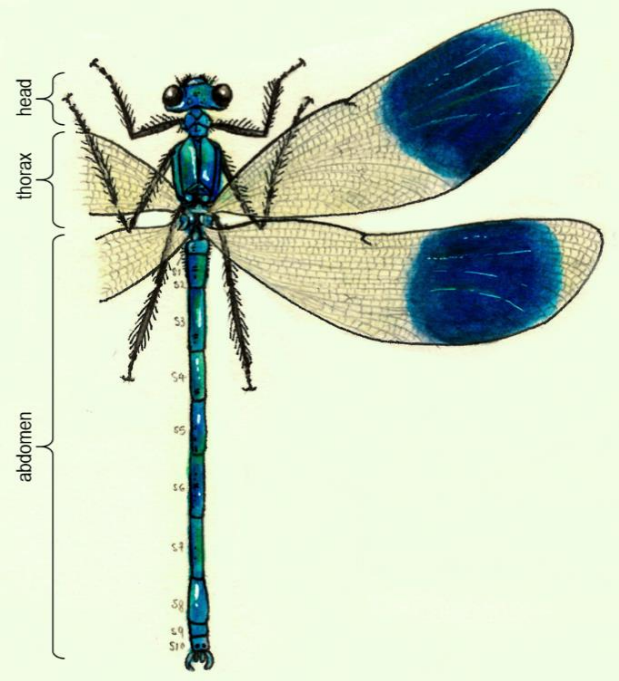


**FIGURE 1.4.** *The three morphological discrete body regions, or tagmata, of insects are the (1) abdomen, (2) thorax, and (3) head. Illustration of* Calopteryx splendens.

The very definition of the word 'head' is ambiguous, because there is no real structural correlate (Scholtz, 2016). Structures associated with the head, such as eyes and mouths, are observed in animals that have secondarily lost the head tagma, such as the mantle margin eyes of pectinid bivalves (Brusca & Brusca, 2002; Scholtz, 2016).

The definition of the 'brain' is equally problematic. If we define the brain as a cluster of nervous cells in the head, we find ourselves in a troubling loop of circular reasoning (Scholtz, 2016). Richter et al. (2011) attempted to circumvent this difficulty by defining the brain as follows, without any reference to the often-ambiguous head tagma:

*"A brain is a cluster of neurons. It is part of the nervous system. It is the most prominent anterior condensation of neurons and may also include further types of cells, including glial cells and pigment cells."*

However, this definition leads to difficulties in defining the brain's posterior boundary, a problem that is also experienced when describing the posterior limits of the head itself, particularly in relatively homogenous animals, such as nematode worms (Scholtz, 2016).

## 1.6. THE PANARTHROPOD HEAD PROBLEM

The panarthropod head is an evolutionarily and morphologically plastic region comprising modified appendage-bearing segments. However, despite decades of genetic, embryological, and palaeontological research, the homologies of these segments remain endlessly disputed (Rempel, 1975). The 'panarthropod head problem' thus stems from difficulties in comparing the anterior segmental composition of various, often-disparate

representatives of Panarthropoda (Ortega-Hernández et al., 2017; Scholtz, 2016; Snodgrass, 1960).

Resolving the nature of anterior segmental organisation is critical to our understanding of the long-debated evolutionary trajectories and phylogenetic relationships of Panarthropoda (see section 1.2; Giribet & Edgecombe, 2012; Ortega-Hernández et al., 2017). There are numerous speculations regarding the composition of panarthropod heads, the number and alignment of their segmental components, and their respective evolutionary histories (Ortega-Hernández et al., 2017). I will briefly recount the foremost four hypotheses here.

### 1.6.1. THE CHEN AND WALOSZEK ET AL. MODEL

Chen, Waloszek and Maas (2004) and Waloszek et al. (2005) suggest that the frontal appendages of megacheirans and radiodontans are deutocerebral, whilst the specialised post-antennal appendages (SPAs) of fuxianhuiids are tritocerebral. An evolutionary trend in which the number of podomeres in megacheiran frontal appendages appears to be decreasing led Chen et al. (2004) to hypothesise that this podomere reduction led to the origin of the bi- or tri-segmental chelicerae found in ancestral representatives of the extant Chelicerata (Chen et al., 2004; Haug et al., 2012; Stein, 2010). By extension, this proposes a deutocerebral origin for the frontal appendages of megacheirans, radiodontans, and gilled lobopodians. Onychophorans are not considered (Figure 1.5).

### 1.6.2. THE SCHOLTZ AND EDGECOMBE MODEL

By utilising the site of appendage-attachment relative to the mouth as a reference point, Scholtz and Edgecombe (2005, 2006) suggest that pre-oral raptorial appendages are homologous deutocerebral structures across Euarthropoda (Ortega-Hernández et al., 2017). It follows that any appendages that attach to a site anterior to the deutocerebral raptorial limbs are protocerebral. Under this model, the fuxianhuiids retain the primary antennae of their ancestors (Figure 1.5).

### 1.6.3. THE LEGG AND VANNIER ET AL. MODEL

Legg, Vannier and colleagues (2013) suggest that the frontal appendages of the bivalved arthropod *Isoxys* are protocerebral, and therefore homologous to the pre-oral raptorial appendages of Radiodonta. They also propose that the specialised post-antennal appendages (SPAs) of the fuxianhuiids are homologous to the megacheiran short-great appendages, both of which correspond to the tritocerebral segment (Figure 1.5).

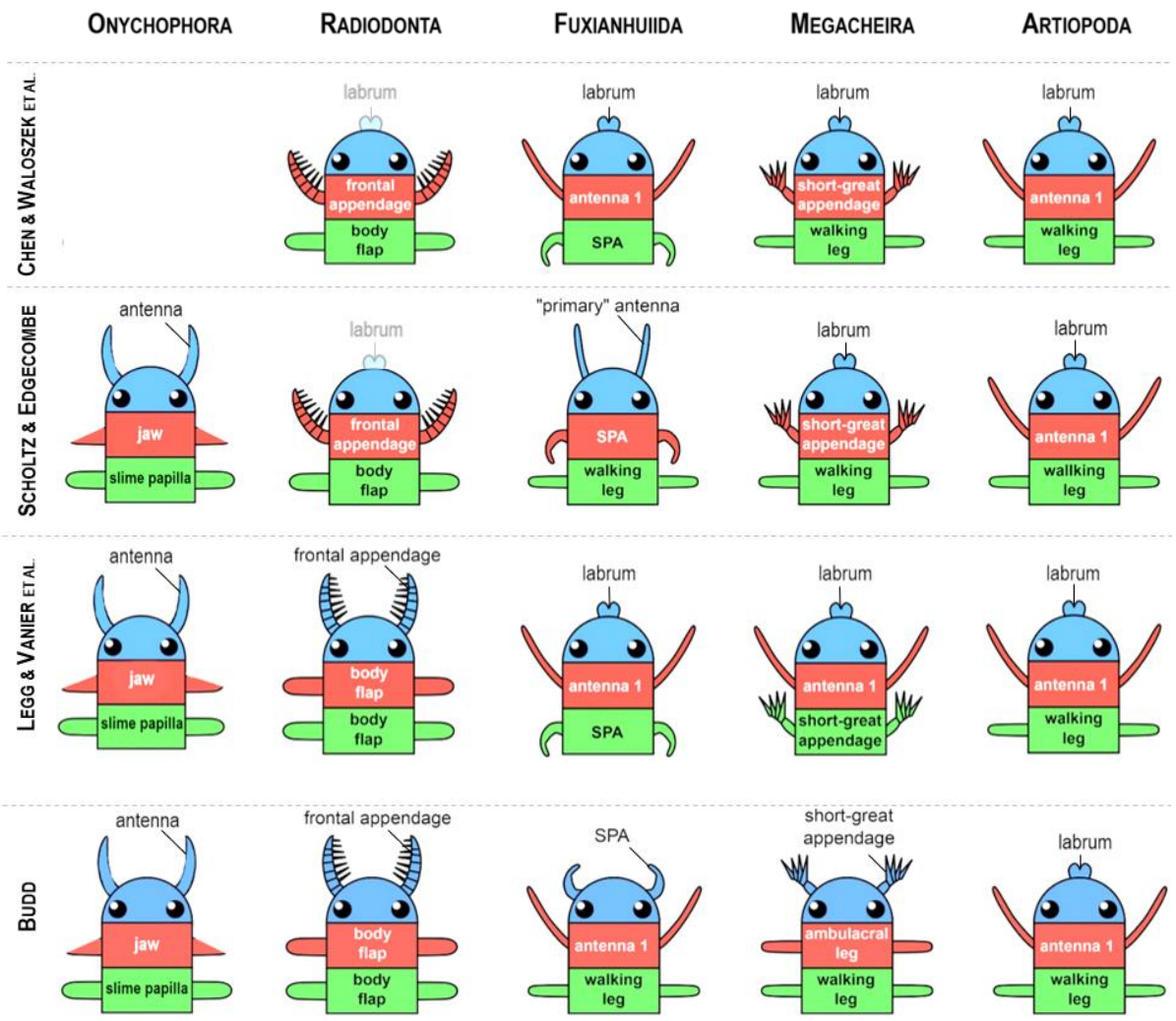


**FIGURE 1.5.** *Foremost hypotheses for the arrangement of head segments in crown-group Onychophora and stem-group Euarthropoda. The protocerebral, deutocerebral, and tritocerebral segments are coloured in blue, red, and green respectively. After Ortega-Hernández et al. (2017),* Branchiocaris *is grouped together with the fuxianhuiids.* (1) *Chen et al. (2004) and Waloszek et al. (2005). See section 1.6.1.* (2) *Scholtz and Edgecombe (2005, 2006). See section 1.6.2.* (3) *Legg and Vannier (2013), and Legg et al. (2013). See section 1.6.3.* (4) *Budd (2002). See section 1.6.4. Structures or taxa not considered by the authors are absent or rendered transparent. Figure adapted from Ortega-Hernández et al., 2017.*

***Abbreviations:*** *SPA, specialised post-antennal appendages.*

### 1.6.4. THE BUDD MODEL

As in the Scholtz and Edgecombe (2005, 2006) model (see section 1.6.2), on account of their robust, spiniferous morphologies, Budd (2002) proposes that all euarthropod pre-oral raptorial appendages are homologous structures (Daley & Budd, 2010; Daley & Edgecombe,

2014; Van Roy, Daley & Briggs, 2015). However, Budd proposes a protocerebral, rather than a deutocerebral, affinity for these structures (Figure 1.5).

Budd also suggests that the raptorial appendages are homologous to the labrum. The onychophoran antennae are structurally similar to the frontal appendages of stem-group euarthropods and basal lobopodians, like *Aysheaia* (Whittington, 1978), indicating that these too are innervated protocerebrally, and are thus homologous to the pre-oral euarthropod labral / raptorial appendages (Figure 1.5).

Despite the fact the specialised post-antennal appendages (SPAs) of Fuxianhuiida are located posteriorly to the antenniform appendages, Budd proposes a protocerebral affinity for the SPAs, suggesting that their preserved placement is a consequence of the ventral rotation of the frontal appendages to follow the migration of the mouth (Budd, 1999; Dewel et al., 1999). However, the other three models suggest the preserved position of the SPAs is a consequence of belonging to a segment located posteriorly to the antennal segment (Figure 1.5).

The Budd model is unique among the competing hypotheses regarding the presence of the labrum. Chen, Waloszek and colleagues (section 1.6.1), Scholtz and Edgecombe (section 1.6.2), and Legg and Vannier et al. (section 1.6.3) all propose the presence of a labrum in the megacheirans, and all but Scholtz and Edgecombe propose that the labrum is present in the fuxianhuiids. These segmental homology models are therefore notably predicated on structures that Budd does not observe in the fossil material (Figure 1.5).

## 1.7. THE BIPARTITE ANCESTRAL PROTOCEREBRUM

Despite the differing segmental affinities of the specialised post-antennal appendages (SPA), frontal appendages, and short-great appendages, the onychophoran antennae, euarthropod labrum, and the eyes are situated in the protocerebrum in all four hypotheses (Figure 1.5).

The protocerebrum is a unique body region formed by the ancient fusion of the ancestral first segment and an apical appendage-bearing non-segmental element (Figure 1.6). These regions are termed the archi-and prosocerebrum respectively, but as these terms are used interchangeably (Strausfeld, 2012; Ortega-Hernández et al., 2017), I will define these regions based on gene expression data. A closer inspection of the constituent protocerebral structures will tell us more about the evolution and formation of the modern protocerebral segment, which is key to homologising the anterior segmental composition of disparate panarthropod taxa.

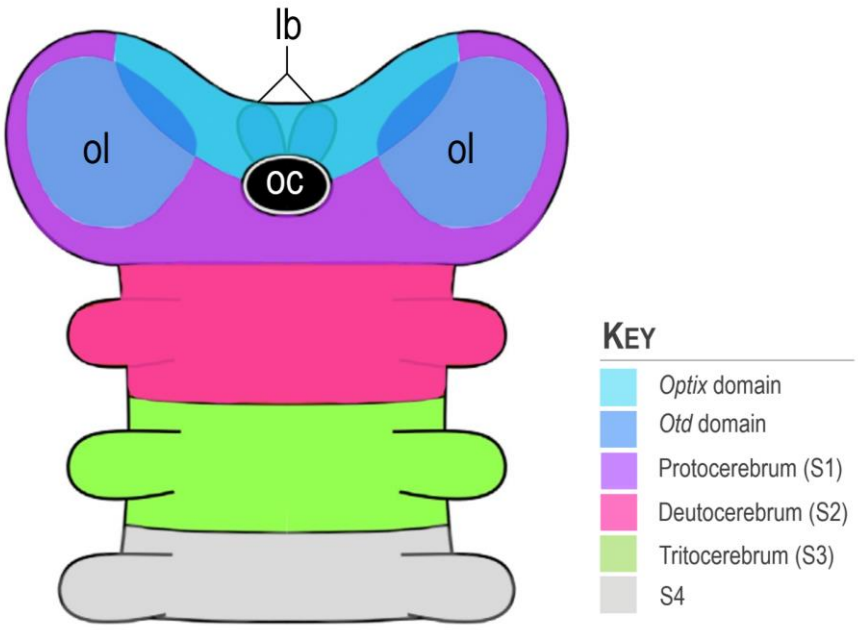


**FIGURE 1.6.** *Anterior gene expression in the embryonic euarthropod protocerebral segment. The protocerebrum is genetically subdivided by the expression of the genes* optix *and* orthodenticle (otd) into the labral and ocular domains respectively*. Diagram modified from Ortega-Hernández et al. (2017). Based on research by Eriksson et al. (2013), Hunnekuhl & Akam (2014), Posnien et al. (2009, 2011), and Steinmetz et al. (2010).*

***Abbreviations:*** *lb, labrum; oc, oral cavity; ol, optic lobe.*

### 1.7.1. THE GENETIC SUBDIVISION OF THE PROTOCEREBRUM

In panarthropods, the protocerebrum is genetically subdivided into two regions by expression of the genes *optix* and *orthodenticle (otd).* The posteriormost protocerebral region is defined by *otd* expression and contains the eyes, whilst the anteriormost protocerebral region expresses *optix* and innervates the labrum / antennae (Figure 1.6; Eriksson, Samadi & Schmid, 2013; Hunnekuhl & Akam, 2014; Janssen, 2013; Ortega-Hernández et al., 2017; Posnien et al., 2011; Steinmetz et al., 2010; Strausfeld, 2012; Urbach & Technau, 2003). The delineation of the *otd* domain's posterior margin by *engrailed* is a clear indicator of the *orthodenticle* domain's segmental origins. However, the lack of an *engrailed* marker in the *optix* domain suggests that the apical protocerebral element is asegmental in origin (Strausfeld, 2012).

The asegmental *optix* and segmental *otd* domains are fused in extant euarthropods (Damen, 2002; Farzana & Brown, 2008; Hunnekuhl & Akam, 2014; Janssen, 2012 & 2013; Posnien et al., 2009 & 2011; Urbach & Technau, 2003 & 2004) and onychophorans (Eriksson

et al., 2013; Eriksson & Stollewerk, 2010) to form the protocerebral region, or the first true body segment (Figure 1.6; Ortega-Hernández et al., 2017; Strausfeld, 2012). The status of the protocerebrum is unclear in the tardigrades (Smith et al., 2016; Smith, Bartels & Goldstein, 2017).

In onychophorans, genes associated with border formation have a clear anterior limit; the anterior margin of *Wingless-related integration site* (*Wnt)*, a gene expressed in a segment-wide domain comparable to the broad domain of *homeobox (Hox)* genes, is situated in the approximate middle of the onychophoran protocerebrum (Hogvall et al., 2014; Hughes & Kaufman, 2002). Conserved *Delta / Notch* signalling, involved in segmentation, also follows a similar pattern; in developing onychophorans, the receptor *Notch (N)* and its ligand *Serrate (Ser)* are expressed at the protocerebral midpoint, forming a genetic boundary that subdivides the head lobes (Eriksson & Stollewerk, 2010; Janssen & Budd, 2016; Pourqui, 2003; Rivera et al., 2005; Stollewerk, Schoppmeier & Damen, 2003; Ortega-Hernández et al., 2017).

The panarthropod protocerebrum is thus genetically subdivided into two functional domains: (1) the apical asegmental *optix* domain containing the euarthropod labrum / onychophoran antennae, mushroom body neuroblasts, and neurosecretory cells, and the (2) segmental *otd* domain, containing the eyes (Figure 1.6; Ortega-Hernández et al., 2017; Strausfeld, 2012; Urbach & Technau, 2003 & 2004). Studies on *optix* expression in fruit flies, flour beetles, and chilopods have demonstrated that the *optix* domain does not overlap with *otd* expression and is constrained to an apical region, effectively confirming the existence of an ancestrally discrete and asegmental element in the euarthropod head (Strausfeld, 2012). The discrete genetic subdivision of the protocerebral segment thus provides evidence for an ancestrally bipartite protocerebrum composed of morphologically discrete regions innervating the anteriormost appendages and the eyes respectively.

The panarthropod's closest relatives are legless, unsegmented roundworms called nematodes. Nematodes possess a circumpharyngeal nerve ring, or brain, that innervates ventral and dorsal cords. An anterior cluster of neuronal cell bodies, the anterior 'ganglion', is positioned anteriorly to the circumoral brain, whilst lateral and ventral 'ganglia' are positioned posteriorly to it (Schmidt-Rhaesa & Henne, 2017; White et al., 1986). Three neurons, defined by the expression of *otd / otx*-like genes, are expressed in the lateral and ventral ganglia of *Caenorhabditis elegans*; expression of the *otx*-like gene *ceh-36* defines the boundaries of the AWC and ASE neuronal cell bodies, whilst the *otx* homologue, *ttx-1,* is expressed in the AFD neurons, all of which are contained within the lateral and ventral ganglia (Figure 1.7; Lanjuin

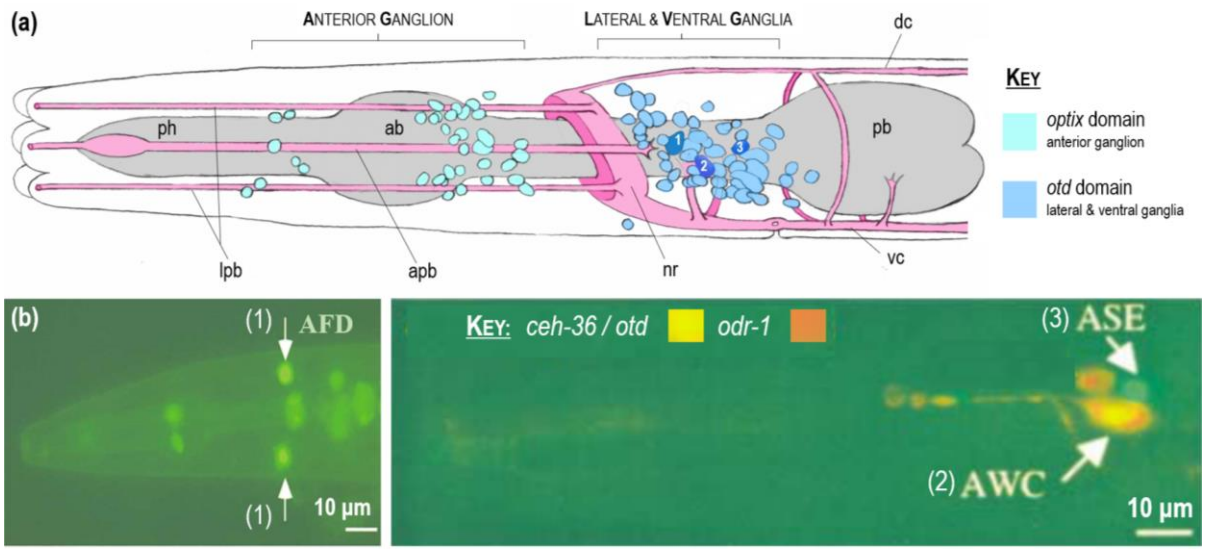


**FIGURE 1.7.** *Expression of* orthodenticle (otd) / otx *like genes in the nematode* Caenorhabditis elegans. *Anterior is left*. (a) *Anterolateral view. A circumpharyngeal nerve ring (nr) functions as the brain, innervating ventral (vc) and dorsal cords (dc). An anterior cluster, or ganglion, of neurons is positioned anteriorly to the brain, whilst lateral and ventral ganglia are positioned posteriorly to it. Three neurons are highlighted in the lateral and ventral ganglia. The identities of these neurons and the* otx*-like genes they express are as follows: (1) AFD,* ttx-1*; (2) AWC,* ceh-36*; (3) ASE,* ceh-36*. I hypothesise that the anterior ganglion is homologous to the panarthropod asegmental* optix *domain. The discrete nature of the proposed* optix *and* otd *domains in* C. elegans *reflects the ancestral bipartite condition of the protocerebrum. Illustration based on research by White et al., 1986, Lanjuin et al., 2003, and Satterlee et al., 2001.* (b) *Ventral view depicting expression of the* otx *homologue* ttx-1*, tagged with green fluorescent protein (GFP), in the left and right AFD neurons (LAFD & RAFD) of the lateral and ventral ganglia. Nuclei are indicated by white arrows.* Ttx-1 *is expressed in the AFD neurons and the pharyngeal marginal cells. Modified from Satterlee et al., 2001.* (c) *Lateral view. A GFP-tagged* ceh-36 *transgene (green) is expressed in the AWC and ASE neurons. Expression of* Odr-1, *tagged with red fluorescent protein (dsRed), is shown in red. Modified from Lanjuin et al., 2003.*

***Abbreviations:*** *ab, anterior bulb of the pharynx; apb, amphid process bundle; dc, dorsal cord; lpb, labial process bundle; nr, nerve ring; pb, posterior bulb of the pharynx; ph, pharynx; vc, ventral cord.*

et al., 2003; Satterlee et al., 2001). I propose that the lateral and ventral ganglia are homologous to the panarthropod *otd* domain, and that the anterior ganglion therefore corresponds to the panarthropod *optix* domain (Figure 1.7). The discrete natures of the proposed *optix* and *otd* domains in *C. elegans* reflects the ancestral bipartite condition of the protocerebrum, suggesting that a fusion event occurred after the evolutionary divergence of nematodes and panarthropods. Although detailed gene expression studies on *optix* / *six3*

homologues in the anterior ganglion are presently lacking, the available morphological and genetic evidence outlined here is entirely consistent with the configuration of the nematode brain as two discrete modules.

### 1.7.2. THE PROTOCEREBRAL APPENDAGES

By definition, a segment can only possess one pair of appendages (see section 1.4; Scholtz, 2002). The presence of more than one pair of appendicular structures in the protocerebrum would therefore indicate that this region was ancestrally divided into two distinct appendage-bearing units.

The appendage indicator gene *distal-less (Dll)* is expressed in the developing optic lobes, the labrum, and the trunk appendages of the amphipod crustacean *Paryhale hawaiensis*, suggesting an appendicular affinity for both the labral and ocular structures (Figure 1.3; Hirth et al., 2003).

Manipulative molecular studies from as early as the 19$^{th}$ century have shown that stalked eyes can transform into limb-like appendages and vice versa, further hinting at the appendicular origins of the ocular structures (Clements et al., 2008; Halder, Callaerts & Gehring, 1995; Herbst, 1896 & 1916; Kumar & Moses, 2001; Milne-Edwards, 1864).

The sensory organisation of the central nervous system, coupled with the physiological and anatomical organisation of eyestalks, also suggest an appendicular origin for the euarthropod eye (Figure 1.8; Strausfeld et al., 2016). The central segregation of axons from peripheral receptors forms discrete synaptic quantities in segmentally iterated ganglia. This ancient arrangement of axon terminals is derived from an ancestral animal with homonomous segments equipped with homonomous ganglia and appendages (Strausfeld et al., 2016). This ancestral condition is observable even in the most modified segmental appendages and ganglia, from thoracic legs and ventral ganglia to uniramous antennae and the deutocerebral ganglion of the panarthropod brain. Leg receptors isolate their axons to distinct domains in the relevant thoracic ganglion, whilst the synaptic mass of the antennal (or olfactory) lobes, known as the olfactory glomerulus, obtains inputs from olfactory receptor neurons situated on the antennal flagellum (Figure 1.8 a; Couto, Alenius & Dickson, 2005; Murphey et al., 1989; Strausfeld et al., 2016). The protocerebrum also possesses distinct domains, the optic glomeruli, which receive outputs from the optic lobes. The neuronal connections of the optic glomeruli are the same as those of the olfactory glomeruli and the sensory domains of the

thoracic ganglia, resolving the neuronal connections of the eyes as typical appendicular connections (Figure 1.8; Mu et al., 2012; Okamura & Strausfeld, 2007; Strausfeld et al., 2016).

The distinctly appendicular innervation of the ocular structures thus provides a clear morphological basis on which to support the genetic evidence for the dual elements of the protocerebrum.

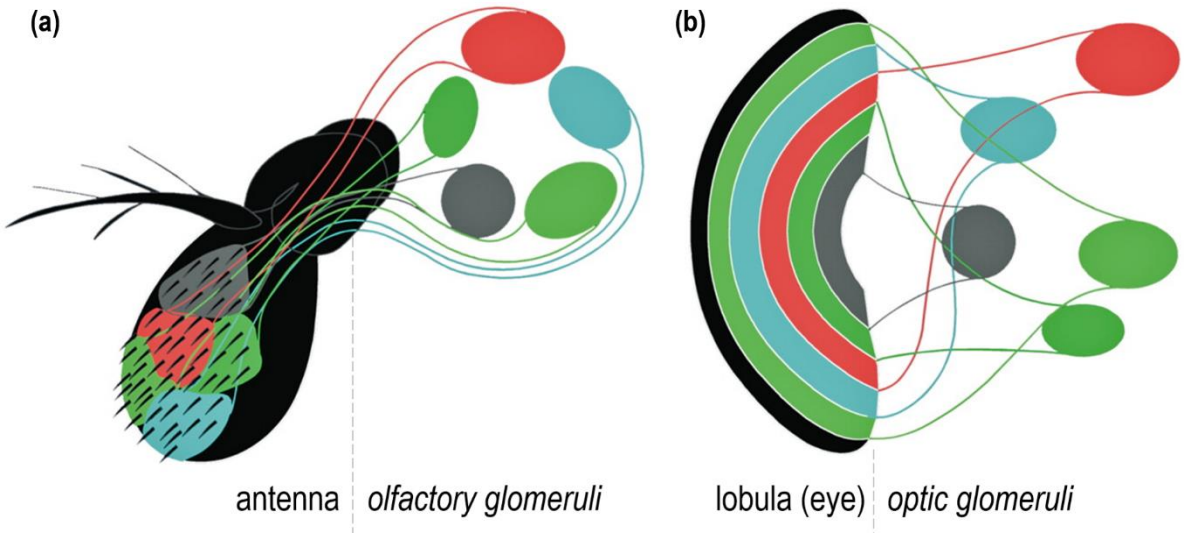


**FIGURE 1.8.** *Illustration documenting the similarities in the central segregation of channels within the* (a) *olfactory and* (b) *optic glomeruli of* Drosophila*. Modified from Mu et al. (2012).*

### 1.7.3. PALAEOANATOMICAL EVIDENCE

Strausfeld proposed that evidence of the bipartite protocerebrum could be expressed in the brains of certain Cambrian lobopodians, particularly in those with simple morphologies (Ortega-Hernández et al., 2017; Strausfeld, 2012). The ancient lobopodian ancestors of extant panarthropods were walking worms with multiple, lobopod-like legs, after which the group was named (Liu & Dunlop, 2014; Smith & Ortega-Hernández, 2014; Zhang et al., 2016), such as the hallucigeniids – a group of animals so bizarre that they were originally interpreted upside down and back to front (Conway Morris, 1977). Lobopodians are found in the both the second (Caron, Smith & Harvey, 2013) and third (Liu et al., 2006) stages of the Cambrian. Increasingly peculiar morphologies typically emerged in the Stage 3 deposits, most notably in the Chengjiang Biota of China, which has yielded more than one third of the total number of lobopod species discovered (Liu et al., 2006; Liu & Dunlop, 2014; Ou et al., 2011).

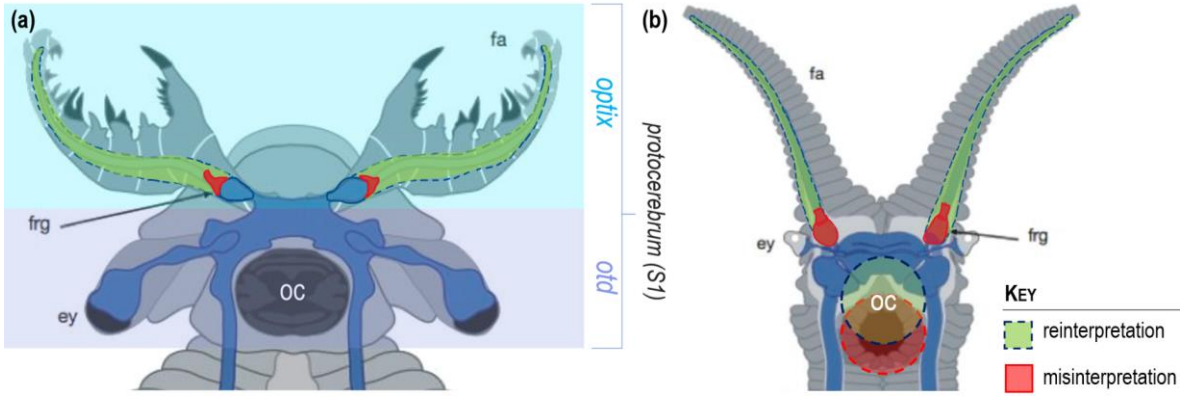


**FIGURE 1.9.** *Anterior segmentation in* (a) Lyrarapax unguispinus, *an early Cambrian anomalocaridid and* (b) *an extant adult onychophoran. Ventral view, anterior is up. Images produced by Cong et al. (2014). Reinterpretations, misinterpretations, and the putative nervous system are coloured green, red, and blue respectively.* (a) *Extensions of the 'frontal ganglia' (frg) are misinterpretations, as they are not observed in the original fossil (Appendix 1.1). I interpret the 'frontal ganglia' as basal elements of the frontal appendages (fa). Hypothetical* optix *and* orthodenticle (otd) *gene expression regions are shaded in pale blue and purple respectively.* (b) *The proposed 'frontal ganglia' of Onychophora were exposed by Mayer et al. (2014) as a misleading sectioning artefact of the antennal base. The oral cavity (oc), incorrectly illustrated to suggest a pre-oral brain, has been redrawn in a more accurate position.*

***Abbreviations:*** *fa, frontal appendage; frg, frontal ganglion; ey, eye; oc, oral cavity.*

Using both palaeo- and modern neuroanatomical data, Cong et al. (2014) proposed that a 'pre-protocerebral' ganglion innervating the frontal appendages was present in the Chengjiang Cambrian anomalocaridid, *Lyrarapax unguispinus*, and persists in the extant Onychophora.

However, the non-preservation of the frontal appendages is insufficient evidence to confirm this bold hypothesis. A misleading illustration artificially constricts the putative nervous tissue to create the appearance of paired ganglia at the presumptive base of the frontal appendages (Figure 1.9 a). However, this constriction is not visible in the fossil material (see Appendix 1.1). A similar error was made in Cong et al.'s interpretation of the modern onychophoran, whereby a sectioning artefact made the basal region of the antennal tract look like a pre-oral ganglion (Figure 1.9 b; Mayer et al., 2014). I therefore reinterpret *Lyrarapax*'s proposed frontal ganglia as basal elements of the frontal appendage tract.

Despite Cong et al.'s (2014) bold proposition, there is also no clear support for a 'pre-protocerebral' panarthropod segment (Mayer et al., 2014). I thus reinterpret *Lyrarapax's* so-called 'pre-protocerebral' region as the apical *optix* domain, which is fused in the fossil to the

succeeding ocular *otd* domain to form the derived unipartite protocerebrum expected of an upper stem-group euarthropod (upper stem-group euarthropod as defined by Ortega-Hernández, 2014).

## 1.8. STUDY AIMS

Developmental gene expression studies suggest that the protocerebral region originated from two discrete appendage-bearing elements. However, there is no evidence for an ancestral bipartite protocerebrum in the fossil record. The evolutionary origins of the protocerebrum thus remain unresolved, awaiting the discovery of new palaeodevelopmental data from Cambrian stem-group taxa.

No larger than a grain of rice, a remarkable early Cambrian embryo with the potential to resolve the panarthropod head problem has been exceptionally preserved by the three-dimensional replication of its tissues in the phosphatic limestones of China's Chengjiang County. This study aims to describe the creature's internal anatomy by manually segmenting Synchrotron X-Ray Computer Tomography (sXCT) data to produce a complete model of the animal.

This thesis offers a remarkable first insight into the developmental processes of early bilaterians, as well as providing the first fossil evidence for an asegmental brain and the ancestrally bipartite protocerebrum, revealing a crucial puzzle piece in the infinite jigsaw puzzle of the panarthropod head problem.

# CHAPTER 2

# MATERIAL & METHODS

- PLEASE REFER TO THE PLATES (PL) LOCATED AT THE END OF THIS THESIS –

---

## 2.1. MATERIALS

This study addresses a millimetric, three-dimensionally preserved phosphatised fossil, Yunnan Key Laboratory of Palaeontology (YKLP) 12387, from the Cambrian Stage 3 Yu'anshan Formation at the Xiaotan section in Yongshan, Yunnan Province, China. YKLP 12387 was recovered from a nodule of limestone in Autumn 2007 via 5% acetic acid digestion of the limestone and extracted from the residue using a stereomicroscope.

## 2.2. IMAGE ACQUISITION

YKLP 12387 was examined via Scanning Electron Microscopy (SEM) in April 2008 in the GeoLab of Northwest University in Xi'an, Shaanxi Province, China, using a Phillip SEM at 20 kV, and in April 2015 at the YKLP, China, using a JCM-6000 benchtop SEM at 10 kV. See

Appendix 2.1 for the SEM photographs.

The specimen was also examined using Synchrotron Radiation X-ray Computed Tomography (sXCT) on the imaging branch of beamline i13, Diamond Light Source (MT15461) under a polychromatic (pink) beam using 3.2 mm Aluminium filters and a 120 ms exposure. 1000 projections were collected on a 180˚ rotation of the fossil at 4× magnification on a pco.edge camera with an effective pixel size of 1.625 µm. Data were reconstructed using i13 standard filter back projection protocols. See Appendix 2.1 for the volume dataset.

## 2.3. Fossil Imaging and Analysis

### 2.3.1. General Methodology

I processed the 3D data in Avizo. Inbuilt Avizo functions are denoted by angular brackets. For the Avizo project and generated model, see Appendix 2.1.

Individual structures were typically mapped manually and assigned to their own label within the <segmentation editor>. The <magic wand> was used to separate the specimen's body from the exterior based on greyscale values. In some regions, traditional methods failed

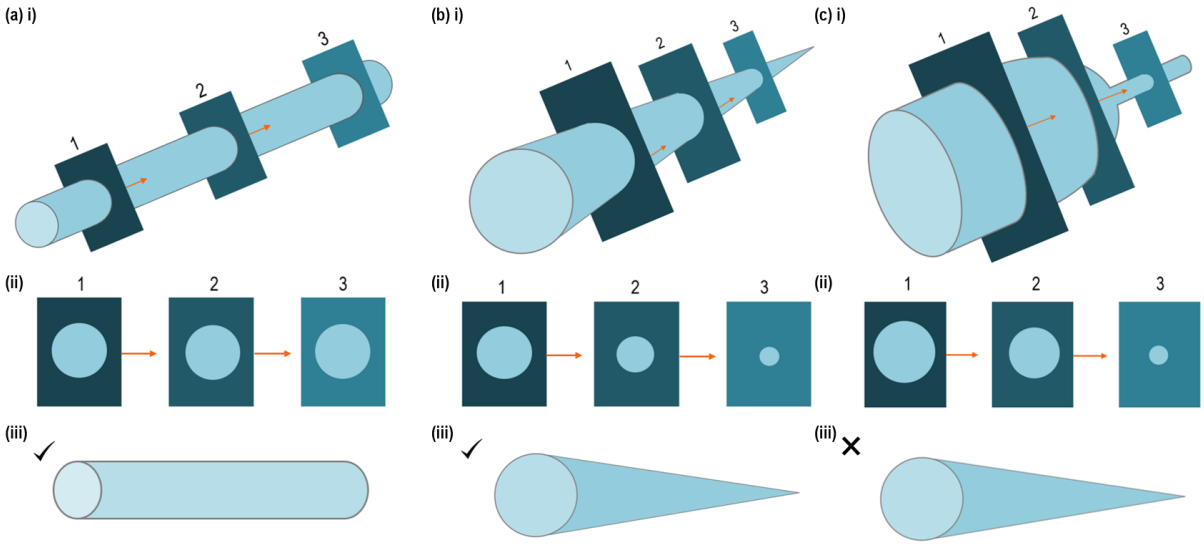


**FIGURE 2.1.** *Segmentation of* (a) *cylindrical,* (b) *conical, and* (c) *wine-glass shaped chambers at 3 regularly spaced intervals. Gaps between the orthoslices are automatically interpolated to produce a 3D model of the structure. Interpolation is indicated by orange arrows.* (a) ii) *Due to the geometric nature of the cylindrical model, the chamber's morphology does not vary between the 3 orthoslices,* (iii) *rendering reconstruction accurate*. (b) ii) *Although the shape of the conical chamber varies between the 3 orthoslices, automatic interpolation assumes gradual change. The original conical morphology is thus reconstructed accurately.* (c) *However, the more complex wine-glass morphology is lost under this assumption.*

to pick up some of the finer internal structures. Where needed, the <brush> tool was used to identify individual internal chambers. By locking the dense tissue previously identified by the <magic wand>, chambers could be traced roughly with the <brush> without editing the tissue label (Appendix 2.2). Chambers were mapped at regular intervals; depending on feature size and how rapidly the morphology changed, slice spacing varied between 2 and 50 slices. The gaps between the slices were then automatically interpolated to produce a 3D model of the structure (Figure 2.1). Following traditional methods, key labelled 3D chambers were measured in Avizo using the 2-point selection <measure> tool. The volume of all labelled 3D chambers can be rapidly measured in Avizo using <Label Analysis>.

### 2.3.2. KEY PROBLEMS AND THEIR SOLUTIONS

#### 2.3.2.1. MISINTERPRETATION OF TAPHONOMIC AND ARTIFICIAL STRUCTURES

Features that look biological, but are not, can be produced by taphonomic processes, such as microborings (Figures 2.2, 2.3 c & 2.4; Zhang & Pratt, 2008), phosphatisation (Figures 2.2 & 2.3; Bengtson & Budd, 2004; Chen et al., 2004; Cunningham et al., 2012; Eriksson et al., 2012), and fractures (Figures 2.2 & 2.3 f & i). Bilateral symmetry was the criterion for biogenicity (Figure 2.5). Features with a similar greyscale value to the fossil, including sulphide contaminants and glue, were manually identified and labelled using <brush> (Figures 2.2, 2.3 g, h & i, & 2.6). The greyscale threshold was adjusted to avoid accretionary artifacts whilst including as much real tissue as possible (Figure 2.7).

#### 2.3.2.2. COMPACTION

Compaction has deformed the specimen's original morphology, making an accurate reconstruction of the affected features difficult and rendering some fine chambers invisible (Figure 2.8). Compaction is often localised to one side of the body. Determining which unmirrored structures were lost due to compaction and which were genuinely absent involved a detailed morphological analysis of the structure in question; if the unmirrored structure resembled an artifact produced by taphonomic (Figures 2.2, 2.3 c-j, 2.4 & 2.6) or methodological (Figures 2.2 & 2.3 a & b) processes, the absence of a bilaterally symmetrical structure was considered genuine. If not, its absence was considered a consequence of compaction (Figure 2.2).

Compaction artificially merges adjacent voids (Figure 2.9). When distinguishing between the taphonomic and original biological boundaries of individual structures, a

subjective decision was made (Figure 2.9). Subjective decisions introduced an element of interpretation into the mapping process, resulting in a degree of unavoidable human bias.

Fluid-filled cavities are more susceptible to compaction than those filled with tissue, as they offer less resistance. Compaction was therefore used to infer the composition of certain chambers (Figure 2.10).

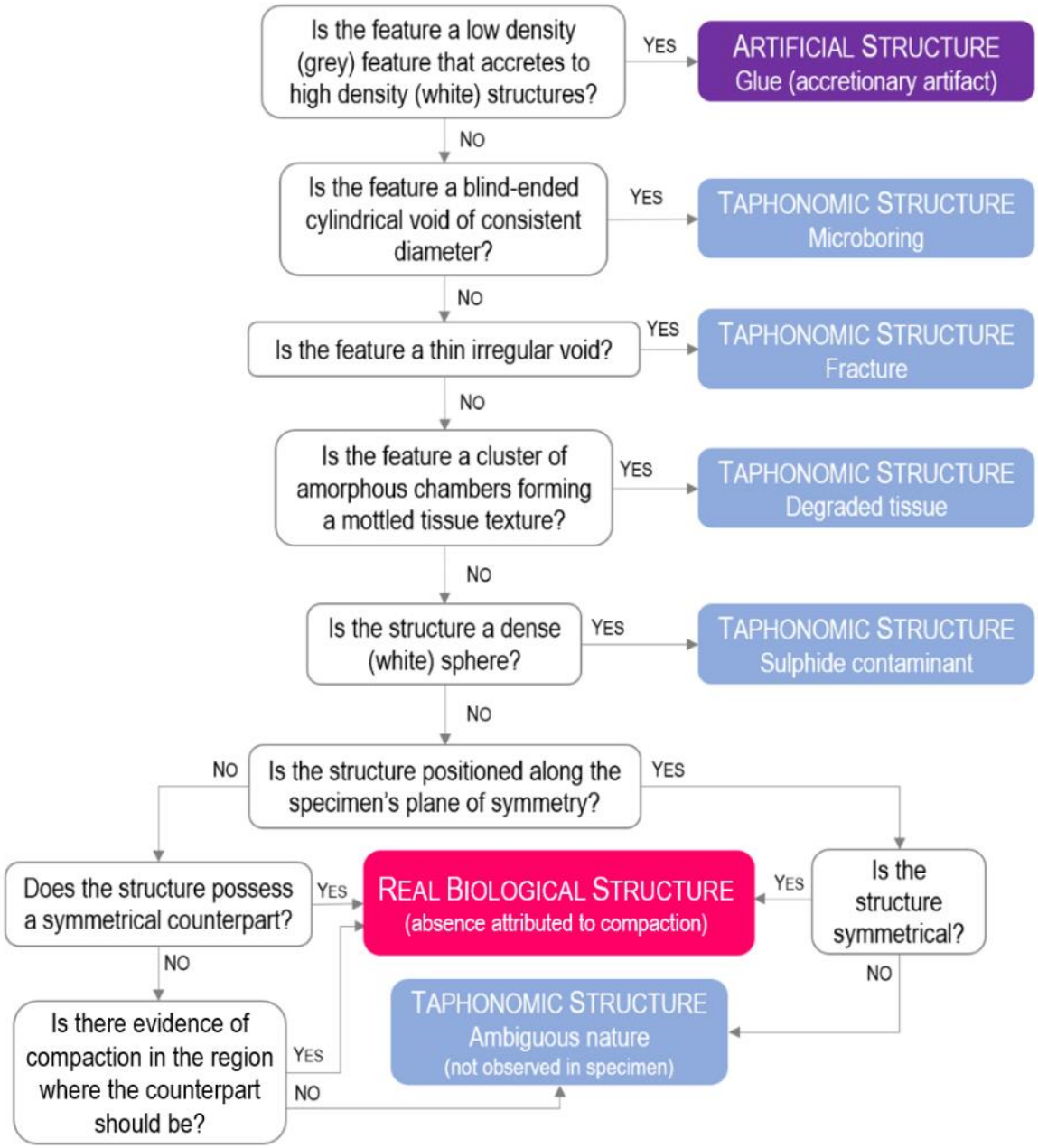


**FIGURE 2.2.** *Decision tree detailing the properties of the various taphonomic, artificial, and real structures observed in the specimen, depicted in lilac, purple, and pink respectively. For images of the various structures described, see Figure 2.3.*

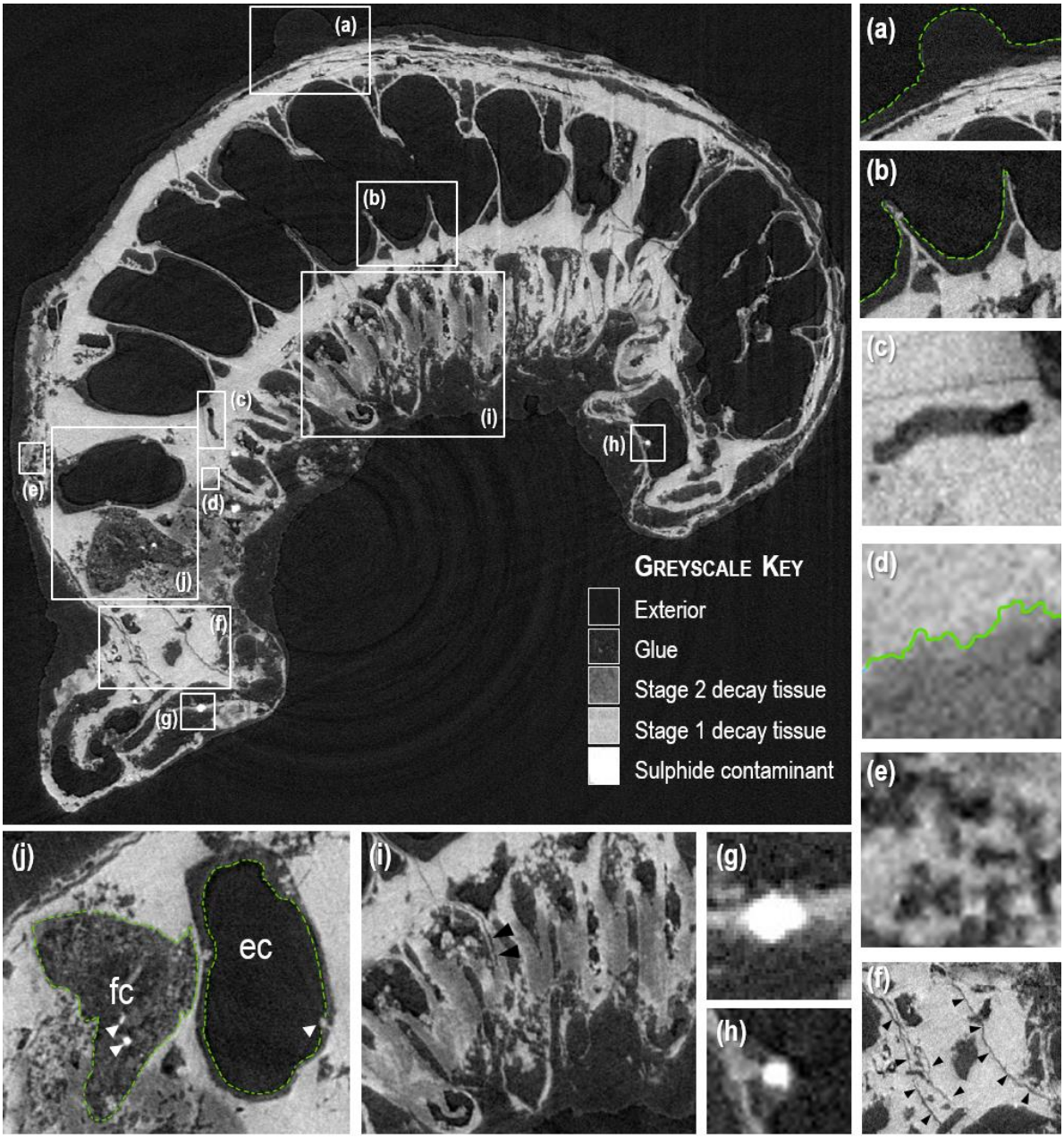


**FIGURE 2.3.** *sXCT micrograph illustrating the key taphonomic and methodological artifacts in the specimen. Figures a-j are close-ups. Accretionary glue artificially extends* (a) *the outer body and* (b) *chamber walls, which are demarcated by green dashes.* (c) *Microboring.* (d) *A green line separates a region of relatively well-conserved tissue (top), which I interpret as in the first stages of decay, from a patch of darker more deteriorated tissue (bottom), which I consider as in the second stages of decay.* (e) *Spongy texture of stage 2 decayed tissue.* (f) *Fractures are indicated by black arrowheads.* (g) *and* (h) *depict bright sulphide contaminants.* (i) *A close-up of the poorly preserved trunk appendages in the second stages of decay. A fracture is indicated by black arrowheads.* (j) *Glue, demarcated by green dashes, has accumulated phosphatic dust and filled a chamber (fc) adjacent to an empty chamber (ec) in which glue has only accreted to the edges (right). Sulphides are indicated by white arrowheads.*

***Abbreviations:*** *ec, empty chamber; fc, filled chamber.*

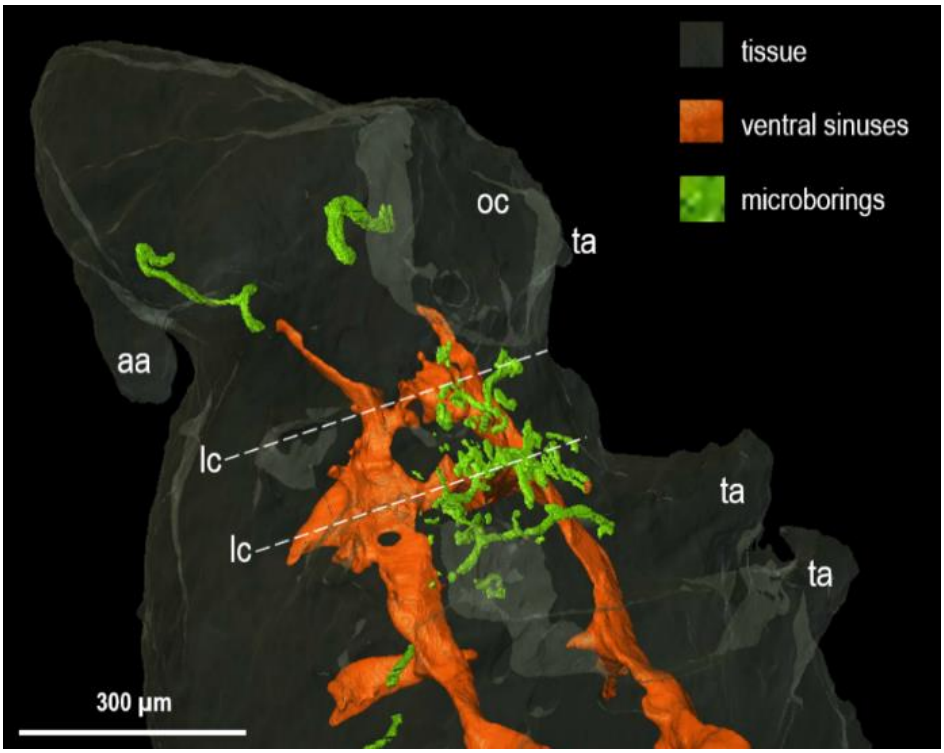


**FIGURE 2.4.** *Avizo surface render depicting a ventrolateral view of the swollen anterior and first trunk appendages. Anterior is up, dorsal is left. A cluster of microborings (green) are shown here to be concentrated in a poorly preserved region located in the ventral aspects of the second and third segments, where they obscure the true connections of the ventral sinuses' (orange) lateral connectives.*

***Abbreviations:*** *aa, anteriormost appendages; lc, lateral connective of the ventral sinuses; oc, oral cavity; ta, trunk appendage.*

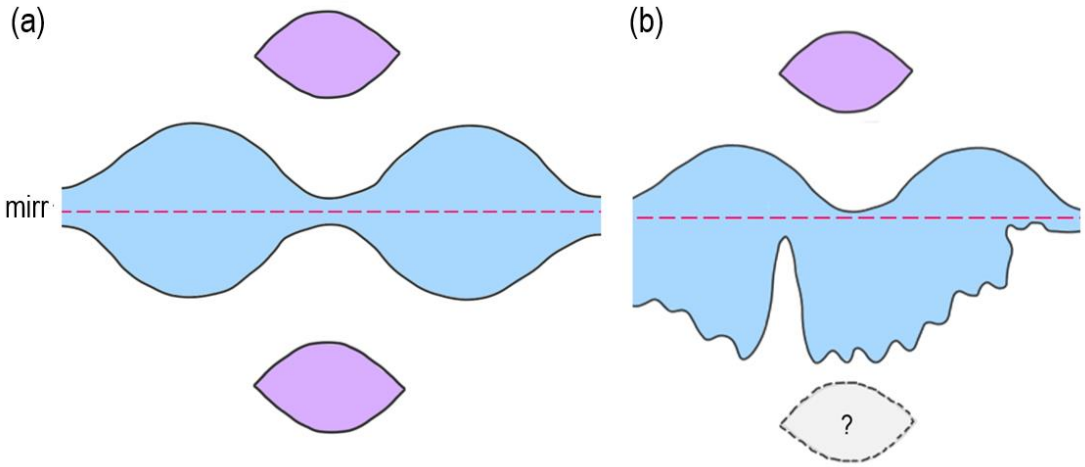


**FIGURE 2.5.** (a) *Bilateral structures are paired on either side of a single mirror plane (mirr), denoted by a dashed line. Biological structures positioned along this plane (shown in blue) are symmetrical. Those positioned elsewhere in the body possess a bilaterally symmetrical counterpart (coloured purple).* (b) *Artificial or taphonomic structures are typically not symmetrical (blue).*

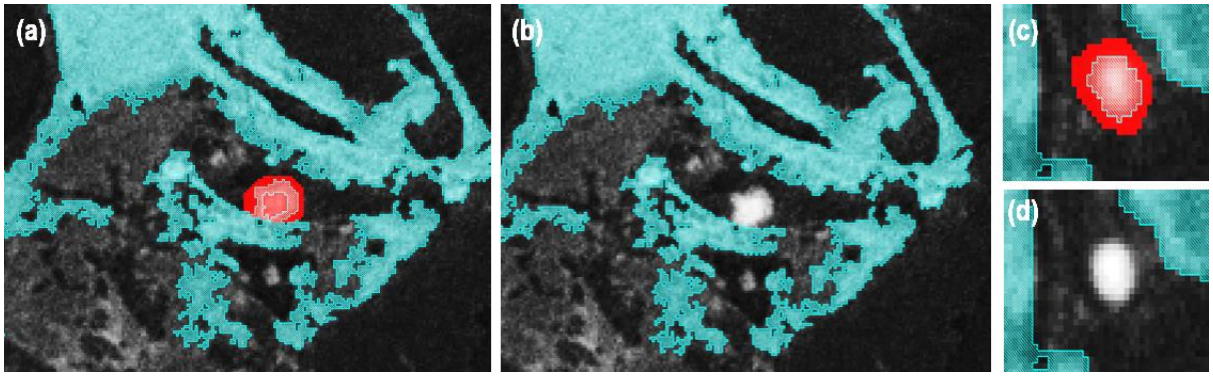


**FIGURE 2.6.** *Manual segmentation of the volume dataset in Avizo using the <brush> tool. Dense contaminant sulphides are visible as bright spots in the sXCT data. Due to similarities in greyscale values, these are easily mislabelled by the <magic wand> as tissue. In* (a) *and* (c), *contaminant sulphides are roughly traced using the <brush> (red) and removed from the tissue material in* (b) *and* (d).

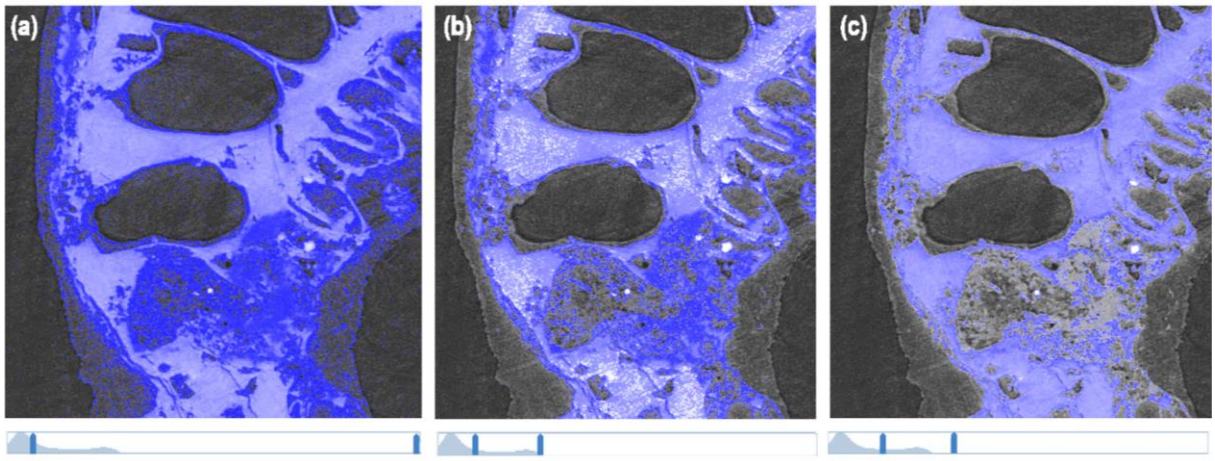


**FIGURE 2.7.** *Semi-manual segmentation of the volume dataset in Avizo using the <magic wand>. Dense contaminant sulphides are visible as bright spots. The relevant greyscale thresholds ($GT_L$ = lower limit, $GT_U$ = upper limit) are displayed below each image.* (a) *$GT_L$ = 12661, $GT_U$ = 65535. A wide greyscale range is picked up by the <magic wand>. Although this picks up all the tissue, it also includes most of the unwanted accretionary glue artifacts*. (b) *$GT_L$ = 14629, $GT_U$ = 23840. A narrow greyscale range which minimises the amount of glue picked up at the expense of excluding patches of real tissue.* (c) *$GT_L$ = 16950, $GT_U$ = 27004. A trade-off between the greyscale ranges of* (a) *and* (b) *to optimise the amount of flesh included and the amount of glue excluded.*

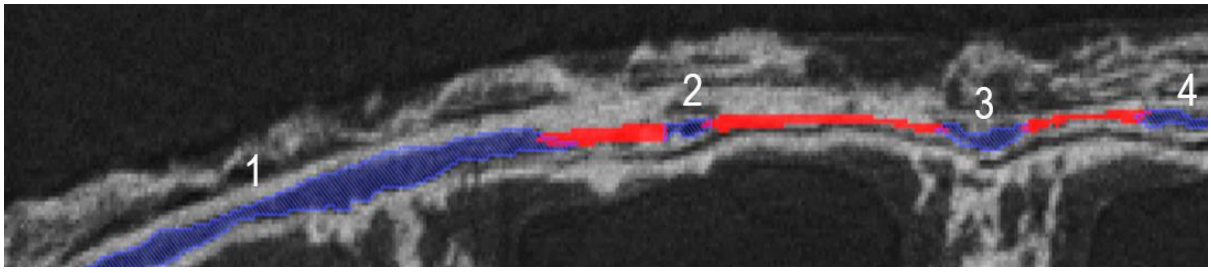

**FIGURE 2.8.** See previous page. *Manual segmentation of the volume data in Avizo using the <brush> (red). A thin chamber (blue) is subdivided into four isolated chambers. The similar position of each isolated chamber relative to the other structures, coupled with their narrow and thus easily compactible natures, leads to the interpretation that these belong to the same chamber. The gaps were manually filled using the <brush>.*

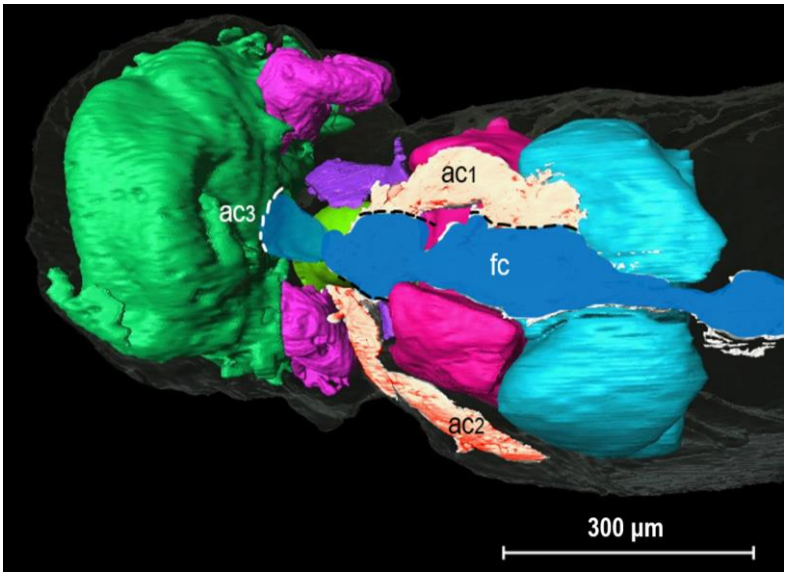


**FIGURE 2.9.** *Avizo surface render. Dorsal view, anterior is left. The focal chamber (fc) runs along the mirror plane of the specimen and merges with three adjacent chambers (ac1-3). ac1, the bilaterally symmetrical counterpart to ac2, merges laterally to the focal chamber in two places, whilst ac1 and ac3 only merge to the focal chamber once. A subjective distinction between the chambers was therefore made to separate the focal cavities from its adjacent cavities.*

***Abbreviations:*** *ac, adjacent chamber; fc, focal chamber.*

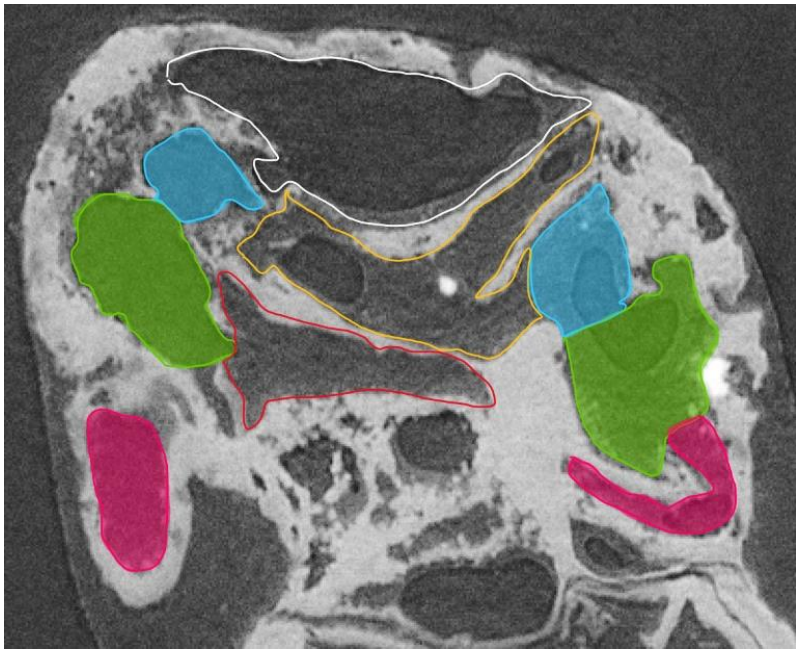

**FIGURE 2.10.** *The roughly symmetrical anterior viewed in Avizo. Symmetrical counterparts are filled in blue, green, and pink respectively.*

*The distorted symmetry is considered a consequence of compaction of easily compactible fluid-filled cavities.*

### 2.3.2.3. DEGREDATION

I interpret regions of tissue with moderate greyscale values (denoting lower density) to have decayed prior to phosphatisation (Figures 2.3 d & i). In parts of the fossil, tissue with a spongy porous texture dissolves the original boundaries of some chambers (Figures 2.4 e, i & 2.11). As when determining the original boundary of a compacted void (see section 2.3.2.2.), a comparison was made to the chamber's symmetrical counterpart, where present, and a subjective decision was made as to where to place the chamber's boundaries (Figure 2.11). This decision was enforced manually using the <brush> tool (Figure 2.11 b). The same methodology also applies to the deformed margins of fractured chambers.

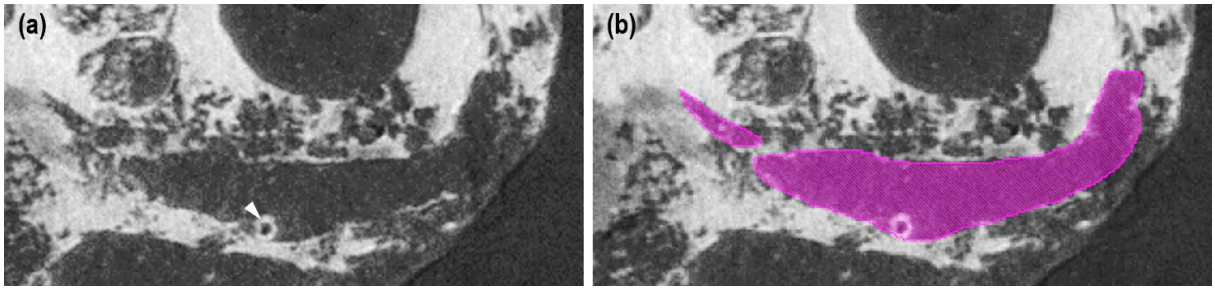


**FIGURE 2.11.** *Orthoslice of the sXCT data.* (a) *The original chamber boundaries have been dissolved by a region of spongy, deteriorated tissue. A sulphide contaminant is indicated by a white arrowhead.* (b) *The biological boundaries of the original chamber and are subjectively enforced using the <brush>.*

Areas of the specimen are damaged; some chamber walls (Figure 2.12) and the distal regions of some appendages (Figure 2.14) are broken. The morphology of broken appendages was inferred from their symmetrical counterparts or, when absent, from the morphology of their proximal regions (Figure 2.14). Damage to the outermost tissue layers of the specimen often results in gaps that link the interior of the fossil to the surrounding exterior / air (Figure 2.12). Gaps in the body wall were thus filled in manually using the <brush> tool to enforce a division between the internal and external void spaces (Figure 2.12 b).

The delicate morphologies of some tissue extensions, coupled with the enforcement of the optimal greyscale threshold values (see Figure 2.7 for more detail), results in gaps in some chamber walls. As with damaged regions (Figure 2.12 b), these gaps are manually segmented using the <brush> tool (Figure 2.13 b).

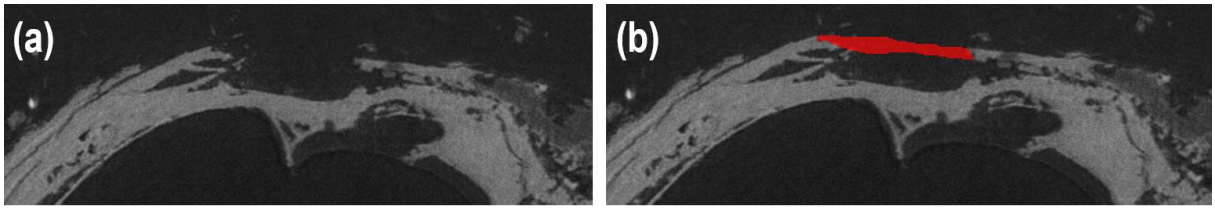


**FIGURE 2.12.** *Orthoslices of the sXCT data in Avizo*. (a) *A delicate outer wall has broken off, thereby connecting the specimen's interior to the exterior.* (b) *The broken wall is reconstructed using the <brush> tool (shown in red).*

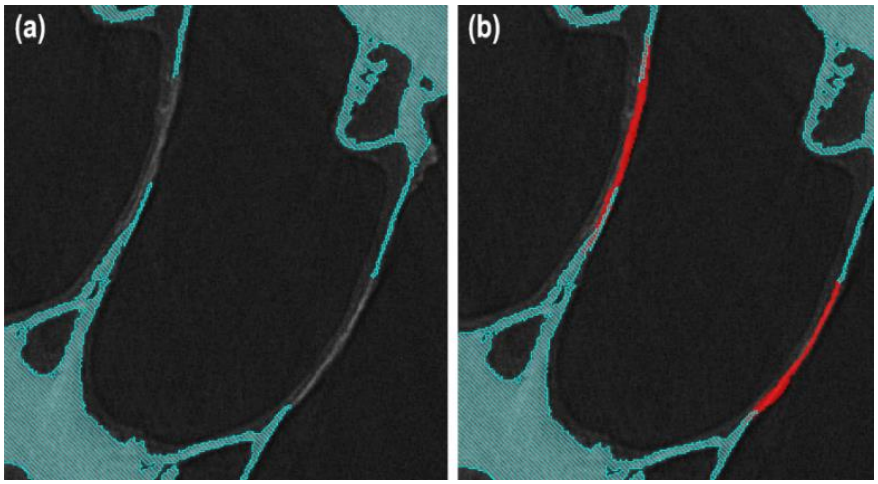


**FIGURE 2.13.** *sXCT dataset viewed in Avizo.* (a) *The delicate chamber walls are not recognised by the optimal greyscale thresholding (recognised tissues shown in blue).* (b) *The unrecognised tissue is subsequently filled using the <brush> tool (red).*

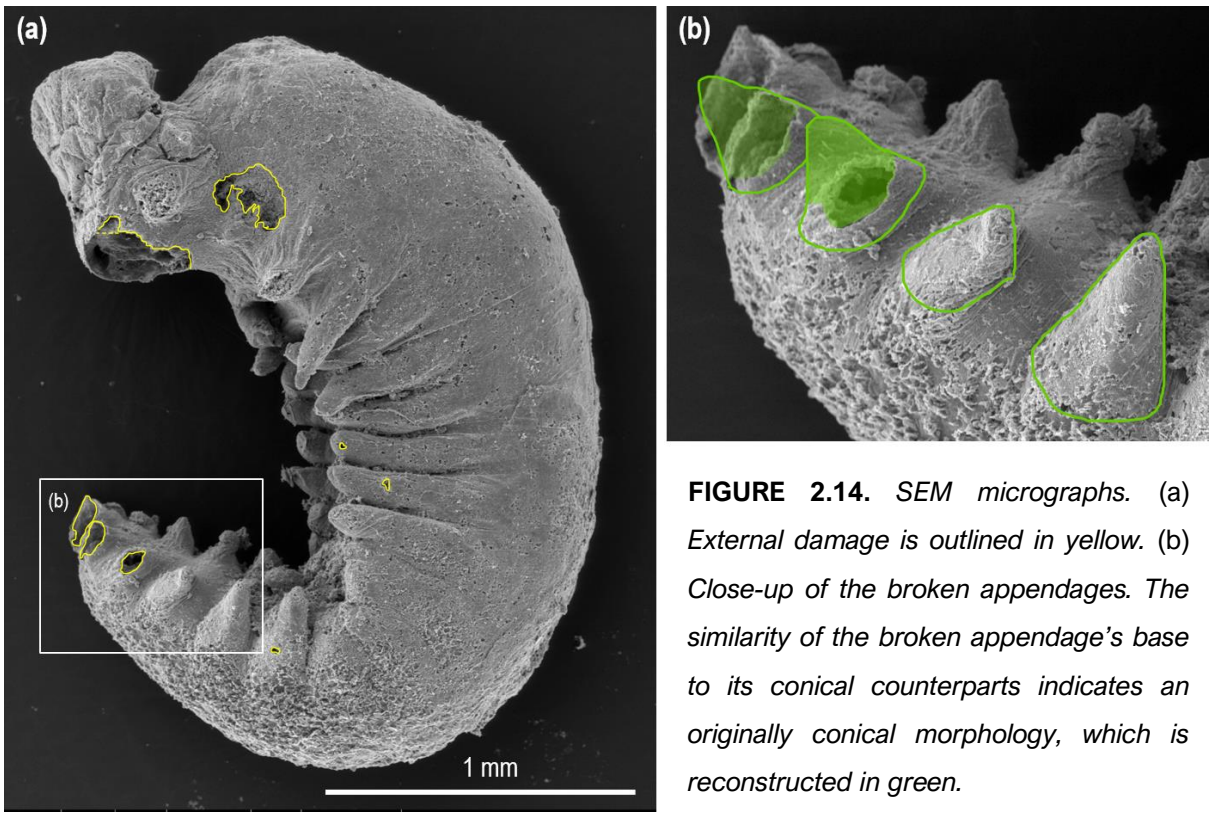


**FIGURE 2.14.** *SEM micrographs.* (a) *External damage is outlined in yellow.* (b) *Close-up of the broken appendages. The similarity of the broken appendage's base to its conical counterparts indicates an originally conical morphology, which is reconstructed in green.*

## 2.4. PHYLOGENETIC ANALYSIS

### 2.4.1. CHARACTER CODING

The new specimen was added to the morphological phylogenetic dataset of Zhang et al. (2016), itself derived from Smith and Ortega-Hernández (2014). Neomorphic characters are either 'present' or 'absent' (*sensu* Sereno 2007). Neomorphic traits that had originally been coded as transformational were therefore recoded accordingly, with inapplicable character states recoded as absent (Brazeau, Guillerme & Smith, 2019; Sereno, 2007 & 2009). The finished matrix contained 50 taxa and 123 unordered characters (see Appendix 2.1 for revised matrix).

Due to numerous similarities to stage IV *Euperipatoides rowelli* (extant onychophoran) embryos, such as the curvature of the body and a posteriad reduction in ventrolateral trunk appendage length, developmental data for extant taxa of an approximately equivalent mid-late developmental stage were selected (pl 1; Walker & Tait, 2004). The following eight characters were added to the dataset:

[116] Nature of the protocerebrum

(0) bipartite
(1) unipartite

A bipartite protocerebrum is identified by the presence of: (1) a morphologically discrete apical asegmental element from which the anteriormost appendages are derived, and (2) a discrete segmental ocular element. The genes *optix* and *orthodenticle (otd)* are expressed in (1) and (2) respectively. In modern euarthropods and onychophorans, these elements are fused to form a genetically subdivided unipartite protocerebrum (see section 5.3; see Ortega-Hernández, Janssen & Budd, 2017, and Strausfeld, 2012). The nature of the protocerebrum is ambiguous in 42 of the 50 taxa, as it requires knowledge of the internal anatomy that is unavailable from most fossil material.

[117] Circumoral nerve ring

(0) present
(1) absent

Circumpharyngeal nerve rings are found in the nematode brain (Schmidt-Rhaesa & Henne, 2017; White et al., 1986) and the anterior nervous systems of extant tardigrades (Mayer et al., 2013a; Smith et al., 2017). As with cerebral nature, the presence of a circumoral nerve

ring is ambiguous in 42 out of 50 taxa, as an insight into the internal anatomy that is unavailable in the majority of fossil material is required to ascertain its presence or absence.

[118] Posteriad reduction in appendage length in mid-late stage embryo

(0) absent
(1) present

Posteriad reduction in appendage length is a developmental trait observed in mid-late stage *Euperipatoides rowelli* (extant onychophoran) embryos (Walker & Tait, 2004). This trait is not observed in the extant tardigrade *Hypsibius dujardini* (see Figure 1 in Gross, Minich & Mayer, 2017). Palaeodevelopmental data is only available from YKLP 12387.

[119] Location of the mouth in mid-late stage embryo

(0) protocerebral segment
(1) elsewhere i.e. deutocerebral segment

The mouth opening migrates during onychophoran ontogeny from a protocerebral to a deutocerebral position. In mid-late stage *E. rowelli* embryos, the mouth opening is located ventrally in the protocerebral segment (Ou, Shu & Mayer, 2012). The terminal position of the mouth in the tardigrade *H. dujardini* (Gross et al., 2017) and the nematode worm *Caenorhabditis elegans* (White et al., 1986) renders the mouths of tardigrades and nematodes protocerebral. Palaeodevelopmental data is only available from the focal fossil of this study.

[120] Annulations in mid-late stage embryo

(0) absent
(1) present

Epidermal annulations first appear in late-stage extant onychophoran embryos. They are absent in mid-late stage *E. rowelli* embryos (Walker & Tait, 2004). As tardigrades and nematodes do not develop annulations, they are also coded as absent in these taxa (Gross et al., 2017; White et al., 1986). Palaeodevelopmental data is only available from YKLP 12387.

[121] Papillae in mid-late stage embryo

(0) absent
(1) present

As with annulations, papillae appear in late-stage extant onychophoran embryos, but are absent in mid-late stage *E. rowelli* embryos (Walker & Tait, 2004). Tardigrades and nematodes do not develop papillae. They are therefore coded as absent in these taxa (Gross et al., 2017; White et al., 1986). Palaeodevelopmental data is only available from YKLP 12387.

[122] Distal specialisation of trunk appendages in mid-late stage embryo

(0) absent
(1) present

The distal differentiation of trunk appendages, such as *Aysheaia*'s multifurcations (Whittington, 1978) and the feet and terminal claws of tardigrades and onychophorans (Gross et al., 2017; Walker & Tait, 2004), present at different developmental stages. As with the other developmental characters, palaeodevelopmental data is only available in the focal fossil of this study – thus the development of *Aysheaia*'s terminally multifurcated appendages is coded as ambiguous. However, modern developmental studies show that the development of feet and claws occurs only in the late stage embryos of extant onychophorans and tardigrades (Gross et al., 2017; Walker & Tait, 2004). Distal specialisation of trunk appendages in the mid-late stage embryos of these taxa is thus coded as absent.

[123] Internal sclerotised jaws in mid-late stage embryo

(0) absent
(1) present

As with the mouth opening, the jaws migrate during onychophoran ontogeny. The jaws are externally visible as lobopodous limbs in mid-late stage *E. rowelli* embryos, migrating internally to form sclerotised jaws in the later stages of embryonic development (Ou et al., 2012; Walker & Tait, 2004). Internal sclerotised jaws are thus coded as absent in extant tardigrades and nematodes (Gross et al., 2017; White et al., 1986). As with the preceding traits, palaeodevelopmental data is only available from YKLP 12387.

### 2.4.2. MAXIMUM PARSIMONY ANALYSIS

Maximum parsimony analysis of the updated matrix was performed in R (R Core Team, 2019) using Ape (Paradis & Schliep, 2018) and TreeSearch, a new R package capable of analysing inapplicable data (Brazeau et al., 2019). A neighbour-joining tree was used as a starting point for analysis. To accelerate the tree search and avoid combinations that would

mix ingroup and outgroup taxa, an outgroup was constrained by enforcing monophyletic relationships for both the outgroup and ingroup taxa. The outgroup contained data from the priapulid worm *Tubiluchus* and protocerebral data from the nematode *Caenorhabditis elegans*. The hybridisation of the outgroup was required due to the absence of gene expression data in Priapulida; although the presence of the *otd* homolog *otx* is observed in the anterior of *Priapulis caudatus*, the extent of its expression is unknown (Martín-Durán & Hejnol, 2015). More refined gene expression studies on the nematode worm *C. elegans* were therefore used in the construction of the outgroup (Lanjuin et al., 2003; Satterlee et al., 2001).

To achieve a better starting point for subsequent ratchet parsimony analysis, the surrounding tree space was searched using Nearest Neighbour Interchanges with the parameters set to default. This step was repeated to further improve the tree.

To escape local optima, a more extensive search for new trees was conducted using Nixon's (1999) parsimony ratchet. The number of ratchet iterations was set to 100, whilst the number of search iterations and search hits were set to 6000 and 65 respectively. Parsimony analysis employed implied weights using 12 variants of Goloboff's (1993) concavity constant between 0.25 and 64 (See Appendix 2.3 for code).

# CHAPTER 3

# DESCRIPTION

- PLEASE REFER TO THE PLATES (PL) LOCATED AT THE END OF THIS THESIS –

---

## 3.1. OVERVIEW OF MORPHOLOGY

YKLP 12387 is a segmented onychophoran-like animal that is approximately 5.7 mm long and 1 mm wide. A prominent constriction distinguishes an anterior unit from an appendage-bearing trunk (Figures 3.1 & 3.2; pl 1, 2 a & 3 a). Internally, the trunk is dominated by an axial cavity, which is subdivided by partial septa into 20 segments (pl 2 a & c). The axial cavity projects into each appendage and surrounds a straight gut (Figures 3.1-3.3 & 3.5; pl 2 a & c). Minor chambers run dorsally above and within the axial cavity, and subordinate longitudinal sinuses occur both dorsally and ventrally to it (Figures 3.1 & 3.3; pl 2). These voids are surrounded by a circumferential chamber (Figures 3.1-3.4).

An additional circumferential cavity occurs dorsally to all other chambers, expanding posteriorly to encompass the specimen's posterior apex (Figures 3.2 & 3.3; Appendix

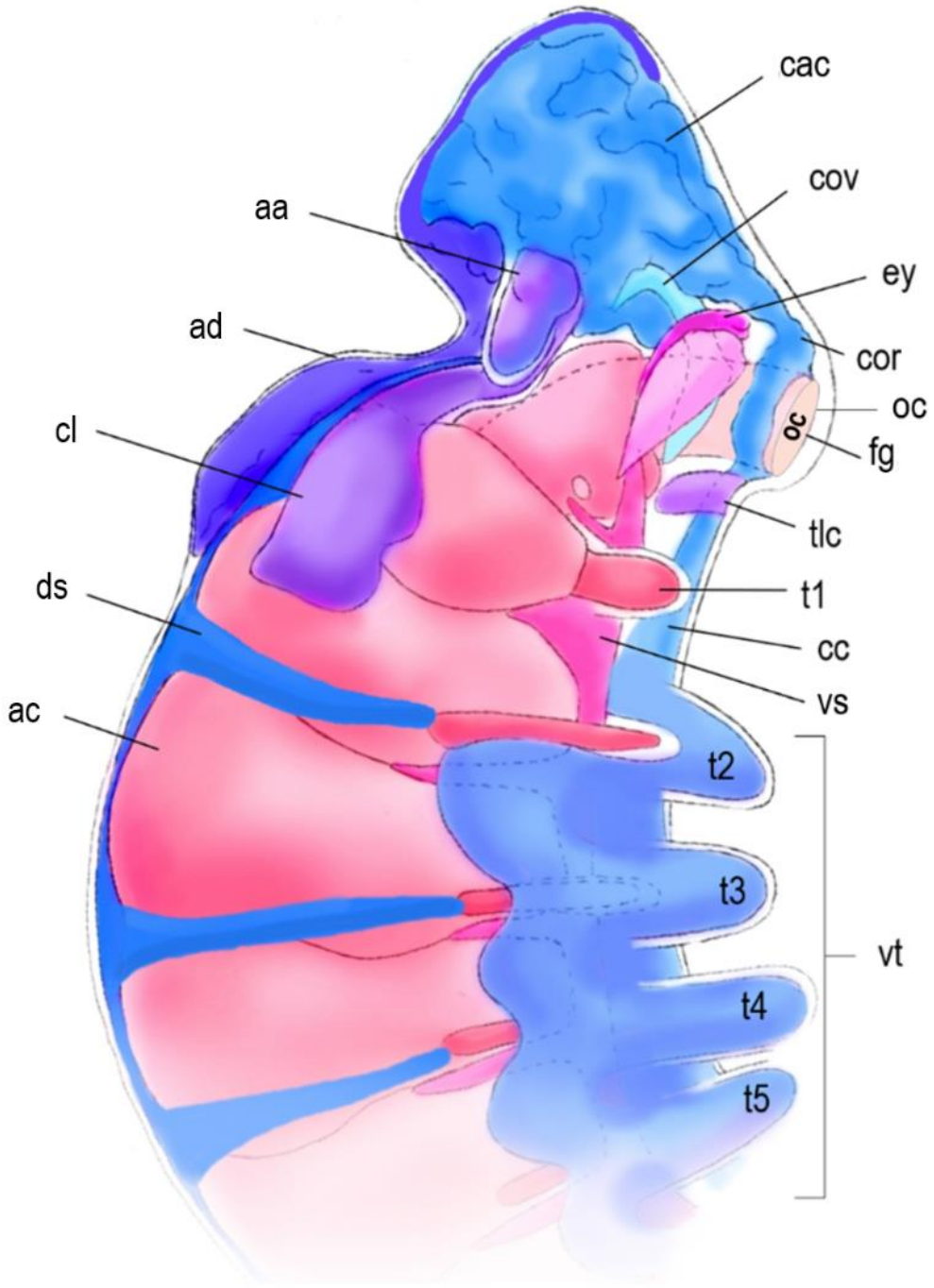


**FIGURE 3.1.** *Illustration of YKLP 12387's anterior internal anatomy. Segmental systems, such as the dorso- (ds) and ventrolateral sinuses (vs), the axial cavity (ac), and the intestinal system (ph) do not extend beyond a prominent constriction that separates the segmental trunk from the additional anterior module. This apical element is predominated by a core anterior cavity (cac), which extends laterally (cl), dorsally, and ventrally (cov & cor).*

***Abbreviations:*** *aa, anteriormost appendages; ac, axial cavity; ad, anterior dorsal cavity; cac, core anterior chamber; cl, cac lateral extension; cor, circumoral ring; cov, cac circumoral ventral extension; ds, dorsolateral sinuses; ey, eye; fg, foregut; oc, oral cavity; ocp, oblate cylindrical projection of flesh; t, trunk appendage; tlc, trilobed chamber; vs, ventrolateral sinuses; vt, ventrolateral trunk appendages*

3.1). The additional anterior region comprises a folded chamber positioned anteriorly to the axial cavity and dorsally to a ventral mouth (pl 2 & 3). It exhibits a nascent pair of dorsolateral appendages that are morphologically distinct from the ventrolateral trunk appendages (Figure 3.1; pl 1-3).

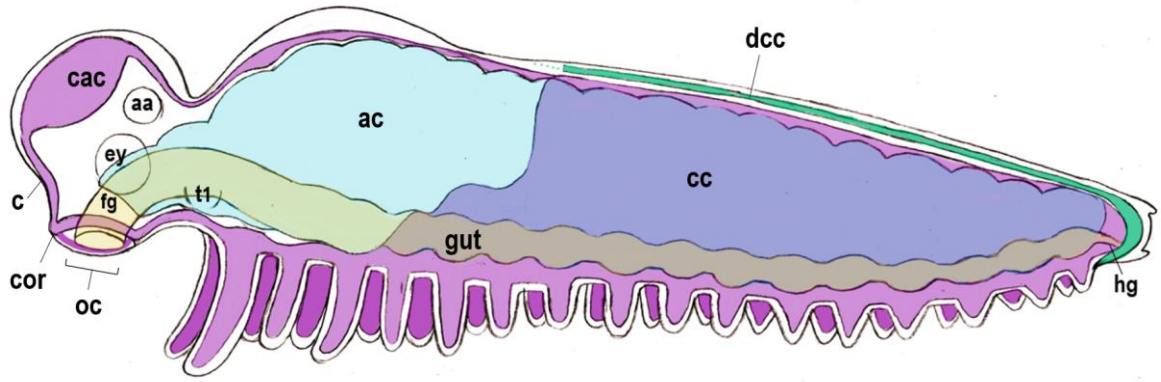


**FIGURE 3.2.** *The specimen's principal body cavities - the intestinal system (yellow), the circumferential chamber (cc; purple), and the axial cavity (ac; pale blue). A cylindrical foregut (fg) opens anteroventrally, leading into a straight ventral gut that terminates in a blind posteroventral hindgut (hg). The circumferential chamber encloses the specimen's posterior, diminishing anteriorly until it encases only the appendages. It is not associated with the first trunk appendage (t1). The circumferential chamber encircles the foregut to form a circumoral ring (cor) before joining the core anterior cavity (cac) that dominates the additional anterior. A dorsal chamber (dcc; green) encases the posterior apex.*

***Abbreviations:*** *aa, anteriormost appendages; ac, axial cavity; c, connecting cord; cac, core anterior cavity; cc, circumferential chamber; cor, circumoral ring; dcc, dorsal circumferential chamber; fg, foregut; hg, hindgut; oc, oral cavity; t1, trunk appendage 1.*

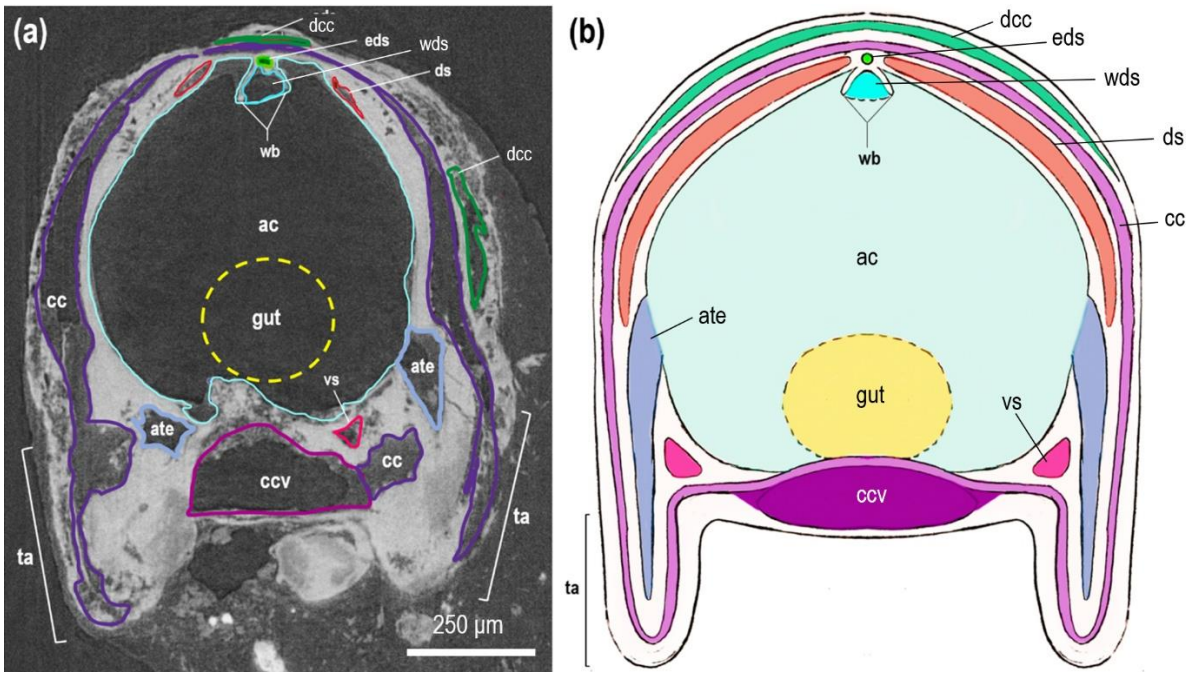

**FIGURE 3.3.** *See previous page. Transverse orthoslice through the midpoint of a typical trunk segment.* (a) *sXCT data and* (b) *illustration. The trunk is dominated by the axial cavity (ac), which projects into the trunk appendages (ta) via ventrolateral extensions (ate). The axial cavity surrounds a straight gut, the presumptive extent of which is indicated by a dashed line. Bifid projections of tissue, which resemble wishbones in transverse cross section (wb), descend from the dorsal surface of the axial cavity. A dorsal vessel (wds) is situated between these bifid tissues. A further sinus (eds) runs along the trunk dorsal to this vessel. The circumferential chamber (cc), which is thinner laterally and dorsally, and thicker ventrally (ccv), encompasses these chambers. A further circumferential chamber (dcc) is positioned dorsally to all other chambers. Additional outer chambers are interpreted as tissue delamination. The serially repeated ventro- (vs) and dorsolateral sinuses (ds) are indicated in pink and orange-red respectively.*

***Abbreviations:*** *ac, axial cavity; ate, axial cavity trunk appendage extension; cc, circumferential chamber; ccv, circumferential chamber ventral component; dcc, dorsal circumferential chamber; ds, dorsolateral sinuses; eds, extra axial cavity dorsal sinus; ta, trunk appendage; vs, ventrolateral sinuses; wb, wishbone-like tissue projections; wds, dorsal sinus between wishbone-like tissue projections.*

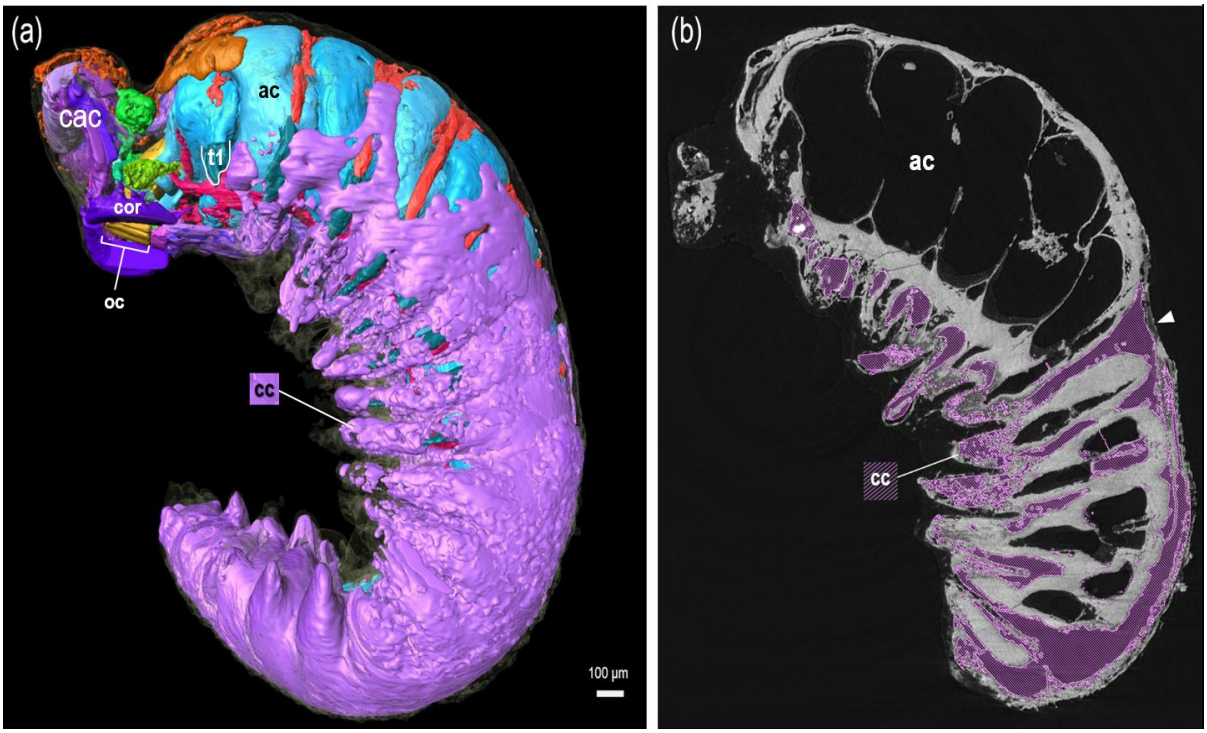


**FIGURE 3.4.** *The extent of the circumferential cavity (cc), shown in purple. Anterior is top left, dorsal is right.* (a) *3D render and* (b) *lateral orthoslice of the sXCT data.* (a) *The circumferential chamber encircles the foregut (yellow) to form a circumoral ring (cor) before joining up with the core anterior cavity (cac). It is not associated with the first trunk appendage (t1).* (b) *The circumferential chamber increases in extent to encase the entire trunk posterior to a swollen septum, indicated by a white arrowhead, situated between the 7$^{th}$ and 8$^{th}$ segments.*

***Abbreviations:*** *ac, axial cavity; cac, core anterior cavity; cc, circumferential chamber; cor, circumoral ring; oc, oral cavity; t1, trunk appendage 1.*

## 3.2. PRINCIPAL BODY CAVITIES

### 3.2.1. THE AXIAL CAVITY

The dorsal section of each axial cavity segment is out of phase with the ventral section (pl 2 a). Sinuses, each 60 µm wide, descend ventrolaterally into the trunk appendages. These sinuses emerge 70% of the way down from the top of the axial cavity and taper to a slender point (Figure 3.1; pl 2 a & c).

A delicate bifid structure, which resembles a wishbone in transverse cross-section, is 100 µm wide and 115 µm tall at the segmental midpoint, and gradually narrows to 40 µm wide and 90 µm tall above each septum (Figure 3.3). This bifid structure extends from the dorsal surface of the axial cavity and runs lengthwise along the body.

In the first segment, the dorsal bifid structure is absent. In the first and 16$^{th}$ to 20$^{th}$ segments, the axial cavity is small and divided by a sagittal wall, forming narrow voids (Figure 3.5; pl 3 a & c). A pair of oblate cylindrical projections of flesh, measuring approximately 20 µm wide and 60 µm tall, puncture the narrow axial cavity at the posterior border of the first segment (Figure 3.1; Appendix 3.2).

The septum between the seventh and eighth segments is 55 µm thick, compared to a typical width of approximately 5 µm.

### 3.2.2. THE INTESTINAL SYSTEM

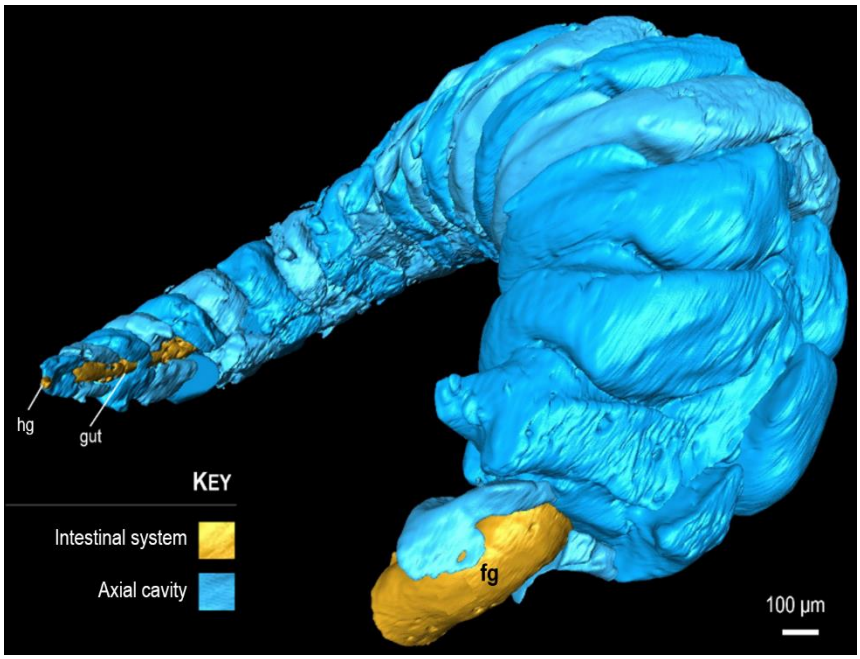


**FIGURE 3.5.** *Avizo 3D render. Anterior is right. The intestinal system (yellow) is surrounded by the axial cavity (blue). Ventral view of posterior, dorsolateral view of anterior. The first axial cavity segment is split into halves that flank the foregut (fg). The 16th-20th axial cavity segments are also split, flanking the gut*

***Abbreviations:*** *fg, foregut; hg, hindhut.*

The intestinal system opens anteriorly into a ventral oral cavity (Figures 3.1, 3.2 & 3.5; pl 2 & 3). A tubular foregut measuring 135 µm in diameter leads into a straight ventral midgut (Figure 3.2). The width of the midgut increases from approximately 55 µm at each septum to a maximum width of 90 µm between septa (Figure 3.3). The intestinal system ends in a blind posteroventral hindgut with a maximum diameter of 25 µm (Figures 3.1 & 3.5; pl 2 a & c).

#### 3.2.3. THE PRINCIPAL CIRCUMFERENTIAL CHAMBER

A circumferential chamber underlies the outer surface (Figures 3.2-3.4). The circumferential chamber's ventral component, which is approximately 55 µm tall, dilates to 85 µm tall at the segmental midpoint (Figures 3.2-3.4). The ventral component is thicker than its lateral and dorsal counterparts, which are each approximately 20 µm thick (Figures 3.1-3.3).

In segments 8-20, the lateral and dorsal extent of the circumferential chamber increases to encase the entire trunk (Figures 3.2 & 3.4). It envelops all but the first highly stunted and uniquely lateral appendage pair (Figures 3.1-3.4; pl 3 a).

## 3.3. LONGITUDINAL SINUS SYSTEMS

### 3.3.1. DORSAL SINUSES

Two sinuses follow the dorsal surface of the axial cavity. The first, with an approximate diameter of 15 µm, occurs above the axial cavity (*eds* in Figure 3.3; see section 3.2.1. for more on the axial cavity). The second is positioned between the flanges of the bifid structure that occupies the dorsal surface of the axial cavity (Figure 3.2). The ventral boundary of this intra-axial-cavity sinus is undefined, as the sinus merges with the axial cavity (Figure 3.2). Both the bifid structure and the associated dorsal chamber are absent in the first segment.

### 3.3.2. DORSOLATERAL SINUSES

Paired dorsolateral sinuses, measuring approximately 10 µm in height, occur in the trunk just below the dorsal boundary of the axial cavity. Their width increases at the lateral margin of each segment boundary, forming regular triangular outgrowths (Figure 3.1; pl 2 a). Dorsolateral processes measuring 60 µm wide extend from the dilations to approximately 70% of the way down each segment from the top of the axial cavity (Figure 3.1; pl 2).

### 3.3.3. VENTROLATERAL SINUSES

The longitudinal ventrolateral sinuses, which measure approximately 20 µm wide and 60 µm tall, occur in the ventrolateral area of the trunk, alongside the axial cavity. They dilate at each segmental midpoint to a width of 50 µm and a height of 95 µm (Figure 3.1; pl 2 a & c).

The ventrolateral sinuses give rise to subsidiary dorsal and ventral processes. Dorsal processes are typically bilobed (Figure 3.6 a). Bilobed processes project to a height that is roughly 30% that of the axial cavity (Figure 3.6 a). The posteriormost lobes are partially obscured by the overlying anterior lobes and are located at the posterior border of each segment (Figures 3.1, 3.6 a & 3.7 a). Anterior lobes are larger than their posterior counterparts, measuring 50 and 20 µm wide respectively (Figure 3.6 a).

The morphology of the dorsal processes changes along the anterior-posterior (AP) axis from the bilobed 'rods' of the first nine segments (Figure 3.6 a) to the unilobed processes of the posteriormost segments (Figure 3.6 b-c). These conical unilobed processes measure approximately 30 µm wide in segments 10 and 11, where they project to approximately 5% the height of the axial cavity (Figure 3.6 b).

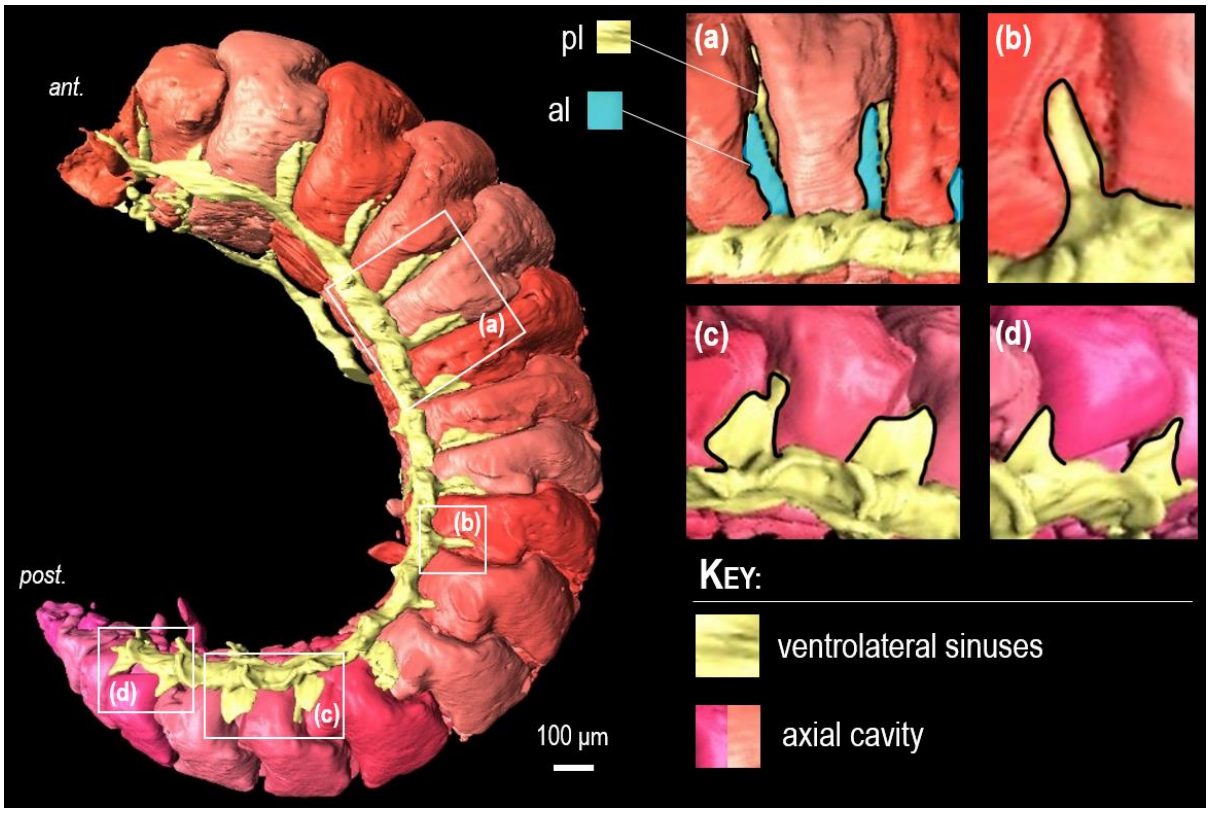


**FIGURE 3.6.** *Avizo 3D render of the ventrolateral sinuses' dorsal processes. Close-ups of the* (a) *bilobed and* (b-c) *unilobed processes.* (a) *The anterior lobes (al) are shorter than the posterior lobes (pl).* (b) *The rod-like unilobed morphology in segment 10 gives way to a* (c) *wide triangular morphology, as shown in segments 13 and 14. (d) The width of this triangular base decreases in segments 15 and 16.*

***Abbreviations:*** *ac, axial cavity; al, anterior process; ant, anterior; pl, posterior lobe; post, posterior.*

In segments 12-14, these transition into wider triangular processes, each 70 µm wide, that project to around 30% the height of the axial cavity (Figure 3.6 c). In segments 15 and 16, the base of these triangular processes decreases to just 55 µm wide and to a height that is only 20% that of the axial cavity (Figure 3.6 d).

Due to posterior compression, the ventrolateral sinuses are not preserved in segments 17-20, but are believed to extend along the ventrum from the first to the 20th segment.

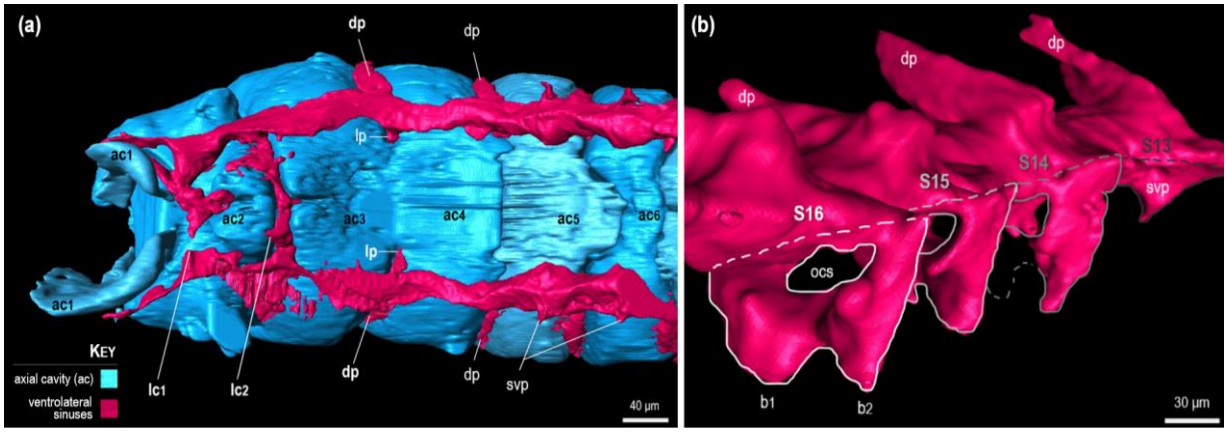


**FIGURE 3.7.** *3D renders generated in Avizo documenting the morphology of the ventrolateral sinuses, shown in pink*. (a) *Close up of the anterior showcasing a ventral view of the lateral connections (lc) of the ventrolateral sinuses. Anterior is left. The ventral processes (svp) can be found from the fifth segment (ac5) onwards.* (b) *Close-up of the posterior detailing the changing morphologies of the ventrolateral processes along the anterior-posterior axis. The ventral processes change from the typically small triangular projections (svp) of the anterior, as shown in segment 13, to the large bifurcating diverticulae of segments 14-16. An oblate cylindrical tissue structure (ocs) punctures the bifurcating ventral processes.*

***Abbreviations**: ac, axial cavity; b, bifurcation; dp, dorsal process; lc, lateral connective; ocs, oblate cylindrical structure; s, segment; svp, small ventral process.*

A small pair of triangular processes, typically measuring 40 µm wide at their base, project ventrally to an approximate distance of 40 µm from the main sinus (Figure 3.7). In the first four segments, the ventrolateral sinuses lack these paired ventral processes (Figure 3.7 a). Here, the ventrolateral sinuses are linked by poorly preserved lateral connectives at the posterior margins of the first and second segments. Lateral triangular processes project inwardly at the posterior margin of segment three. No such lateral processes are observed in segment four (Figure 3.7 a).

The size, shape, and position of the ventral processes changes along the anterior-posterior (AP) axis; the ventral processes gradually shift towards the posterior border, forming

bifurcating triangular diverticulae that project from the exterior-facing side of each sinus in segments 14-16 (Figure 3.7 b). The ventral processes also transition along the AP axis from small triangular projections to relatively large 100 μm wide and 50 μm high bifurcating diverticulae in segments 14-16 (Figure 3.7 b). Bifurcations are rounded structures measuring approximately 15 μm wide. An oblate cylindrical tissue structure measuring approximately 50 μm wide and 35 μm high punctures the midpoint of each of the bifurcating ventral processes (Figure 3.7 b).

## 3.4. TRUNK APPENDAGES

The first eight ventrolateral appendages are rounded, whereas trunk appendages 13-17 are short and conical. The shapes of trunk appendages 10–12 are not preserved (pl 1). The innermost trunk appendage chamber is the slender rod-like projection of the axial cavity. This is separated from an envelope of circumferential chamber by a layer of tissue. Excluding the first two ventrolateral trunk appendages (corresponding to segments 3 & 4), the ventrolateral appendages are also associated with small triangular ventrally descending processes of the ventrolateral sinuses (Figures 3.7 & 3.8 i).

The first pair of trunk appendages are distinct from the subsequent appendages on account of their lateral location, short length, and unique internal composition; they are not encased by the circumferential chamber (Figures 3.1 & 3.8; pl 3 a); neither are they associated with ventral projections of the ventrolateral sinuses (Figures 3.7 a & 3.8 ii).

## 3.5. THE ANTERIORMOST SEGMENTS

The anteriormost region of the specimen, corresponding to segments 1-3, deviates from the typical template described (pl 2 & 3).

Segment one hosts three ventral openings, including those allied with the outer circumferential chamber and the intestinal system. An additional post-oral opening corresponds to a small chamber with three round blind-ended lobes (Figure 3.9; pl 1, pl 2 a & c, & pl 3 a & c; Appendix 3.3).

Bulbous lateral outgrowths are positioned at the segment's anterior border (Figures 3.1, 3.2 & 3.10; pl 1-3). These structures are allied with the dilated end of internal teardrop-shaped chambers, composed of thicker outer and narrower inner structures, measuring approximately 30 and 20 μm at their dilated ends respectively (Figure 3.10; pl 2 & 3). Their

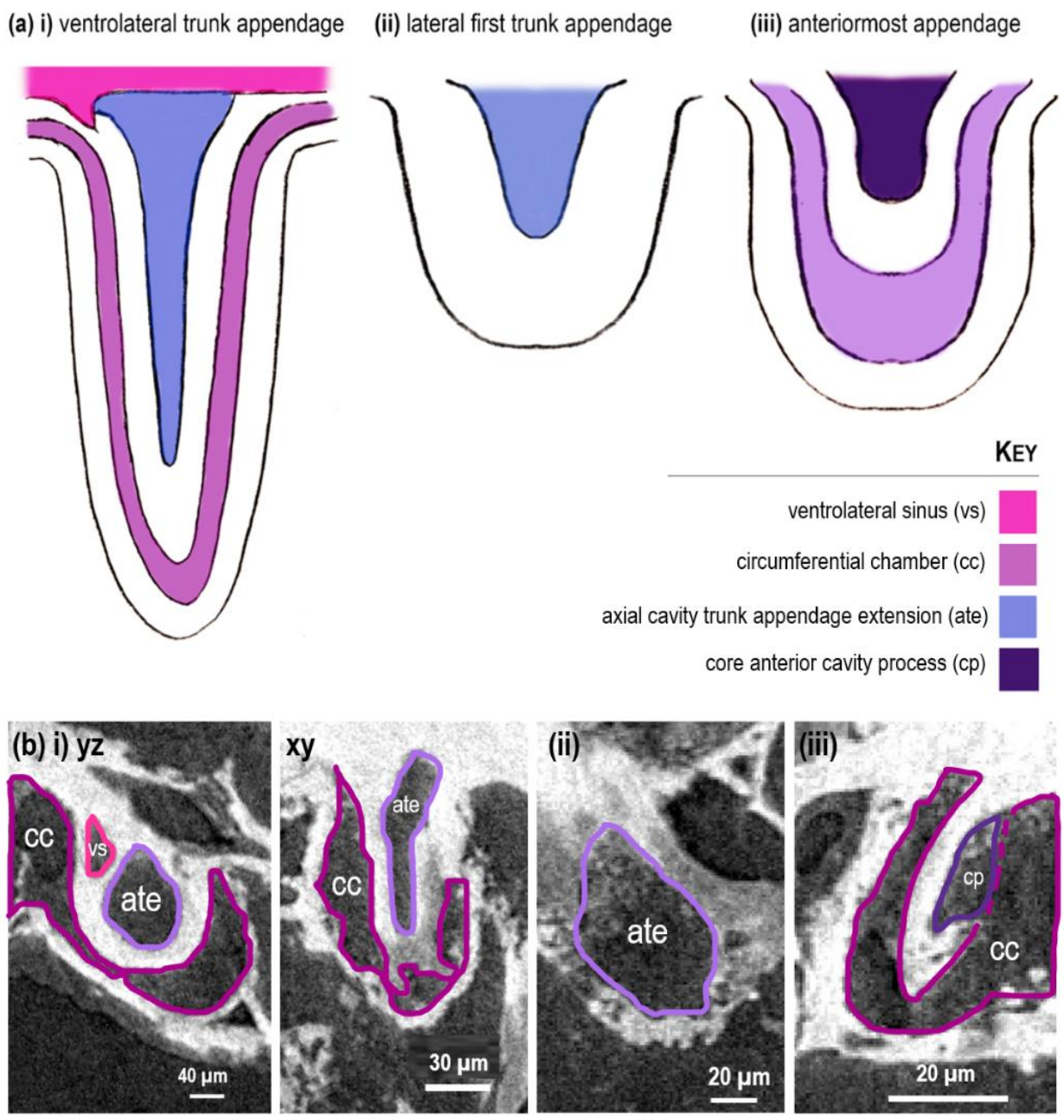


**FIGURE 3.8.** *Internal anatomy of* (i) *a typical ventrolateral trunk appendage,* (ii) *the uniquely lateral and stunted first trunk appendage, and* (iii) *the nascent anteriormost appendages. Illustrations are depicted in* (a). *sXCT orthoslices are shown in* (b). (i) *A typical trunk appendage is shown in both yx and xy orientations, whilst* (ii) *the first trunk appendage and the* (iii) *anteriormost appendages are shown in the yz orientation.* (i-ii) T*he trunk appendages are defined by their association with the axial cavity, which forms the innermost chamber.* (ii) *Unlike a typical appendage* (i), *the first limb pair is not associated with the circumferential chamber of the ventral projections of the ventrolateral sinuses.* (iii) *Like the ventrolateral trunk appendages* (i), *the anterior module's appendages are also composed of inner and outer chamber layers; a process of the core anterior cavity that dominates is encased by the circumferential chamber.*

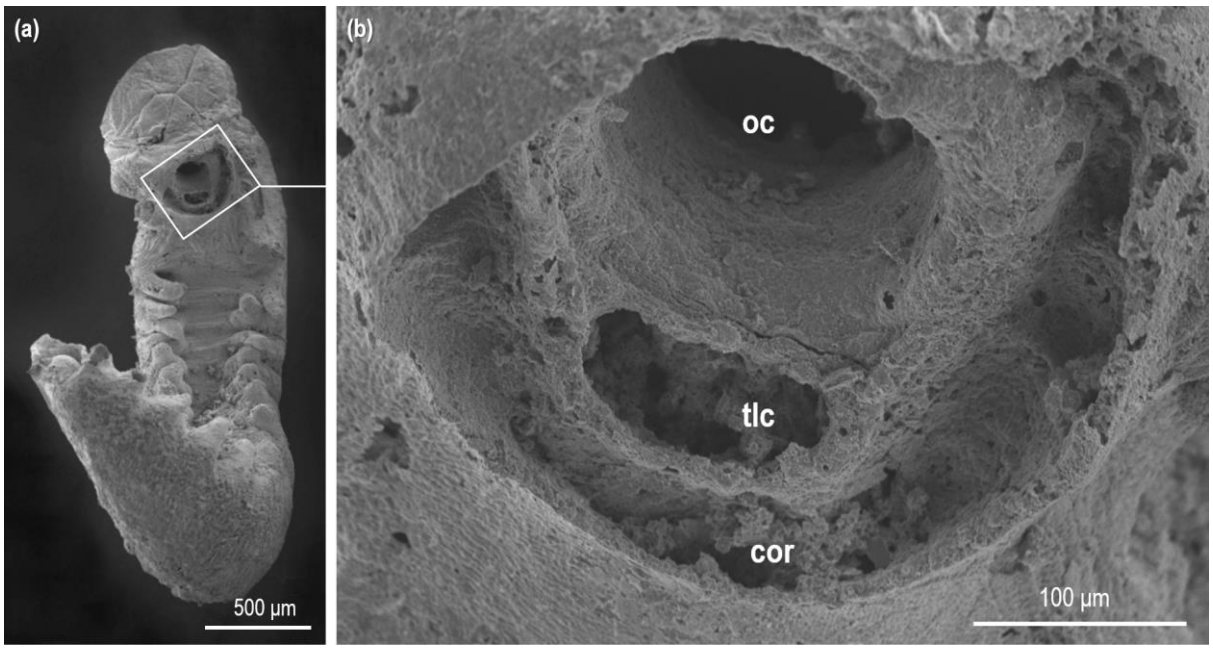


**FIGURE 3.9.** *SEM micrographs of the specimen detailing the ventral openings. Ventral view, anterior is up.* (a) *Full body*. (b) *Close-up of the circular oral cavity (oc), the oval cavity associated with the trilobed chamber (tlc), and the circumoral depression (cor) that encircles both.*

***Abbreviations:*** *cor, circumoral ring; oc, oral cavity; tlc, trilobed chamber.*

position at the anterior border of the first segment places them at the base of a nascent pair of dorsolateral appendages associated with the additional anterior region (Figures 3.1 & 3.2; pl 2 & 3). Due to their morphology and their position anterior to the base of the anteriormost trunk appendages, I will refer to these para-oral bumps as eyes.

## 3.6. THE ANTERIOR UNIT

The anterior unit is an additional body region that is situated anteriorly to the segmental organ systems described in the previous sections (Figure 3.1; pl 2 & 3). It contains two chambers, neither of which is segmented: (1) the dorsal sac, and (2) the 'core' anterior cavity, from which the anteriormost appendages are derived (Figure 3.8). These voids are separated by a thin ventral / dorsal partition and are bent by a single fold, the hinge axis of which is positioned in the specimen's apex (pl 2 a & 3 a).

The dorsal sac encompasses the specimen's apex and occurs in the first three segments in a region positioned dorsally to the sheath-like circumferential chamber (Figure 3.1; pl 2 b, 3 a & b).

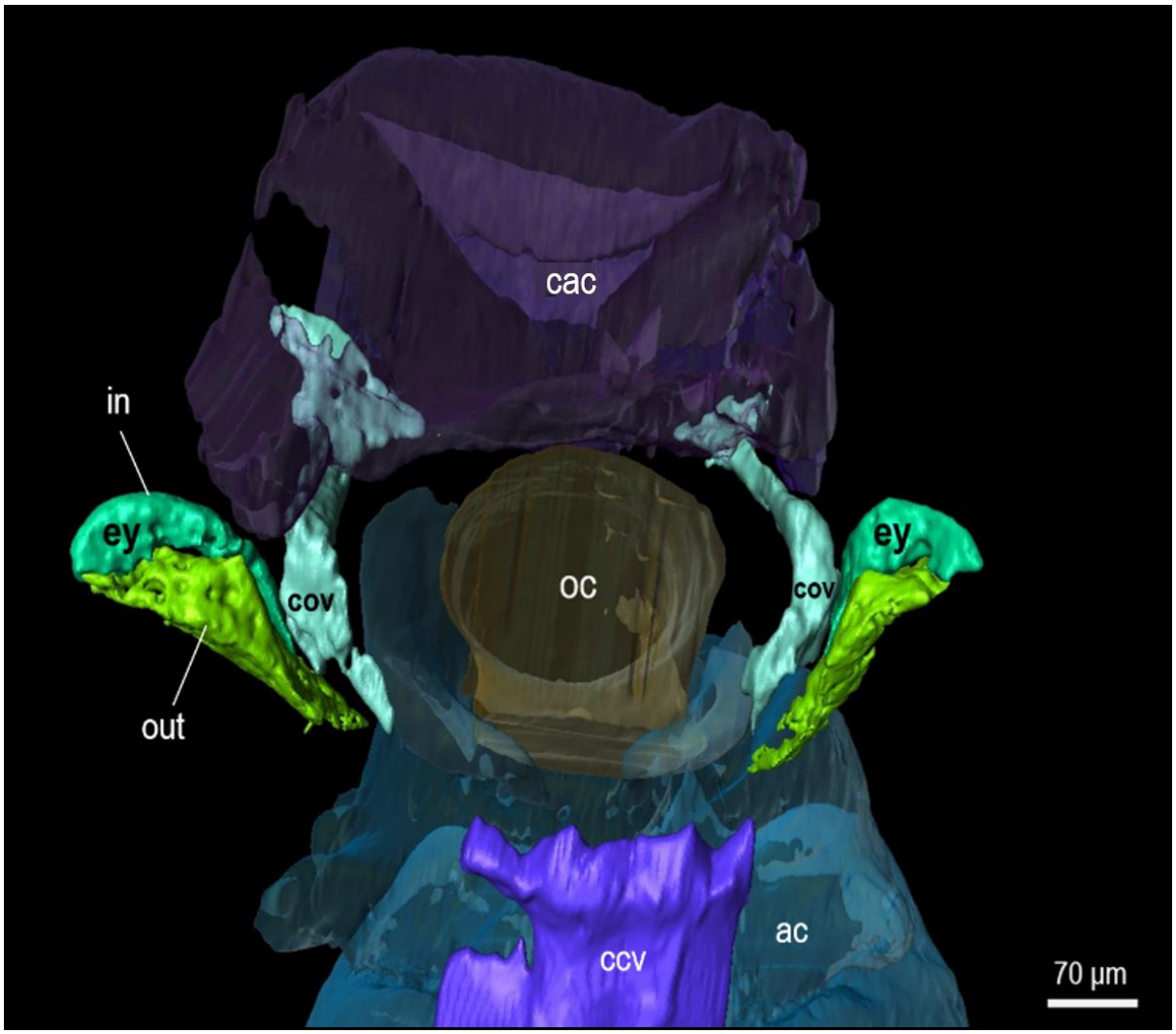


**FIGURE 3.10.** *3D render of the eyes generated in Avizo. Ventral view, anterior is up. Circumoral ventrolateral processes (cov) descend from the core anterior cavity (cac). These ventrolateral processes make glancing connections to the paraoral ocular structures (ey). The ocular structures are composed of teardrop-shaped inner (in) and outer (out) voids.*

***Abbreviations:*** *ac, axial cavity; cac, core anterior cavity; ey, eye; in, inner ocular structure; oc, oral cavity; out, outer ocular structure.*

### 3.6.1. THE CORE ANTERIOR CAVITY

The core anterior cavity dominates the additional anterior module (Figure 3.1; pl 2 & 3). It extends laterally, dorsally, and ventrally from a central void positioned at the fold axis in the specimen's apex (pl 3 a). Narrow lateral chambers, which do not occur beyond the third segment, originate from the central void's dorsal edge (Figure 3.1; pl 2, 3 a & c).

A ventral component of the central void runs along the specimen's plane of bilateral symmetry before connecting to a circumoral depression positioned in the first segment. This depression connects to the thickened ventral component of the sheath-like circumferential chamber (Figures 3.1, 3.2, 3.4, & 3.9; pl 2 a, 3 a & c).

A pair of ventrally descending circumoral processes project from the core aspect of the central void (Figure 3.10; pl 2 c & 3 c). The processes measure approximately 120 µm wide and 100 µm tall at their base, narrowing to just 20 µm wide and 40 µm tall upon their ventrolateral descent before dilating in their terminal ventral position to a width and height of 60 and 140 µm respectively. The ventral dilations of these processes make glancing connections to the ocular structures (Figure 3.10; pl 2 c, 3 a & 3 c; see section 3.5 for more on the ocular structures).

A dorsal extension of the core anterior cavity's central void extends into the trunk region. Although the dorsal extension is poorly preserved in this region, due to its morphology and location it is believed to merge with the circumferential chamber, connecting this sheath-like void to the core anterior chamber that predominates the anterior unit (Figures 3.1, 3.2 & 3.4; pl 2 b).

### 3.6.2. THE ANTERIORMOST APPENDAGES

The nascent appendages originate laterally from the additional anterior module (Figure 3.1; pl 1-3). The appendages are linked by a tubular, lateral connective measuring approximately 15 µm wide and 290 µm long (pl 3 c).

The appendages' inner component is derived from the central aspect of the core anteior cavity's central void, whilst the outer component originates from the central void's dorsal component, which merges posteriorly with the circumferential chamber (see section 3.2.3 for more on the circumferential chamber). The anteriormost appendages are thus composed of an internal core separated from an outer, sheath-like layer of the circumferential chamber via a layer of tissue (Figure 3.8 iii).

# CHAPTER 4

# INTERPRETATION

- PLEASE REFER TO THE PLATES (PL) LOCATED AT THE END OF THIS THESIS –

---

YKLP 12387 is a Cambrian stage 3 lobopodian. On account of numerous morphological similarities, the anatomy of extant onychophorans are used to interpret the specimen.

## 4.1. THE CENTRAL NERVOUS SYSTEM

The core anterior cavity, the circumoral ring, and the ventral and ventrolateral aspects of the principal circumferential chamber correspond in position to the nervous systems of extant panarthropods (Yang et al., 2016). That these structures are preserved as voids likely reflects the rapid decay of nervous tissue (Murdock et al., 2014).

The anterior unit is clearly distinct from the succeeding body region as it is not associated with any of the segmental organ systems; the intestinal system, the axial cavity, and the longitudinal dorso- and ventrolateral sinuses do not proceed beyond the ocular segment (pl 2 & 3). I therefore interpret this unit as asegmental. Due to the core anterior cavity's location

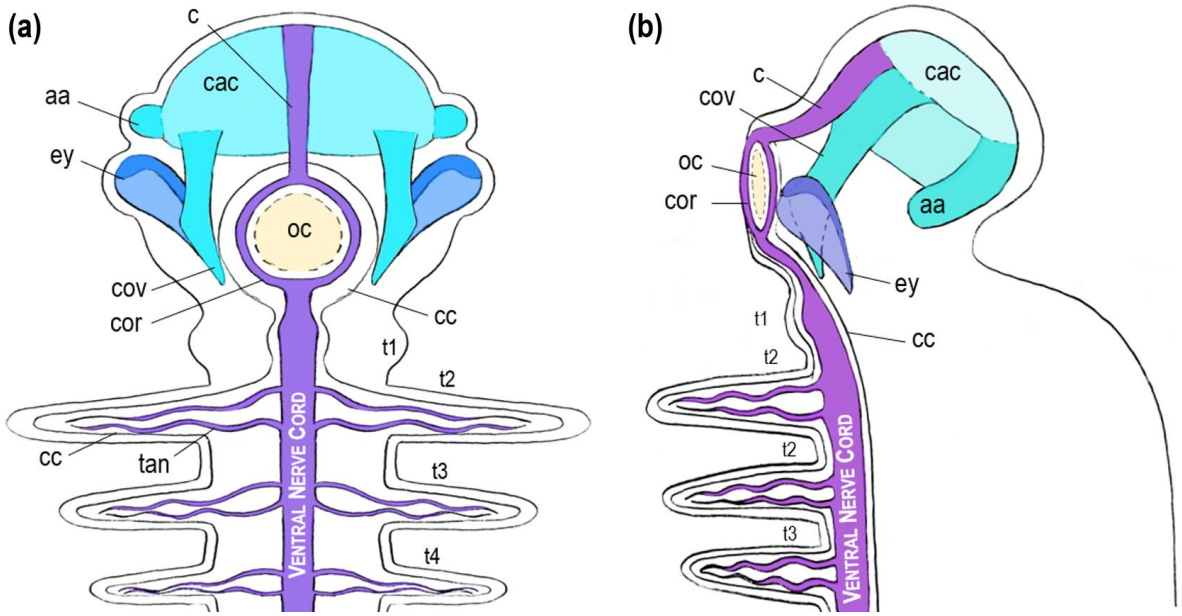


**FIGURE 4.1.** *YKLP 12387's putative central nervous system (CNS). Anterior is up.* (a) *Ventral view.* (b) *Lateral view. Dorsal is right. The CNS is situated in the principal circumferential chamber (cc). A ventral nerve cord directly innervates the trunk appendages (t) via ventrolateral nerves (tan). The nerve cord opens anteroventrally into a circumoral nerve ring (cor). This nerve ring connects to the core anterior cavity (cac), or asegmental brain, via a connecting cord (c). The antennae (aa) are directly innervated by the brain.*

***Abbreviations:*** *aa, anteriormost appendages (antennae); cac, core asegmental cavity (brain); c, connecting cord; cc, circumferential chamber; cor, circumoral ring (nerve ring); cov, circumoral ventrally descending voids; ey, eye; oc, oral cavity; t, trunk appendage; tan, trunk appendage nerve.*

relative to the brains of extant onychophorans, and its position in the asegmental unit, I interpret this structure as an asegmental brain (Figure 4.1; pl 2 & 3).

The anteriormost appendages are directly innervated by a brain process, which forms the innermost component of the appendages (Figure 3.8 iii). This configuration is suggestive of a sensory function equivalent to the antennae of extant onychophorans (Figure 4.1; Martin et al., 2017). I therefore interpret the anteriormost appendages as asegmental sensory antennae. Due to their position in the first true segment, I propose a protocerebral affinity for the eyes (Ortega-Hernández et al., 2017).

The ventral nerve cord opens anteroventrally into a circumoral nerve ring, which is linked to the brain via a ventral connecting cord. Peripheral ventrolateral extensions of the ventral nerve cord directly innervate the trunk appendages via a single nervous connection (Figure 4.1).

The specimen's central nervous system is thus composed of a ventral nerve cord, a circumoral nerve ring, and an asegmental brain, which innervates a set of asegmental antennae (Figure 4.1; pl 3 a & c). I interpret the antennal, ocular, and oral region anterior to the trunk constriction as the specimen's head.

## 4.2. THE APPENDICULAR EYES

In extant panarthropods, the anteriormost eye pair is always derived from the first 'ocular' segment, and is innervated protocerebrally (Ortega-Hernández et al., 2017). The innervation of YKLP 12387's ocular structures by the asegmental brain therefore indicates that the antennae and eyes do not belong to discrete segmental units, but rather to a single element – the protocerebrum (pl 3 a & c).

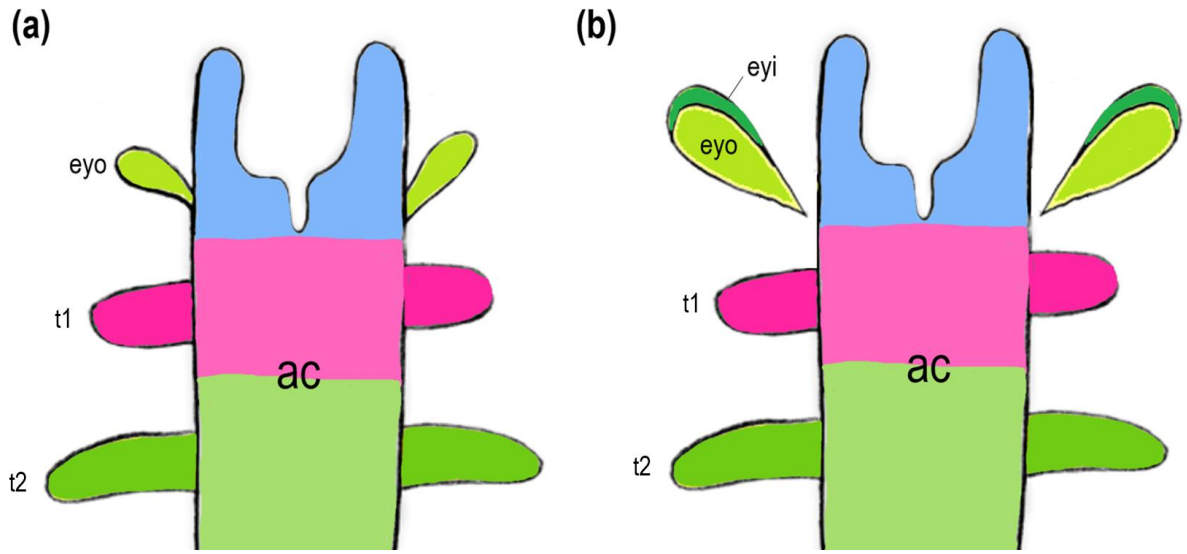


**FIGURE 4.2.** *Anterior is up. Hypothetical reconstruction detailing the appendicular origins of the eyes in YKLP 12387.* (a) *Like the inner void of the succeeding appendages, I propose that the outer ocular structure originates from the posterior margin of the first axial cavity segment.* (b) *This structure likely budded off to form the fossil's outer ocular structure. The protocerebral (first), deutocerebral (second), and tritocerebral (third) segments are coloured in lilac, pink, and green respectively.*

***Abbreviations:*** *ac, axial cavity; eyi, eye inner structure; eyo, eye outer structure; t, trunk appendage.*

The eyes express a remnant of the internal 'bilayered' condition of the trunk appendages. This is reflected in their dual inner and outer structures, which are partially separated from one another via a thin layer of flesh (Figures 3.8, 3.10 & 4.2; pl 2 & 3). The outermost ocular structures, teardrop-shaped voids that run parallel to the narrower inner voids, form discrete cavities that bud off from the posterior margin of the first axial cavity

segment (Figures 3.10 & 4.2; pl 2 & 3). I hypothesise that the specimen's outer ocular structure is derived from the posterior margin of the first segment of the axial cavity (Figure 4.2). This suggests that the core ocular chamber is derived from the axial cavity, just as the core chambers of the trunk appendages are (Figures 3.8 & 4.2; pl 2 a & c, pl 3 a & c). The composition of the eyes thus reflects their appendicular origins.

By definition, each body segment must bear a single pair of appendages (see section 1.4; Scholtz, 2002). The appendicular eyes thus support the interpretation of the ocular domain as the first true body segment.

## 4.3. THE DEUTOCEREBRAL APPENDAGES

The protocerebral location of the specimen's eyes and ventral oral cavity reflects the condition of extant onychophoran embryos (Figure 4.3; Ou, Shu & Mayer, 2012). The succeeding deutocerebral appendages of the fossil are stunted lobopodous outgrowths, positioned on either side of the protocerebral oral cavity (Figure 4.1; pl 2 a & c, 3 a & c).

The shortened morphology of the specimen's deutocerebral limbs relative to the succeeding trunk appendages argues against an ambulatory function, whilst the absence of clear direct innervation, such as that observed for the asegmental antennae (see section 4.1), militates against a sensorial function, such as that of the deutocerebral antennae of the then-contemporary trilobites (Figure 4.1; pl 2 & 3; Ortega-Hernández et al., 2017).

Instead, the specimen's paraoral limb buds more closely resemble the developing paraoral jaws of early stage IV onychophoran embryos. In *Euperipatoides rowelli* embryos, the deutocerebral appendages are visible as modified limbs until the later phases of stage IV, when they are readily distinguishable from the succeeding appendages on account of their unique internal migration (Figure 4.3; pl 1 a; Ou et al., 2012; Walker & Tait, 2004). The ventral mouth also migrates during onychophoran development, shifting from the embryonic protocerebrum to the adult deutocerebrum (Figure 4.3; Ou et al., 2012). The modification of deutocerebral limbs is also observed in the extinct *Antennacanthopodia gracilis*, a stem-group Chengjiang onychophoran and contemporary of the specimen, albeit into slender elongated appendages instead of jaws (Ou et al., 2011; Walker & Tait, 2004).

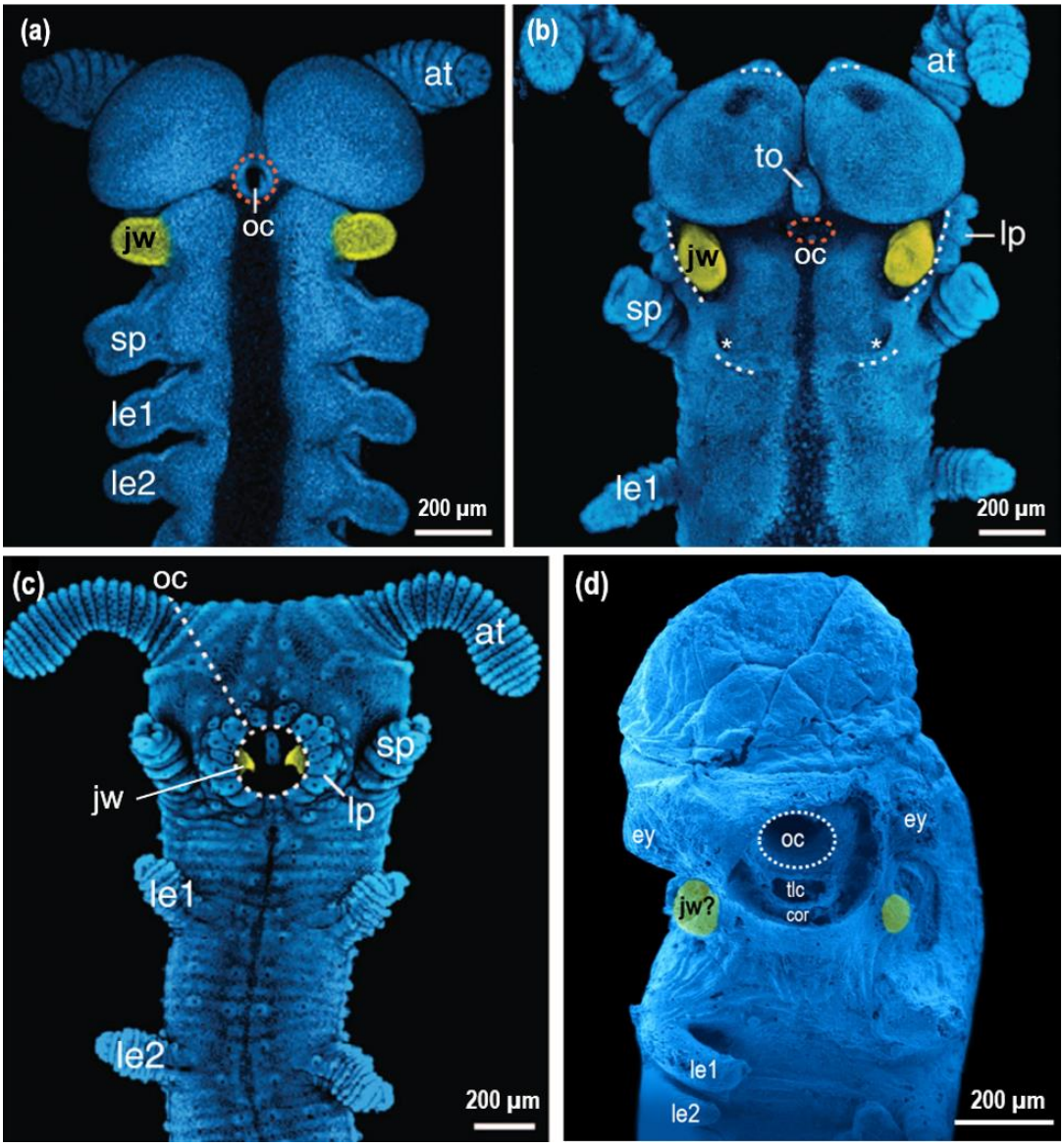


**FIGURE 4.3.** *Ventral view, anterior is up. Deutocerebral appendages are artificially coloured yellow. Oral cavities (oc) are indicated via dashed lines.* (a-c): *Confocal micrographs of* Euperipatoides rowelli *(onychophoran) embryos labelled with the DNA-marker Hoechst at subsequent developmental stages. These images depict the migration and / or modification of the jaws (jw) and oral cavity. Three consecutive oral openings arise during ontogeny. The second and third openings are indicated here via orange and white dashed lines respectively*. (a) *Early stage IV embryo. The stomodaeum, an early oral cavity, is situated at the posterior border of the protocerebral segment. The jaws are visible as external lobopodous appendages.* (b) *Late stage IV embryo. The jaws migrate inwardly.* (c) *Stage VII embryo. The deutocerebral jaws are internalised and sclerotised. Modified from Ou, Shu & Mayer (2012).* (d). *YKLP 12387. False-coloured SEM. Modified deutocerebral appendages are positioned laterally to either side of a well-developed oral cavity and resemble the limb-like jaws of early stage IV* E. rowelli *embryos.*

***Abbreviations:*** *at, antennae; cor, circumoral ring; ey, eye; jw, jaw; jw?, putative jaw; le, leg; lp, lips; oc, oral cavity; sp, slime papillae; tlc, trilobed chamber; to, presumptive tongue.*

## 4.4. THE WALKING LEGS

Excluding the deutocerebral appendages, the shortened length of which is attributed to modification (see section 4.3), the specimen exhibits a distinctive posteriad reduction in ventrolateral trunk appendage length (pl 1). The underdevelopment of posterior trunk limbs with respect to their anterior counterparts is a characteristic trait of developing euarthropods and onychophorans; in these taxa, the posteriormost segments are the youngest, most recently formed components of the body, whilst those in the anterior are older and thus more fully developed (pl 1; Walker & Tait, 2004). The variation in limb length along the fossil's anterior-posterior (AP) axis is therefore attributed to development. The cause of morphological variation from the anterior rounded limbs to the posterior conical protuberances is also considered developmental (pl 1).

YKLP 12387's tritocerebral appendages are the anteriormost pair of unmodified trunk appendages. Due to similarities to the ambulatory lobopods of onychophorans, I interpret the typical trunk appendages as walking limbs, which are directly innervated via peripheral lateral extensions of the ventral nervous system (Figure 4.1; pl 3 a).

Distal claws had evolved and were maintained in the early Cambrian onychophoran stem lineage; YKLP 12387's Cambrian contemporaries, such as the hallucigeniids, possessed claws (Smith & Ortega-Hernández, 2014). However, distal limb differentiation does not occur in onychophoran ontogeny until stages V and VI respectively (Walker & Tait, 2004). Given the specimen's numerous morphological similarities to the onychophoran lineage, it is therefore likely that feet and terminal claws were present in later ontogenetic stages of the fossil organism.

## 4.5. BODY CAVITIES AND GERM LAYERS

In invertebrates, body cavities are split into one of two structural groups: (1) primary body cavities and (2) secondary coelomic spaces (see Appendix 4.1 for more detail; Schmidt-Rhaesa, 2007). I will therefore identify both primary and secondary body cavities in the fossil.

### 4.5.1. THE PRIMARY BODY CAVITY

In developing coelomates, both the nerve cord and the gut are derived from the primary body cavity. The nerve cord arises ventrally in the primary body cavity as neuroectoderm (Figure 4.4 aii). The location of YKLP 12387's ventral nerve cord thus reveals the primary nature of the sheath-like circumferential chamber (Figure 4.4 b). The

specimen's circumferential primary body cavity is thus bordered by mesoderm on its internal margins and ectoderm on its external margins, as is the arrangement within the Onychophora (Figure 4.4; Appendix 4.1; Bartolomaeus, & Ruhberg, 1999; Schmidt-Rhaesa, 2007).

In coelomate animals, the gut, enclosed in endoderm, is derived from a section of primary body cavity contained within a transverse partition that splits the coelom into adjacent voids (Figure 4.5; Wilmer, 1990). Although this partition, or mesentery, is present in many extant protostomes, such as the annelids, it is absent in extant onychophorans (Figure 4.4 a; Brusca & Brusca, 2003). The fossil's ventral gut is thus presumed to have arisen from a conserved pocket of primary body cavity (Figure 4.4 bi). Due to the preservation of structures of a similarly delicate nature, the absence of a mesentery in the fossil is considered genuine, reflecting the condition of the extant Onychophora (Figure 4.4 a). However, midgut's absence is deemed taphonomic, as the foregut and hindgut are still visible (pl 2 a & c).

### 4.5.2. THE COELOM AND ITS PARTIAL SEPTA

Due to its position within the primary body cavity and its ventral extensions into the trunk appendages, I interpret the axial cavity as the coelom (Figure 4.4). By comparison with

**FIGURE 4.4.** *See following page. Cross sections through the trunk.* (a) *Extant onychophorans.* (i) *Adult. The primary and secondary cavities are fused into a mixocoel (mx) in which organs are suspended. A dorsal vessel (dv) is situated in the pericardial sinus (ps). This is separated from the axial cavity by the pericardial floor (pf). Based on Brusca & Brusca, 2003 and Mayer et al., 2005.* (ii) Segment 3 of Opisthopatus roseus *embryo. The gut is bordered by endoderm (en) and mesoderm (me). The transitory embryonic coelom (co), bordered by mesoderm, flanks the gut, which is bordered by endoderm. The coelom extends (cx) into the anlagen of the slime papillae appendages (sp). The primary body cavity is bordered by mesoderm internally and ectoderm (ec) externally and gives rise to the neuroectoderm (ne). Modified from Mayer et al., 2005.* (b) *YKLP 12387.* (i) *The pale blue region is not preserved in* (ii)**,** *alongside the gut*. (ii) *sXCT data viewed in Avizo. The coelom, bordered by mesoderm, extends into the appendages (ta). A dorsal vessel (dv) is situated within the mesoderm and is separated from the coelom by a dorsal floor (df). The dorsal sinuses are interpreted as pockets of primary body cavity and are thus bordered internally by mesoderm and externally by ectoderm. The ventral nerve cord is contained within the primary body cavity, which envelops the coelom like a thin sheath.*

***Abbreviations:*** *cl, claw; cm, circular muscle; co, coelom (or axial cavity); cx, coelomic extension; ds, dorsal sinus; dv, dorsal vessel; ec, ectoderm; en / endo, endoderm; ft, foot; lm, lateral longitudinal muscle; m, muscle; me / meso, mesoderm; mx, mixocoel; nc, nerve cord; ne / neuro, neuroectoderm; pbc, primary body cavity (or circumferential chamber); pf, pericardial floor; ps, pericardial sinus; sa, salivary gland; sg, slime gland; som, superficial oblique muscle; sp, slime papillae; ta, trunk appendage; vs, ventral sinus.*

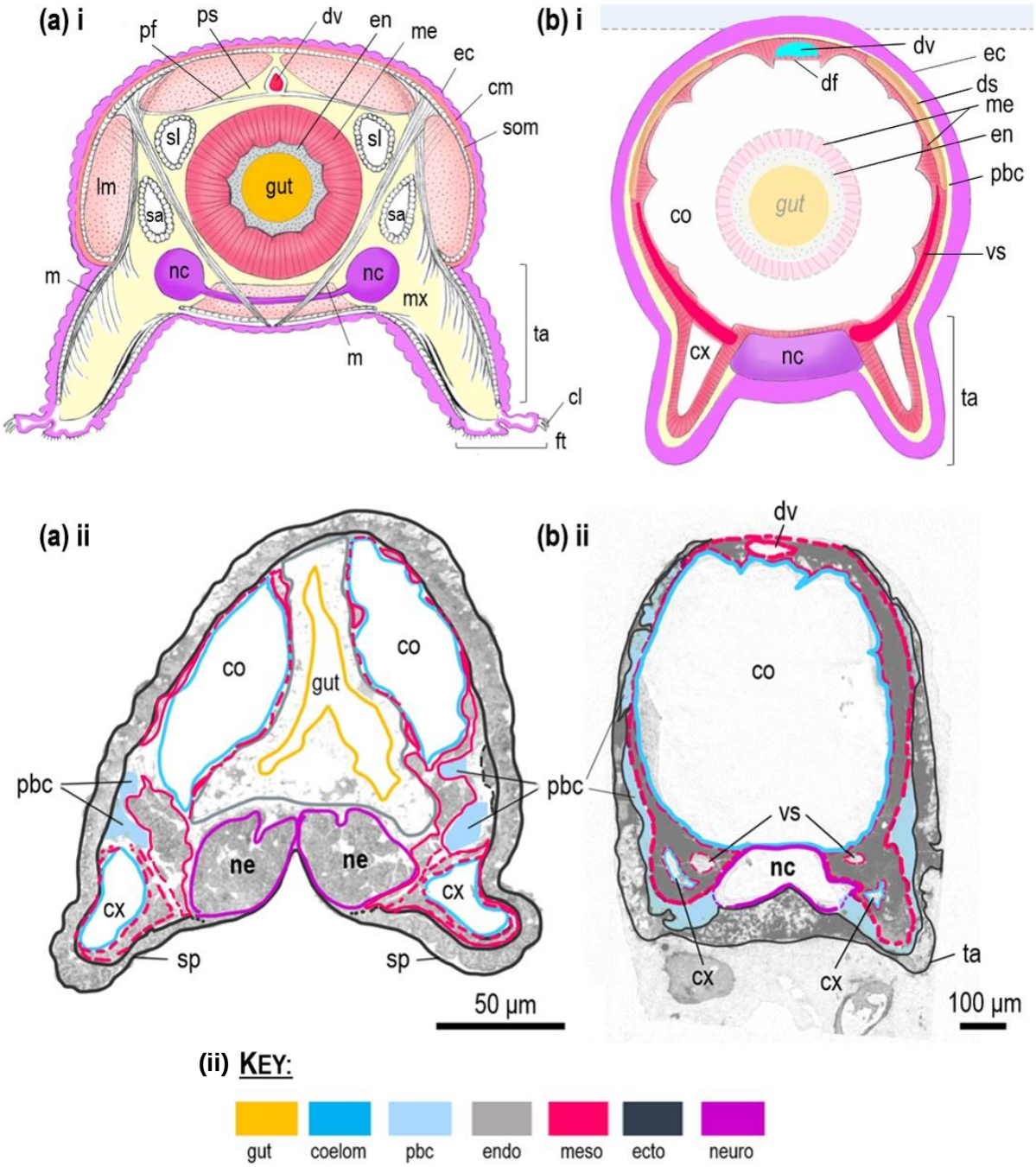


extant taxa, the surrounding tissue is thus reconstructed as mesoderm (Figures 4.4 & 4.5; Bartolomaeus, & Ruhberg, 1999; Mayer at al., 2004 & 2005; Schmidt-Rhaesa, 2007; Wilmer, 1990). Partial septa subdivide the fossil's coelomic space into segments but are absent in extant adult panarthropods (Brusca & Brusca, 2003). However, septa composed of an outer layer of ectoderm and an inner layer of mesoderm are present in extant onychophoran embryos during the early stages of somite formation and mesoderm proliferation (Figure 4.6; Anderson, 1973; Manton, 1949). These early partitions may thus be homologous to the mesodermal septa of the fossil embryo, vanishing in later ontogenetic stages.

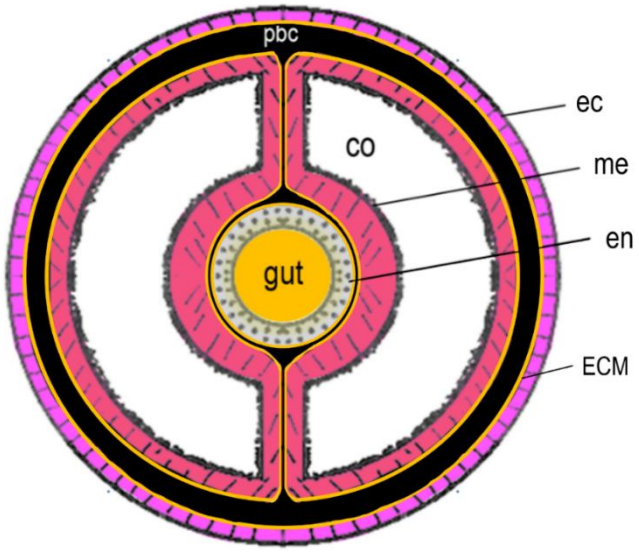


**FIGURE 4.5.** *The coelomate condition. The gut, enclosed by an endodermal layer (en), is positioned within the primary body cavity (pbc). The primary body cavity is primarily bordered by extracellular matrix (ECM). It is secondarily bordered by mesoderm (me) internally and ectoderm (ec) externally. The coelom (co) is situated within the mesoderm (me). Modified from Wilmer, 1990.*

***Abbreviations:*** *co, coelom (or axial cavity); ec, ectoderm; ECM, extracellular matrix; en, endoderm; me, mesoderm; pbc, primary body cavity (or circumferential chamber).*

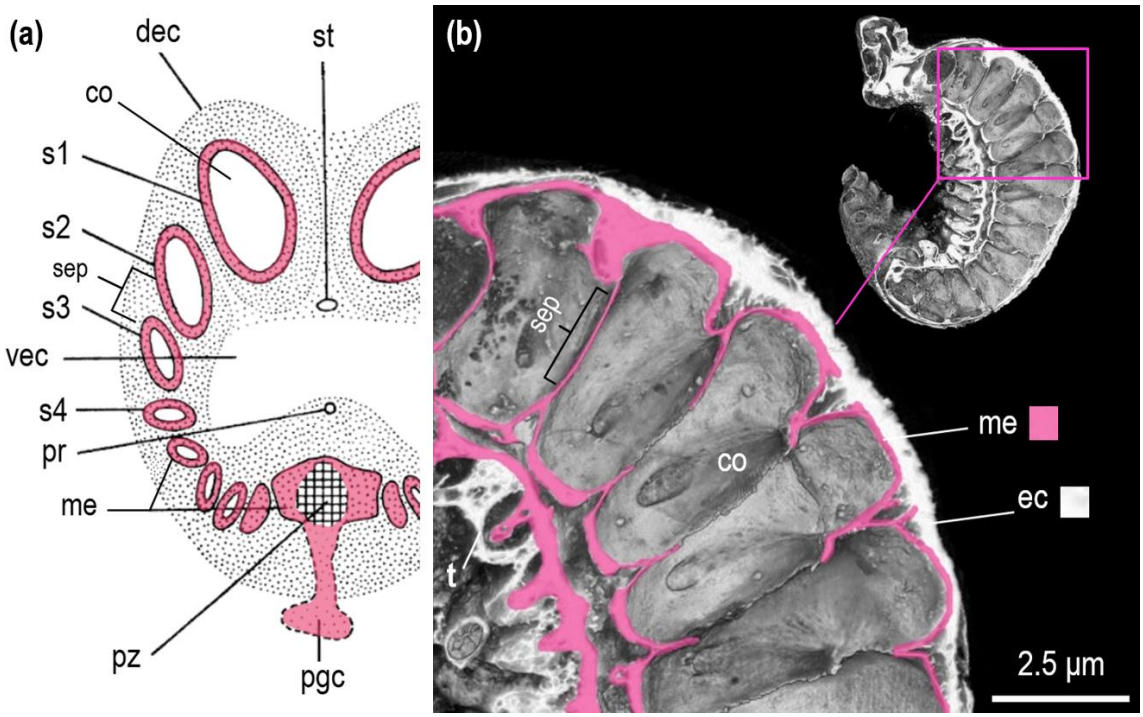


**FIGURE 4.6.** *See following page. Mesodermal septa.* (a) Peripatopsis sedgwicki *(extant onychophoran) embryo. Anterior is up. Somites (s) are distinctly separated by septa composed of an outer layer of embryonic ectoderm (eec) and an inner layer of mesoderm (me). Modified from Anderson, 1973, and Manton, 1949.* (b) *sXCT data of YKLP 12387 viewed in Avizo. Mesoderm is artificially coloured pink. Anterior is top left, dorsal is right.*

***Abbreviations:*** *co, coelom; dec, dorsal embryonic ectoderm; ec, ectoderm; me, mesoderm; pgc, primordial germ cells; pr, proctodeum; pz, proliferation zone; s, somite; sep, septum; st, stomodeum; vec, ventral embryonic ectoderm.*

### 4.5.3. EXTRAEMBRYONIC ENDORDERMAL SAC

YKLP 12387's anterodorsal cavity occurs in the proto- and deutocerebral regions and extends into the anteriormost aspect of the tritocerebral segment (Figure 4.7; pl 2 a & b, pl 3 a & b). Some ovoviviparous onychophorans retain large portions of dorsal extraembryonic ectoderm during the later stages of development. *Peripatopsis sedgwicki* and *Peripatopsis moseleyi* retain an anterodorsal pocket of extraembryonic ectoderm as a swollen sac. This sac gradually shrinks as the embryo elongates (Figure 4.7 a; Anderson, 1973; Manton, 1949). In *P. sedgwicki*, the extraembryonic sac is attached dorsally to a narrow neck in the region corresponding to the proto- and deutocerebral segments (Figure 4.7 a; Anderson, 1973).

Due to the anterodorsal cavity's position, morphology, size, and asegmental nature in the fossil, I interpret this cavity as a sac of extraembryonic ectoderm (Figure 4.7 b). This pocket of dorsal ectoderm may have formed an extraembryonic sac with a narrow dorsal attachment which was compacted dorsally during preservation (Figure 4.7 bi), or it may have formed an intraembryonic dorsal 'hump' (Figure 4.7 bii). Due to a lack of clear evidence for the compaction of an externalised sac in the SEMs, I favour the latter hypothesis (Figure 4.7 bii).

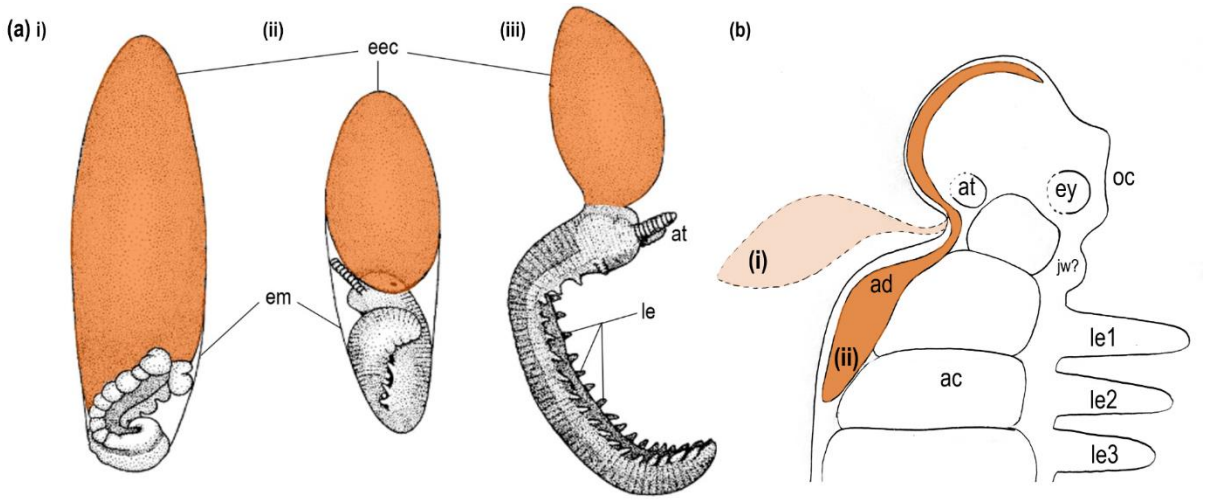


**FIGURE 4.7.** *Anterodorsal sacs*. (a) *Reduction of the extraembryonic ectodermal sac (eec; orange) through development in* Peripatopsis sedgwickii. *Anterior is up. (i) Early stage embryo. (ii) Mid-stage embryo. (iii) Late stage embryo. Modified from Anderson, 1973, and Manton, 1949.* (b) *YKLP 12387's anterodorsal cavity (ad) extends from the anterior unit into the anteriormost limits of the third segment (which bears the second pair of walking legs, le2).* Hypothesis (i): *The anterodorsal sac was an external, extraembryonic feature that was compacted dorsally as a consequence of preservation. This interpretation is illustrated with a dashed outline.* Hypothesis (ii): *The anterodorsal sac is intraembryonic.*

***Abbreviations:*** *ac, axial cavity; ad, anterodorsal cavity; at, antenna; eec, dorsal extraembryonic ectoderm; em, egg membrane; ey, eye; jw?, putative developing jaw; le, leg; oc, oral cavity.*

## 4.6. PHYLOGENETIC ANALYSIS

### 4.6.1. YKLP 12387 IS A STEM-GROUP ONYCHOPHORAN

Maximum parsimony analysis consistently resolved YKLP 12387 as a stem-group onychophoran (Figure 4.8). Ortega-Hernández et al.'s (2017) key for determining anterior segmental affinities across extant and extinct panarthropods also resolves the specimen as an onychophoran (Appendix 4.2). The position of the eyes at the base of the first appendage pair, the ventrally oriented mouth, the absence of a hypostome, the presence of a multisegmented head, and the protocerebral affinity and preoral location of the anteriormost appendages are key characters used to define the onychophoran lineage (Appendix 4.2; Brusca & Brusca, 2012; Ortega-Hernández et al., 2017).

### 4.7.2. YKLP 12387 IS AN ONYCHOPHORAN EMBRYO

YKLP 12387 resembles onychophoran embryos, but not adults, in four respects: (1), a curved body, (2), posteriad reduction in appendage length, (3), a blind gut, and thus a developing intestinal system, and (4) an anterodorsal sac of extraembryonic ectoderm. I therefore interpret the fossil as an embryonic stem-group onychophoran, preserved in an approximately equivalent developmental phase to that of stage V *Euperipatoides rowelli* embryos (pl 1).

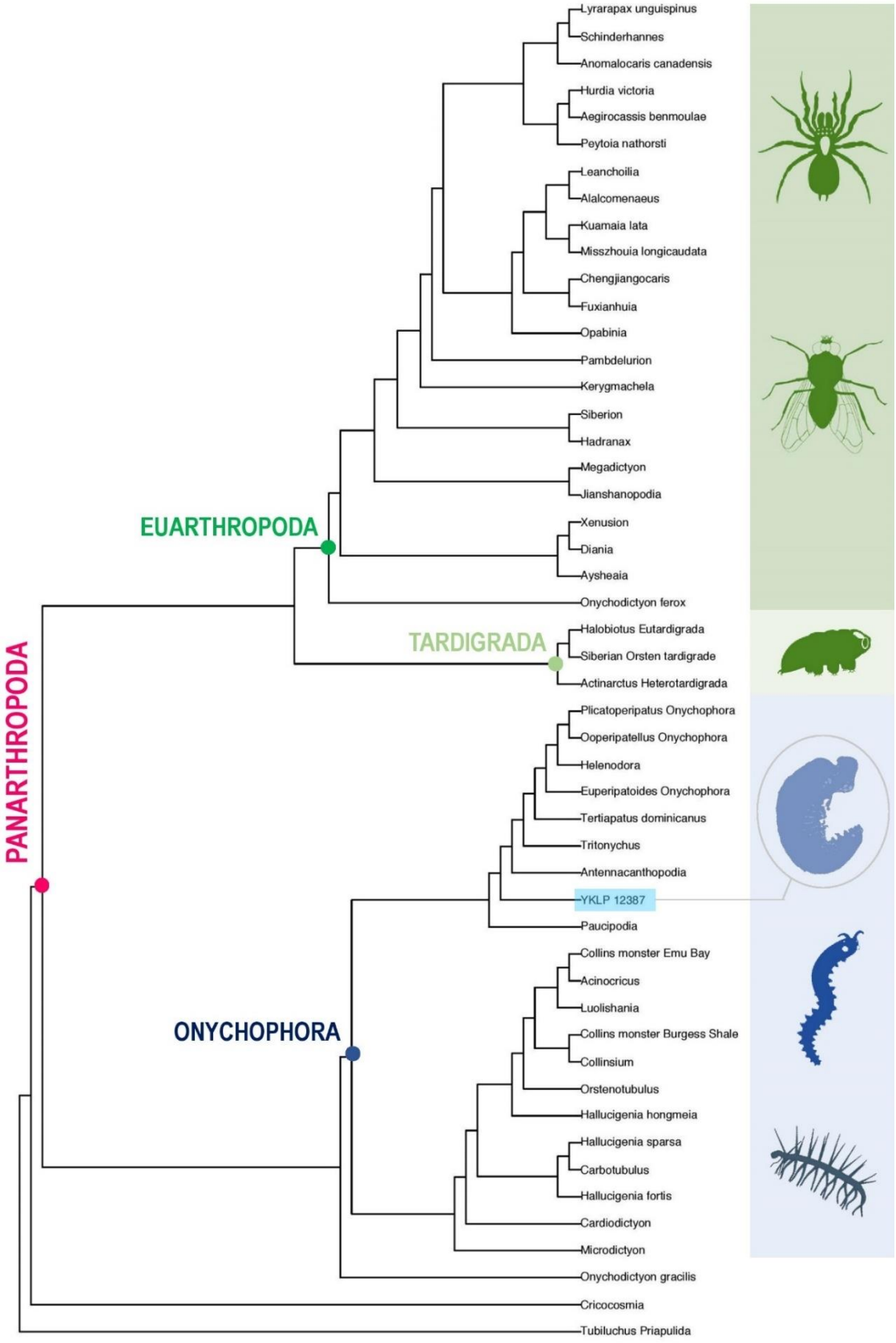


**FIGURE 4.8**. *The phylogenetic relationships of various extinct and extant. Maximum parsimony tree using the default concavity constant of k = 4. YKLP 12387 (highlighted) is resolved as a stem-group onychophoran.*

# CHAPTER 5

# DISCUSSION

- PLEASE REFER TO THE PLATES (PL) LOCATED AT THE END OF THIS THESIS –

---

## 5.1. SEGMENTAL HOMOLOGY OF THE HEAD IN YKLP 12397

As a Cambrian stem-group onychophoran, YKLP 12387 is usefully placed to illuminate the early evolution of the panarthropod anterior nervous system. This remarkably preserved fossil sheds new light on the series of evolutionary steps that transformed the simple circumoral nerve ring of the last common ancestor of Nematoda and Panarthropoda into the compact yet complex dorsal brains of crown-group Euarthropoda and Onychophora.

YKLP 12387 has two protocerebral domains: (1) an apical dorsal void (*cac* in plates), or the asegmental brain, innervates a pair of asegmental antennae and a pair of (2) segmental eyes, which are located in the first true body segment (Figure 5.1). I interpret the specimen's antennal and ocular domains as homologous to the fused protocerebral *optix* and *orthodenticle (otd)* domains of extant panarthropods respectively (Figures 5.1 & 5.2). In view

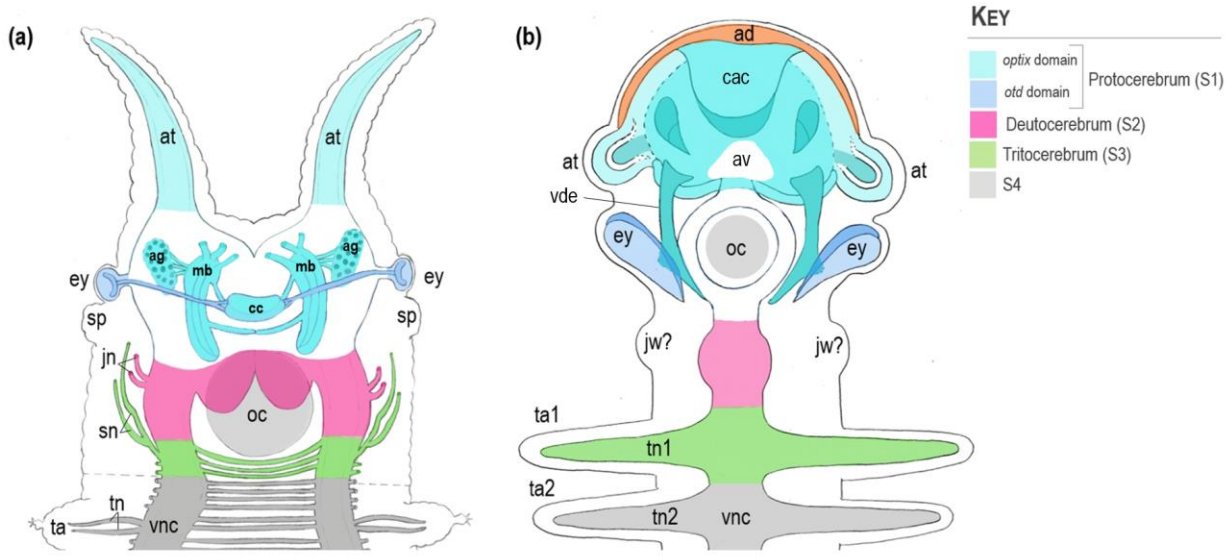


**FIGURE 5.1.** *Illustration depicting the central nervous system in* (a) *an adult onychophoran and* (b) *YKLP 12387, an early Cambrian stem-group onychophoran embryo. The* optix *domain contains the antennae, the mushroom bodies, and the central complex, whilst the* orthodenticle (otd) *domain contains the eyes.* (a) *In extant onychophorans, the antennal and ocular domains are fused to form a unipartite protocerebral segment.* (b) *In YKLP 12387, the antennal and ocular domains are discrete, resulting in a bipartite protocerebrum. Adult onychophoran illustration based on Mayer (2016) and Schürman (1987).*

***Abbreviations:*** *ad, anterodorsal cavity (or ectodermal sac); ag, antennal glomeruli; at, antenna; av, asegmental ventral cavity; cac, core anterior cavity; cc, central complex; ey, eye; jn, jaw nerve; jw?, putative developing jaw; mb, mushroom body (also known as the corpora pedunculata); oc, oral cavity; s, segment; sn, slime papilla nerve; sp, slime papilla, ta, trunk appendage; tn, trunk appendage nerve; vde, ventrally descending process of the core anterior cavity vnc, ventral nerve cord.*

of the asegmental origins of YKLP 12387's brain and the antennae it innervates, this structure is likely homologous to a highly conserved central complex located in the brains of euarthropods and onychophorans (Appendix 5.1).

The bipartite protocerebrum is followed by the unipartite deutocerebral and tritocerebral segments respectively. The internal sclerotised jaws of crown-group Onychophora are thus homologous to the short deutocerebral outgrowths of the stem-group (Figure 5.1; pl 1). In the aquatic Cambrian lobopodian, YKLP 12387, the tritocerebral appendages represent the first pair of walking legs. Subsequent modification of the tritocerebral appendages into slime papillae likely post-dates the terrestrialisation of the Onychophora and is thus not apparent in the Cambrian stem-group (Garwood et al., 2016).

## 5.2. THE PANARTHROPOD HEAD PROBLEM

As Graham Budd (2002) remarked almost two decades ago, the difficulties that arise when homologising the anterior segmental configurations of disparate panarthropods can be resolved by the very rocks beneath our feet, in the ancient fossil record.

The proposal that pre-oral raptorial-like appendages are deutocerebral, as suggested in the Scholtz and Edgecombe (2005, 2006; see section 1.6.2) and Chen et al. (2004) and Waloszek et al. (2005; see section 1.6.1) models, is not clearly supported by the fossil evidence. The anterior location and innervation of YKLP 12387's nascent antennae discourage a deutocerebral interpretation in favour of homology to the protocerebral *optix* domain. Similarly, the apical location and innervation of the frontal appendages of the Cambrian radiodontans *Lyrarapax unguispinus* (Cong et al., 2014) and *Kerygmachela kierkegaardi* (Park et al., 2018) also refute a deutocerebral interpretation, and are more likely homologous to the protocerebral *optix* domain. Nevertheless, Budd's (2002) model, which proposes protocerebral affinities for these structures, (2002) does not consider the discrete origins of the ocular and antennal / labral structures, or the appendicular origins of the eyes, a critical component to unravelling the mysteries of appendage homology.

The configuration of YKLP 12387's eyes provides morphological support for their appendicular origins, suggesting that eyes, rather than antennae, are the protocerebral appendages of onychophorans. A recent unpublished study on the flour beetle *Tribolium castaneum* supports this hypothesis, by showing that the central neural complex evolved through the integration of neural cells from an ancestral apical neuroendocrine centre, which eventually gives rise to the labrum (He et al., 2019). The homology between the asegmental euarthropod labrum and the asegmental onychophoran antennae to the pre-oral raptorial-like appendages and labral complexes of the other euarthropods suggests that these too are asegmental.

By combining Strausfeld's (2012) model of protocerebral evolution with Budd's (2002) model of appendage homology and the fossil evidence that eyes, not antennae, are the protocerebral appendages of panarthropods, a convincing hypothesis supported by the fossil material outlined in this study emerges (Figure 5.2).

Using the ancient labral / *optix* and ocular / *orthodenticle (otd)* domains as reference points, the protocerebral domain of the unsegmented nematode is defined by the posterior

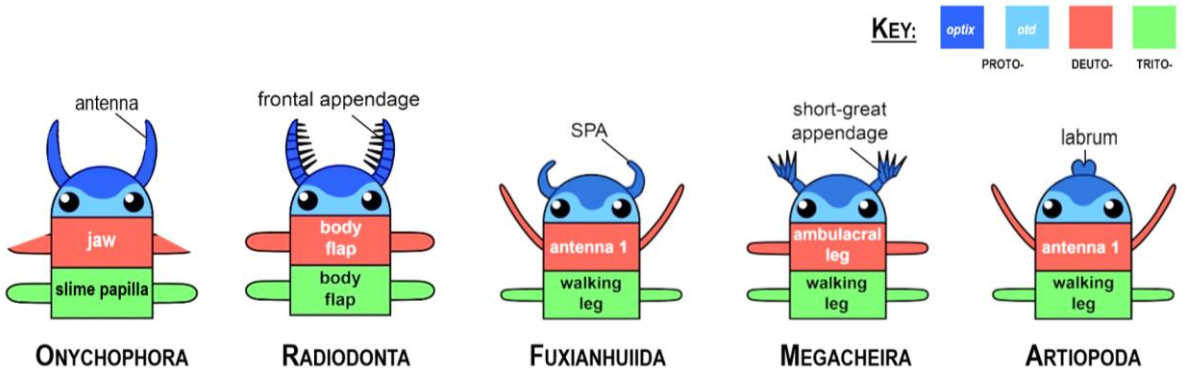


***FIGURE 5.2.*** *The Long model of Panarthropod segmental homology. The protocerebral, deutocerebral, and tritocerebral segments are coloured in blue, red, and green respectively. The ancestral protocerebrum was morphologically and genetically divided into two regions: (1) the asegmental* optix *region is coloured dark blue, and (2) the segmental* orthodenticle (otd) *domain is coloured pale blue. The protocerebral segmental appendages are defined here as eyes instead of the pre-oral raptorial-like appendages, which are asegmental. Figure adapted from Ortega-Hernández et al., 2017.*

***Abbreviations:*** *SPA, specialised post-antennal appendages.*

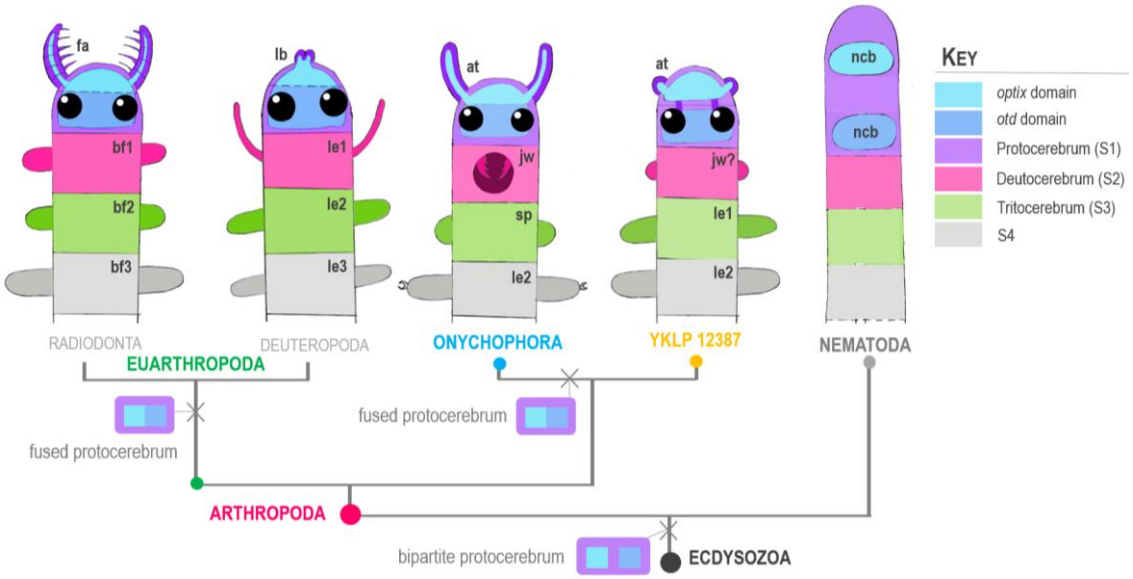


**FIGURE 5.3.** *The dual origin of the bipartite protocerebrum in Ecdysozoa. Gene expression studies support the ancestral division of the protocerebrum into: (1) the asegmental antennal / labral* optix *domain, and the (2) segmental ocular* orthodenticle (otd) *domain (Strausfeld, 2012). These units are fused in modern euarthropods and onychophorans. YKLP 12387 provides the first fossil evidence of the ancestral bipartite protocerebrum. Euarthropod and onychophoran homologies based on Ortega-Hernández et al. (2017). Nematode homologies based on Lanjuin et al. (2003). Tardigrades are excluded due to a lack of gene expression studies in this group.*

***Abbreviations:*** *at, antennae; bf, body flap; fa, frontal appendage; jw, jaw; lb, labrum; le, walking leg; ncb, neuronal cell bodies; sp, slime papillae.*

border of *otd* expression (Figures 1.7 & 5.3), whilst the antennal prostomium and ocular peristomium of the distantly related annelids correspond to the asegmental *optix / Six3* and segmental *otd / otx* domains respectively (Appendix 5.2; Strausfeld, 2012). These regions of gene expression therefore not only allow us to homologise regions within Panarthropoda, but throughout the protostomes, and even the deuterostomes (Appendix 5.3; Riebli & Reichert, 2016). This ancient genetic and morphological division is thus the key to understanding the anterior organisation of vastly disparate groups, separated by hundreds of millions of years of evolution to branches far and wide across the tree of life.

## 5.3. CONVERGENCE AND THE CASE FOR TACTOPODA

In the panarthropod stem lineage, the ganglionation of the ventral nerve cord gave rise to the earliest tactopods (Euarthropoda + Tardigrada). However, prior to the divergence and diversification of the panarthropods, a series of evolutionary alterations took place, transforming the simple legless ancestor of Nematoda and Panarthropoda into a walking worm-like creature with an increasingly compact anterior nervous configuration, whose first set of trunk appendages were modified to construct a pair of segmental eyes.

Nervous compactification occurred by linking the discrete *optix* and *orthodenticle (otd)* gene expression domains by means of the circumoral nerve ring, which is retained in extant tardigrades. The presence of this structure in YKLP 12387 suggests that the nerve ring was retained in the ancestral panarthropod before its independent secondary loss in both crown-group Euarthropoda and Onychophora. The ventral oral cavity of YKLP 12387 also indicates that nerve ring loss occurred after the ventralisation of the mouth in the onychophoran lineage.

YKLP 12387 provides the first fossil evidence of the ancestrally bipartite protocerebrum, suggesting that the protocerebrum was likely unfused in the last common ancestor (LCA) of Panarthropoda (see section 5.1; pl 2 & 3). The protocerebrum is thus revealed to have a more complex evolutionary history than previously thought, as fusion occurred separately in the onychophoran and euarthropod lineages to give rise to the unipartite protocerebral segments of the respective crown-groups (Figures 5.3 & 5.4).

The convergent evolution of the morphologically similar anterior nervous configurations in Euarthropoda and Onychophora suggests a compact nervous arrangement confers a distinct evolutionary advantage (Figure 5.4). I propose that fusion of the labral and ocular domains into a single compact region played a significant role in ensuring the enduring evolutionary success of Panarthropoda.

As a stem-group Onychophoran, the nerve ring, bipartite protocerebrum, ventral mouth, and appendicular eyes of YKLP 12387 illuminates the convergent evolutionary pathways of crown-group panarthropods. Despite remarkable similarities in the construction of the euarthropod and onychophoran brains, the loss of the ancestral nerve ring, the fusion of the protocerebral elements into a single unit, the incorporation of the second trunk appendage into the head, and the ventralisation of the mouth occurred separately in both groups via convergent evolution. The fact that such a substantial subset of similarities in the composition of the euarthropod and onychophoran brains are unequivocally convergent suggests that the morphological argument for the proposed sister-group relationships of these taxa needs serious rethinking. The independent evolution of these neuroanatomical traits weakens the case that these phyla form a clade, and is thus consistent with fossil, musculoskeletal, and neurological evidence that tardigrades are the sister group to the euarthropods (the Tactopoda hypothesis; see section 1.3).

The discovery of a discrete dorsal brain and circumoral nerve ring in the stem-group Onychophoran YKLP 12387 adds an intriguing piece of evidence to the evolutionary history of the modern panarthropod brain (Figures 5.2 & 5.4; pl 2 & 3). A series of evolutionary transformations from the primitive circumoral nerve ring of Nematoda, to the separate ring and dorsal brain of stem-group Onychophora, to the fused, adjacent ring and dorsal brain of the tardigrades and the tripartite dorsal brains that evolved separately in the euarthropods and onychophorans, can thus be mapped (Figure 5.4). YKLP 12387's distinct nerve ring and discrete antennal and ocular elements, innervated by a complex asegmental brain, likely reflects the ancestral condition of Panarthropoda, thus offering a remarkable first glimpse at the evolutionary origins of the most successful group of animals to have ever swam, flown, or walked on planet Earth.

***Figure 5.4.*** *See following page. Phylogenetic tree illustrating the hypothetical transition from a simple nerve ring to a complex dorsal brain in Ecdysozoa. The Tactopoda hypothesis is assumed. The numbering system is used to denote traits that evolved independently multiple times in the euarthropod and onychophoran lineages. The deutocerebrum and tritocerebrum are coloured pink and green, whilst the protocerebral* optix *and* orthodenticle (otd) *domains are coloured pale and dark blue respectively. Purple denotes the circumoral nerve ring. Euarthropod and onychophoran homologies based on Ortega-Hernández et al. (2017). Nematode homologies based on Lanjuin et al. (2003). Tardigrade homologies based on Ou et al. (2012) and Smith et al. (2017).*

***Abbreviations:*** *ag, anterior ganglion; at, antenna; jw, jaw; lc, labral complex; le, leg; lvg, lateral and ventral ganglia; md, modified deutocerebral appendage; sp, slime papilla; ta, trunk appendage.*

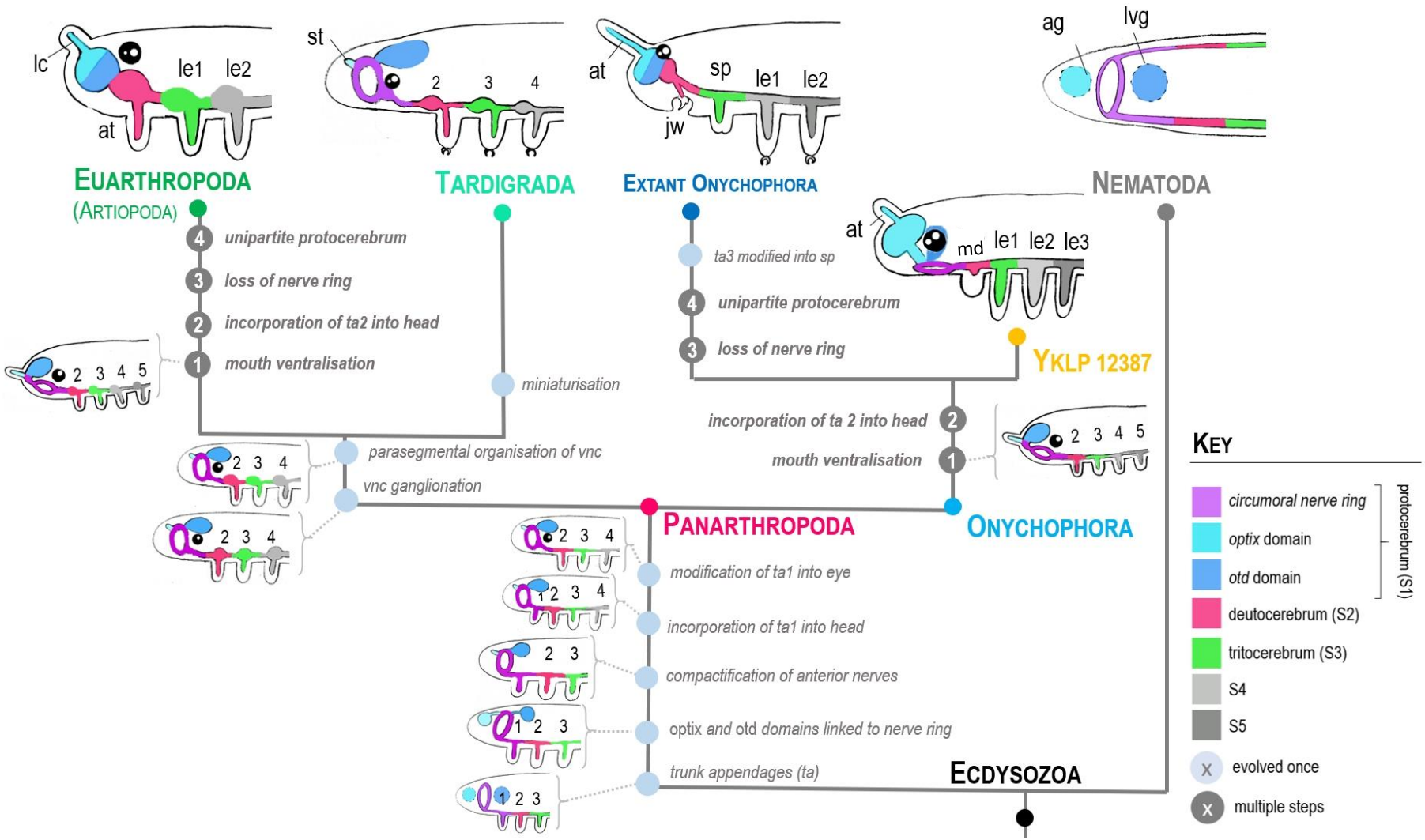
lc
le1
le2
at
EUARTHROPODA
(ARTIOPODA)
4 unipartite protocerebrum
3 loss of nerve ring
2 incorporation of ta2 into head
1 mouth ventralisation
2 3 4 5
st
2 3 4
TARDIGRADA
miniaturisation
parasegmental organisation of vnc
vnc ganglionation
2 3 4
2 3 4
at
sp
le1
le2
jw
EXTANT ONYCHOPHORA
ta3 modified into sp
4 unipartite protocerebrum
3 loss of nerve ring
YKLP 12387
incorporation of ta 2 into head
2
mouth ventralisation
1
2 3 4 5
ONYCHOPHORA
ag
lvg
NEMATODA
at
md
le1 le2 le3
2 3 4
2 3 4
1 2 3 4
2 3
1 2 3
1 2 3
PANARTHROPODA
modification of ta1 into eye
incorporation of ta1 into head
compactification of anterior nerves
optix and otd domains linked to nerve ring
trunk appendages (ta)
ECDYSOZOA
KEY
circumoral nerve ring
optix domain
otd domain
protocerebrum (S1)
deutocerebrum (S2)
tritocerebrum (S3)
S4
S5
x evolved once
x multiple steps

# REFERENCES


1. Aguinaldo, A.M.A., Turbeville, J.M., Lindford, L.S., Rivera, M.C., Garey, J.R., Raff, R. & Lake, J.A. (1997). Evidence for a clade of nematodes, arthropods and other moulting animals. *Nature,* 387: 489–93.

2. Anderson D.T. (1973). Embryology and phylogeny in annelids and arthropods. Oxford: Pergamon Press.

3. Anderson, D.T. (1973). Onychophorans. In: *Embryology and Phylogeny in Annelids and Arthropods* 1st ed. (pp. 93-126). Oxford: Pergamon Press.

4. Babcock, L.E., Zhang, W. & Leslie, S.A. (2001). The Chengjiang Biota: Record of the Early Cambrian Diversification of Life and Clues to Exceptional Preservation of Fossils. *GSA Today*, 11: 4-9.

5. Baguñà, J., Martinez, P., Paps, J. & Riutort, M. (2008). Back in time: a new systematic proposal for the Bilateria. *Philos. Trans. R. Soc. B*., 363: 1481–1491.

6. Balavoine, G., de Rosa, R. & Adouette, A. (2002). *Hox* clusters and bilaterian phylogeny. *Mol. Phylogenet. Evol.,* 24: 266–373.

7. Bartolomaeus, T. & Ruhberg, H. (1999). Ultrastructure of the body cavity lining in embryos of *Epiperipatus biolleyi* (Onychophora, Peripatidae) – a comparison with annelid larvae. *Invertebr. Biol.,* 118: 165-174.

8. Beermann, A., Jay, D.G., Beeman, R.W., Hulskamp, M., Tautz, D. Jurgens, G. (2001). The short antennae gene of *Tribolium* is required for limb development and encodes the orthologue of the *Drosophila distal-less* protein. *Development,* 128: 287– 297.

9. Bourlat, S.J., Nielsen, C., Economou, A.D. & Telford, M.A. (2008). Testing the new animal phylogeny: a phylum level molecular analysis of the animal kingdom. *Mol. Phylogenet. Evol*., 49: 23–31.

10. Boyan, G. & Williams, L. (2002). A single cell analysis of engrailed expression in the early embryonic brain of the *Schistocerca gregaria*: ontogeny and identity of the secondary headspot cells. *Arthropod Struct. Dev.*, 30: 207-218.

11. Brazeau, M.D., Guillerme, T. & Smith, M.R. (2019). An algorithm for Morphological Phylogenetic Analysis with Inapplicable Data. *Syst. Biol*., 68: 619-631.

12. Browne, W.E., Price, A.L., Gerberding, M. & Patel, N.H. (2005). Stages of Embryonic Development in the Amphipod Crustacean, *Parhyale hawaiensis. Genesis*, 42: 124-149.

13. Brusca, R.C. & Brusca, G.J. (2003). *Invertebrates* 2nd ed. Sunderland, Massachusetts: Sinauer Associates.

14. Budd, G.E. (1999). The morphology and evolutionary significance of *Kerygmachela kierkegaardi* Budd (Buen Formation, Lower Cambrian, North Greenland). *Trans. R. Soc. Edinb. Earth Sci.,* 89: 249–290.

15. Budd, G.E. & Jensen, S. (2000). A critical reappraisal of the fossil record of the bilaterian phyla. *Biol. Rev.,* 75: 253–295.

16. Budd, G.E. (2001). Tardigrades as 'stem-group arthropods': the evidence from the Cambrian fauna. *Zool. Anz*., 240: 265–279.

17. Budd, G.E. (2002). A palaeontological solution to the arthropod head problem. *Nature*, 417: 271-274.

18. Caron, J-B., Smith, M.R. & Harvey, T.H.P. (2013). Beyond the Burgess Shale: Cambrian microfossils track the rise and fall of hallucigeniid lobopodians. *Proc. R. Soc. B.,* 280: 20131613.

19. Chen, J.-Y., Waloszek, D. & Maas, A. (2004). A new 'great-appendage' arthropod from the Lower Cambrian of China and homology of chelicerate chelicerae and raptorial antero-ventral appendages. *Lethaia,* 15: 3-20.

20. Clements, J., Lu, Z., Gehring, W.J., Meinertzhagen, I.A., Callaerts, P. (2008). Central projections of photoreceptor axons originating from ectopic eyes in Drosophila. *PNAS USA*, 105: 8968-8973.

21. Cong, P., Ma, X., Xian-Guang, H., Edgecombe, G.D. & Strausfeld, N.J. (2014). Brain structure resolves the segmental affinity of anomalocaridid appendages. *Nature*, 513: 538-542.

22. Conway Morris, S. (1977). A new metazoan from the Cambrian Burgess Shale of British Columbia. *Palaeontology*, 20: 623–640.

23. Conway Morris, S. (1979). Middle Cambrian Polychaetes from the Burgess Shale of British Columbia. *Philos. Trans. R. Soc. Lond. B. Biol. Sci*., 285: 227–274.

24. Couto, A., Alenius, M. & Dickson, B.J. (2005). Molecular, anatomical, and functional organization of the *Drosophila* olfactory system. *Curr. Biol.,* 15: 1535-1547.

25. Cuvier, G. (1817). Le Règne animal distribué d'après son organisation, VIII Articulés. *(The Animal Kingdom, Distributed According to Its Organization, VIII Articulata.)* Paris: Chez Deterville. In French.

26. Daley, A.C. & Budd, G.E. (2014). New anomalocaridid appendages from the Burgess Shale, Canada. *Palaeontology*, 53: 721-738.

27. Daley, A.C. & Edgecombe, G.D. (2014). Morphology of *Anomalocaris canadensis* from the Burgess Shale. *J. Paleontol.,* 88: 68-91.

28. Damen, W.G.M. (2002). Parasegmental organization of the spider embryo implies that the parasegment is an evolutionary conserved entity in arthropod embryogenesis. *Development,* 129: 1239-1250.

29. Darwin, C.R. (1859*). On the origin of species by means of natural selection, or, the preservation of favoured races in the struggle for life*. London: J. Murray.

30. de Rosa, R., Grenier, J.K., Andreeva, T., Cook, C.E., Adouette, A., Akam, M., Carroll, S.B. & Balavoine, G. (1999). Hox genes in brachiopods and priapulids and protostome evolution. *Nature*, 399: 772–776.

31. Dewel, R.A., Budd, G.E., Castano, D.F. & Dewel, W.C. (1999). The organization of the subesophageal nervous system in tardigrades: insights into the evolution of the arthropod hypostome and tritocerebrum. *Zoologischer Anzeiger,* 238: 191–203.

32. Economou, A.D. & Telford, M.J. (2009). Comparative gene expression in the heads of *Drosophila melanogaster* and *Triboleum castaneum* and the segmental affinity of the *Drosophila* hypopharyngeal lobes. *Evol. Dev.,* 11: 88-96.

33. Edgecombe, G.D. (2009). Palaeontological and Molecular Evidence Linking Arthropods, Onychophorans, and other Ecdysozoa. *Evo. Edu. Outreach*, 2: 178–190.

34. Edgecombe, G.D. (2010). Arthropod phylogeny: an overview from the perspectives of morphology, molecular data and the fossil record. *Arthropod Struct. Dev*., 39: 74–87.

35. Eriksson, B.J. & Stollewerk, A. (2010). The morphological and molecular processes of onychophoran brain development show unique features that are neither comparable to insects nor to chelicerates. *Arthropod Struct. Dev*., 39: 478-490.

36. Eriksson, B.J., Samadi, L. & Schmid, A. (2013). The expression pattern of the genes *engrailed, pax6, otd* and *six3* with special respect to head and eye development in *Euperipatoides kanangrensis* Reid 1996 (Onychophora: Peripatopsidae). *Dev. Genes Evol.,* 223: 237-246.

37. Eriksson, B.J., Tait, N.N. & Budd, G.E. (2003). Head development in the onychophoran *Euperipatoides kanangrensis* with particular reference to the central nervous system. *J. Morphol.*, 255: 1-23.

38. Eriksson, M.E. & Tait, N.N. (2012). Early development in the velvet worm *Euperipatoides kanangrensis* Reid 1996 (Onychophora: Peripatopsidae). *Arthropod Struct. Dev.,* 41: 483-493.

39. Erwin, Valentine & Jablonski (1997). The Origin of Animal Body Plans: Recent fossil finds and new insights into animal development are providing fresh perspectives on the riddle of the explosion of animals during the Early Cambrian. *Am. Sci*., 85: 126-137.

40. Farzana, L. & Brown, S.J. (2008). Hedgehog signalling pathway function conserved in *Tribolium* segmentation. *Dev. Genes Evol*. 218, 181-192.

41. Fortey, R.A. & Thomas, R.H. (1998). Preface. In: R.A. Fortey & R.H. Thomas (eds.) *Arthropod Relationships, Systematics Association Special Volume Series 55*. (pp. xi-xii). London: Chapman & Hall.

42. Fortey, R.A., Fjose, A., McGinnis, W. & Gehring, W.J. (1985). Isolation of a homeobox-containing gene from the *engrailed* region of *Drosophila* and the spatial distribution of its transcript. *Nature,* 313: 284-289.

43. Garwood, R.J., Edgecombe, G.D., Charbonnier, S., Chabard, D., Sotty, D. & Giribet, G. (2016). Carboniferous Onychophora from Montceau-les-Mines, France, and onychophoran terrestrialisation. *Invertebr. Biol.*, 135: 179-190.

44. Giribet, G. & Edgecombe, G.D. (2017). Current understanding of Ecdysozoa and its internal phylogenetic relationships. *Integr. Comp. Biol.*, 57: 455–466.

45. Giribet, G. (2003). Molecules, development and fossils in the study of metazoan evolution; Articulata versus Ecdysozoa revisited. *Zoology*, 106: 303–326.

46. Giribit, G. & Edgecombe, G.D. (2012). Reevaluating the arthropod tree of life. *Ann. Rev. Entomol*., 57: 67-86.

47. Goloboff, P.A. (1993). Estimating character weights during tree search. *Cladistics*, 9: 83-91.

48. Goodrich, E. J. (1897). On the relation of the arthropod head to the annelid prostomium. *Quart. J. Micr. Sci.,* 40: 259–268.

49. Halder, G., Callaerts, P. & Gehring, W.J. (1995). Induction of ectopic eyes by targeted expression of the *eyeless* gene in *Drosophila. Science*, 267: 1788-1792.

50. He, B., Buescher, M., Farnworth, M.S., Strobl, F., Stelzer, E., Dieter, N., Koniszewski, B., Mühlen, D. & Bucher, G. (2019). An ancestral apical brain region contributes to the central complex under the control of *foxQ2* in the beetle *Tribolium castaneum*. In review.

51. Heinze, S. & Homberg, U. (2007). Maplike representation of celestial E-vector orientations in the brain of an insect. *Science*, 315: 995–997.

52. Helmkampf, M., Bruchhaus, I. & Hausdorf, B. (2008). Multigene analysis of lophophorate and chaetognath phylogenetic relationships. *Mol. Phylogenet. Evol.,* 46: 206–214.

53. Herbst, C. (1896). Über die Regeneration von antennähnlichen Organen an Stelle von Augen *(On the regeneration of antennae-like organs instead of eyes). Arch. Entw. Mech.,* 2: 544-558. In German.

54. Herbst, C. (1916). Über die Regeneration von antennähnlichen Organen an Stelle von Augen. VII. Die Anatomie der Gehirnnerven und des Gehirns bei Krebsen mit Antennulis an Stelle von Augen (*On the regeneration of antennae-like organs instead of eyes. VII. The anatomy of brain*

*nerves and the brain in crabs with antennules instead of eyes)*. *Arch. Entw. Mech.*, 42: 407-489. In German.

55. Hildebrand, J.G. & Shepherd, G.M. (1997). Mechanisms of olfactory discrimination: converging evidence for common principles across phyla. *Annu. Rev. Neurosci.*, 20: 593-631.

56. Hogvall, M., Schoenauer, A., Budd, G.E., McGregor, A.P., Posnien, N. & Janssen, R. (2014). Analysis of the *Wnt* gene repertoire in an onychophoran provides new insights into the evolution of segmentation. *Evodevo,* 5: 14.

57. Hughes, C.L. & Kaufman, T.C. (2002). *Hox* genes and the evolution of the arthropod body plan. *Evol. Dev*., 4: 459-499.

58. Hughes, N.C. (2003). Trilobite body patterning and the evolution of arthropod tagmosis. *Bioessays*, 25: 386-395.

59. Hunnekuhl, V.S. & Akam, M. (2014). An anterior medial cell population with an apical- organ-like transcriptional profile that pioneers the central nervous system in the centipede *Strigamia maritima. Dev. Biol.,* 396: 136-14.

60. Janssen, R. & Budd, G.E. (2016). Gene expression analysis reveals that *Delta/Notch* signalling is not involved in onychophoran segmentation. *Dev. Genes Evol.,* 226: 69-77.

61. Janssen, R. (2013). Developmental abnormalities in *Glomeris marginata* (Villers 1789) (Myriapoda: Diplopoda): implications for body axis determination in a myriapod. *Naturwissenschaften*, 100: 33-43.

62. Janssen, R. (2017). A molecular view of onychophoran segmentation. *Arthropod Struct. Dev.,* 46: 341-353.

63. Janssen, R., Prpic, N.-M. & Damen, W.G.M. (2004). Gene expression suggests decoupled dorsal and ventral segmentation in the millipede *Glomeris marginata* (Myriapoda: Diplopoda). *Dev. Biol.* 268, 89-104.

64. Kay, L.M. & Stopfer, M. (2006). Information processing in the olfactory systems of insects and vertebrates. *Semin. Cell Dev. Biol*., 17: 433-442.

65. Kimm, M.A. & Prpic, N.M. (2006). Formation of the arthropod labrum by fusion of paired and rotated limb-bud-like primordia. *Zoomorphology,* 125: 147– 155.

66. Kimmel, C.B. (1996). Was *Urbilateria* segmented? *Trends Genet.,* 12: 329-331.

67. Kocot, K.M. (2016). On 20 years of Lophotrochozoa. *Org. Divers Evol.,* 16: 329–343.

68. Kornberg, T.B., Siden, I., O'Farrell, P.H. & Simon, M. (1985). The *engrailed* locus of *Drosophila*: *in situ* localization of transcripts reveals compartment-specific expression. *Cell*, 40: 45-53.

69. Kumar, J.P. & Moses, K. (2001). *EGF* receptor and *notch* signaling act upstream of *Eyeless/Pax6* to control eye specification. *Cell*, 104: 687-697.

70. Kusche, K., Bangel, N., Mueller, C., Hildebrandt, J.-P. & Weber, W.-M. (2005). Molecular cloning and sequencing of the Na+/K+ -ATPase αsubunit of the medical leech *Hirudo medicinalis* (Annelida) – implications for modelling protostomian evolution. *J. Zoolog. Syst. Evol. Res.*, 43: 339–342.

71. Lanjuin, A., VanHoven, M.K., Bargmann, C.I., Thompson, J.K. & Sengupta, P. (2003). *Otx/otd* Homeobox Genes Specify Distinct Sensory Neuron Identities in *C. elegans*. *Dev. Cell,* 5: 621–633.

72. Lankester, E.R. (1904). The structure and classification of Arthropoda. *Q. J. Microsc. Sci*., 47: 523–582.

73. Lankester, E.R. (1904). The structure and classification of the Arthropoda. *J. Cell Sci*., 47: 523-582.

74. Legg, D.A. & Vannier, J. (2013). The affinities of the cosmopolitan arthropods *Isoxys* and its implications for the origin of arthropods*. Lethaia*, 46: 540-550.

75. Legg, D.A., Sutton, M.D. & Edgecombe, G. (2013). Arthropod fossil data increase congruence of morphological and molecular phylogenies. *Nat. Comm*., 4: 2485.

76. Liu, J. & Dunlop, J.A. (2014). Cambrian lobopodians: A review of recent progress in our understanding of their morphology and evolution*. Palaeogeogr. Palaeoclimatol. Palaeoecol*., 398: 4-15.

77. Liu, J., Shu, D., Jian, H., Zhang, Z. & Zhang, X. (2006). A large xenusiid lobopod with complex appendages from the Lower Cambrian Chengjian Lagerstätte. *Acta Palaeontol. Pol*., 51: 215-222.

78. Loesel, R., Nässel, D.R. & Strausfeld, N.J. (2002). Common design in a unique midline neuropil in the brain of arthropods. *Arthropod Struct. Dev.,* 31: 77–91.

79. Maas, A., Braun, A., Dong, X.-P., Donoghue, P.C.J., Müller, K.J., Olempska, Repetski, J.E., Siveter, D.J., Stein, M. & Waloszek, D. (2006). The 'Orsten'—More than a Cambrian Konservat-Lagerstätte yielding exceptional preservation. *Palaeoworld*, 15: 266-282.

80. Mallatt, J.M. & Giribet, G. (2006). Further use of nearly complete 28S and 18S rRNA genes to classify Ecdysozoa: 37 more arthropods and a kinorhynch. *Mol. Phylogenet. Evol*., 40: 772–794.

81. Mallatt, J.M., Garey, J.R. & Shultz, J.W. (2004). Ecdysozoan phylogeny and Bayesian inference: first use of nearly complete 28S and 18S rRNA gene sequences to classify the arthropods and their kin. *Mol. Phylogenet. Evol.,* 31: 178–191.

82. Manton, S.M. (1949). Studies on the Onychophora VII. The early embryonic stages of *Peripatopsis* and some general considerations concerning the morphology and phylogeny of the Arthropoda. *Phil. Trans. R. Soc. B*, 233: 483-580.

83. Marchioro, T., Rebecchi, L., Cesari, M., Guldberg Hansen, J., Viotti, G. & Guidetti, R. (2013). Somatic musculature of Tardigrada: phylogenetic signal and metameric patterns. *Zool. J. Linn. Soc*., 169: 580–603.

84. Marshall, C.R. (2006). Explaining the Cambrian "explosion" of animals. *Annu. Rev. Earth Planet. Sci.,* 34: 355-384.

85. Martin, C., Gross, V., Hering, L., Tepper, B., Jahn, H., Oliveira, I.S., Stevenson, P.A. & Mayer, G. (2017). The nervous and visual systems of onychophorans and tardigrades: learning about arthropod evolution from their closest relatives. *J. Comp. Physiol. A*., 203: 565-590.

86. Martín-Durán, J.M. & Hejnol, A. (2015). The study of *Priapulus caudatus* reveals conserved molecular patterning underlying different gut morphogenesis in the Ecdysozoa. *BMC Biology*, 13: 29.

87. Mayer, G. (2016). Onychophora. In: A. Schmidt-Rhaesa, S. Harzsch and G. Purschke (eds.), *Structure and Evolution of Invertebrate Nervous Systems* (pp. 390-401). Oxford: Oxford University Press.

88. Mayer, G., Bartolomaeus, T. & Ruhberg, H. (2005). Ultrastructure of Mesoderm in Embryos of *Opisthopatus roseus* (Onychophora, Peripatopsidae): Revision of the "Long Germ Band" Hypothesis for *Opisthopatus. J. Morphol.,* 263: 60-70.

89. Mayer, G., Kauschke, S., Rüdiger, J. & Stevenson, P.A. (2013a). Neural markers reveal a one-segmented head in tardigrades (water bears). *PLoS ONE*, 8: e59090.

90. Mayer, G., Martin, C., Rüdiger, J., Kauschke, S., Stevenson, P.A., Poprawa, I., Hohberg, K., Schill, R.O., Pflüger, H.-J. & Schlegel, M. (2013b). Selective neuronal staining in tardigrades and onychophorans provides insights into the evolution of segmental ganglia in panarthropods. *BMC Evol. Biol*., 13: 230.

91. Mayer, G., Ruhberg, H. & Bartolomaeus, T. (2004). When an epithelium ceases to exist – an ultrastructural study on the fate of the embryonic coelom in *Epiperipatus biolleyi* (Onychophora, Peripatidae). *Acta Zoologica*, 85: 163–170.

92. Mayer, G., Whitington, P.M., Sunnucks, P. & Pfluger, H.-J. (2010). A revision of brain composition in Onychophora (velvet worms) suggests that the tritocerebrum evolved in arthropods. *BMC Evol. Biol.,* 10: 1–10.

93. Milne-Edwards, A. (1864). Sur un cas de transformation du peduncle oculaire en une antenne, observe chez une Langouste *(On a case of transformation of the ocular peduncle into an antenna, observed in a lobster). C. R. Acad. Sci.,* 59: 710-712. In French.

94. Mu, L., Ito, K., Bacon, J.P. & Strausfeld, N.J. (2012). Optic glomeruli and their inputs in *Drosophila* share an organizational ground pattern with the antennal lobes. *J. Neurosci.*, 32: 6061-6071.

95. Murdock, D.J.E., Gabbott, S.E., Mayer, G. & Purnell, M.A. (2014). Decay of velvet worms (Onychophora), and bias in the fossil record of lobopodians. *BMC Evol. Biol.,* 14: 222.

96. Murphey, R.K., Possidente, D., Pollack, G. & Merritt, D.J. (1989). Modality-specific axonal projections in the CNS of the flies *Phormia* and *Drosophila. J. Comp. Neurol.,* 290: 185-200.

97. Nagy, L.M. & Carroll, S. (1994). Conservation of wingless patterning functions in the short-germ embryos of *Tribolium castaneum*. *Nature*, 367: 460– 463.

98. Nielsen, C. (1995). *Animal Evolution, Interrelationships of the Living Phyla*. Oxford: Oxford University Press.

99. Nielsen, C. (2001). *Animal evolution.* Oxford: Oxford University Press.

100. Nixon, K.C. (1999). The Parsimony Ratchet, a New Method for Rapid Parsimony Analysis. *Cladistics,* 15: 407–41.

101. Okamura, J.Y. & Strausfeld, N.J. (2007). Visual system of calliphorid flies: motion- and orientation-sensitive visual interneurons supplying dorsal optic glomeruli. *J. Comp. Neurol*., 500: 189-208.

102. Oliveira, I.D.S., Kumerics, A., Jahn, H., Müller, M., Pfeiffer, F. & Mayer, G. (2019). Functional morphology of a lobopod: case study of an onychophoran leg. *R. Soc. Open Sci*., 6: 191200.

103. Oliveira, I.S. & Mayer, G. (2013). Apodemes associated with limbs support serial homology of claws and jaws in onychophora (velvet worms). *J. Morphol*., 274: 1180-1190.

104. Ortega-Hernández, J. (2014). Making sense of 'lower' and 'upper' stem-group Euarthropoda, with comments on the strict use of the name Arthropoda von Siebold, 1848. *Biol. Rev.,* 91: 255-273.

105. Ortega-Hernández, J., Janssen, R. & Budd, G.E. (2017). Origin and evolution of the panarthropod head - A palaeobiological and developmental perspective. *Arthropod Struct. Dev.*, 46: 354-379.

106. Ou, Q., Liu, J., Shu, D., Han, J. & Zhang, X.-G. (2011). A rare onychophoran-like lobopodian from the lower Cambrian Chengjiang Lagerstätte, Southwestern China, and its phylogenetic implications. *J. Paleontol.,* 85: 587-594.

107. Ou, Q., Shu, D. & Mayer, G. (2012). Cambrian lobopodians and extant onychophorans provide new insights into early cephalization in Panarthropoda. *Nat. Commun*., 3: 1261.

108. Paradis, E. & Schliep, K. (2018). Ape 5.0: an environment for modern phylogenetics and evolutionary analyses in R. *Bioinformatics*, 35: 526-528.

109. Park, T.S., Kihm, J., Woo, J., Park, C., Lee, W.Y., Smith, M.P., Harper, D.A.T., Young, F., Nielsen, A.T. & Vinther, J. (2018). Brain and eyes of *Kerygmachela* reveal protocerebral ancestry of the panarthropod head. *Nat. Commun.,* 9: 1019.

110. Patel, N.H., Kornberg, T.B. & Goodman, C.S. (1989b). Expression of engrailed during segmentation in grasshopper and crayfish. *Dev.*, 107: 201-212.

111. Patel, N.H., Martin-Blanco, E., Coleman, K.G., Poole, S.J., Ellis, M.C., Kornberg, T.B. & Goodman C.S. (1989a). Expression of *engrailed* proteins in arthropods, annelids, and chordates. *Cell*, 58: 955-968.

112. Petrov, N.B. & Vladychenskaya, N.S. (2005). Phylogeny of molting protostomes (Ecdysozoa) as inferred from 18S and 28S rRNA gene sequences. *Mol Biol*., 39: 590–601.

113. Pfeiffer, K. & Homberg, U. (2014). Organization and functional roles of the central complex in the insect brain. *Annu. Rev. Entomol*., 59: 165–184.

114. Philippe, H., Lartillot, N. & Brinkmann, H. (2005). Multigene analyses of bilaterian animals corroborate the monophyly of Ecdysozoa, Lophotrochozoa, and Protostomia. *Mol. Biol. Evol*., 22: 1175–1184.

115. Podsiadlowski, L., Braband, A., Mayer, G. (2008). The complete mitochondrial genome of the onychophoran *Epiperipatus biolleyi* reveals a unique transfer RNA set and provides further support for the Ecdysozoa hypothesis. *Mol. Biol. Evol*., 25: 42–51.

116. Posnien, N., Koniszewski, N.D.B., Hein, H.J. & Bucher, G. (2011). Candidate gene screen in the red flour beetle *Tribolium* reveals *six3* as ancient regulator of anterior median head and central complex development. *PLoS Genet*. 7, e1002416.

117. Pourqui, O. (2003). The segmentation clock: converting embryonic time into spatial pattern. Science, 301: 328-330.

118. Prpic, N.M., Wigand, B., Damen, W.G. & Klingler, M. (2001). Expression of *dachshund* in wild-type and *distal-less* mutant *Tribolium* corroborates serial homologies in insect appendages. *Dev. Genes Evol.,* 211: 467– 477.

119. R Core Team. (2019). R: A language and environment for statistical computing. R Foundation for Statistical Computing, Vienna, Austria. URL https://www.R-project.org/.

120. Rempel, J.G. (1975). The Evolution of the Insect Head: The Endless Dispute. *Quaest. Entomol.,* 11: 7-25.

121. Richter, S., Loesel, R., Purschke, G., Schmidt-Rhaesa, A., Scholtz, G., Stach, T., Vogt, L., Wanninger, A., Brenneis, G., Döring, C., Faller, S., Fritsch, M., Grobe, P., Heuer, C.M., Kaul, S., Møller, O.S., Müller, C.H., Rieger, V., Rothe, B.H., Stegner, M.E. & Harzsch, S. (2010).

Invertebrate neurophylogeny: suggested terms and definitions for a neuroanatomical glossary. *Front. Zool*., 46: 354-379.

122. Riebli, N. & Reichert, H. (2016). Perspective – The First Brain. In: In: A. Schmidt-Rhaesa, S. Harzsch & G. Purschke (eds.) *Structure and Evolution of Invertebrate Nervous Systems.* (pp. 67-73) Oxford: Oxford University Press.

123. Rivera, A.S., Gonsalves, F.C., Song, M.H., Norris, B.J. & Weisblat, D.A. (2005). Characterization of Notch-class gene expression in segmentation stem cells and segment founder cells in *Helobdella robusta* (Lophotrochozoa; Annelida; Clitellata; Hirudinida; Glossiphoniidae). *Evol. Dev.*, 7: 588-599.

124. Ruiz-Trillo, I., Paps, J., Loukota, M., Ribera, C., Jondelius, U., Bagunà, J. & Riutort, M. (2002). A phylogenetic analysis of myosin heavy chain type II sequences corroborates that Acoela and Nemertodermatida are basal bilaterians. *Proc. Natl. Acad. Sci. USA*, 99: 11246–51.

125. Sanchez-Salazar, J., Pletcher, M.T., Bennett, R.L., Brown, S.J., Dandamudi, T.J., Denell, R.E. & Doctor, J.S. (1996). The *Tribolium decapentaplegic* gene is similar in sequence, structure, and expression to the *Drosophila dpp* gene. *Dev. Genes Evol.*, 206: 237– 246.

126. Sanes, J.R. & Zipursky, S.L. (2010). Design principles of insect and vertebrate visual systems. *Neuron,* 66: 15-36.

127. Satterlee, J.S., Sasakura, H., Kuhara, A., Berkeley, M., Mori, I. & Sengupta, P. (2001). Specification of thermosensory neuron fate in *C. elegans* requires *ttx-1*, a homolog of *otd/Otx*. *Neuron*, 31: 943–956.

128. Schinko, J.B., Kreuzer, N., Offen, N., Posnien, N., Wimmer, E.A. & Bucher, G. (2008). Divergent functions of *orthodenticle*, empty spiracles and buttonhead in early head patterning of the beetle *Tribolium castaneum* (Coleoptera). *Dev. Biol*., 317: 600-613.

129. Schmidt-Rhaesa, A. & Henne, S. (2017). Cycloneuralia (Nematoda, Nematomorpha, Priapulida, Kinoryhnca, Loricifera). In: A. Schmidt-Rhaesa, S. Harzsch, & G. Purschke (eds.) *Structure and Evolution of Invertebrate Nervous Systems.* Oxford: Oxford University Press.

130. Schmidt-Rhaesa, A. (2007). Body Cavities. In: *The Evolution of Organ Systems*. (pp. 148-169) Oxford: Oxford University Press.

131. Scholtz, G. & Edgecombe, G.D. (2005). Heads, Hox and the phylogenetic position of trilobites. In: S. Koenemann & R.A. Jenner (eds.) *Crustacea and Arthropod Relationships* (pp. 139-165). Boca Raton, Florida: CRC Press.

132. Scholtz, G. & Edgecombe, G.D. (2006). The evolution of arthropod heads: reconciling morphological, developmental and palaeontological evidence. *Dev. Genes Evol*., 216: 395-415.

133. Scholtz, G. (1998). Cleavage, germ band formation and head segmentation: the ground pattern of the Euarthropoda. In: R.A. Fortey & R.H. Thomas (eds.) *Arthropod Relationships, Systematics Association Special Volume Series 55* (pp. 317-332). London: Chapman & Hall.

134. Scholtz, G. (2002). The Articulata hypothesis – or what is a segment? *Org. Divers. Evol*., 2: 197–215.

135. Scholtz, G. (2016). Perspective – Heads and Brains in Arthropods: 40 years after the 'Endless Dispute'. In: A. Schmidt-Rhaesa, S. Harzsch & G. Purschke (eds.) *Structure and Evolution of Invertebrate Nervous Systems.* (pp. 402-418) Oxford: Oxford University Press.

136. Schulze, C. & Persson, D. (2016). Tardigrada. In: A. Schmidt-Rhaesa, S. Harzsch, & G. Purschke (eds.) *Structure and Evolution of Invertebrate Nervous Systems.* (pp. 383-389) Oxford: Oxford University Press.

137. Schulze, C. & Schmidt-Rhaesa, A. (2011). Organisation of the musculature of *Batillipes pennaki. Meiofauna Mar.,* 19: 195–207.

138. Schumann, I., Kenny, N., Hui, J., Hering, L. & Mayer, G. (2018). Halloween genes in panarthropods and the evolution of the early moulting pathway in Ecdysozoa. *R. Soc. Open Sci.,* 5: 180888.

139. Schürman, F.W. (1987). Histology and Ultrastructure of the Onychophoran Brain. In: A.P. Gupta (ed.) *Arthropod Brain: Its Evolution, Development, Structure, and Functions.* (pp. 158-180) New York: A Wiley-Interscience Publication, John Wiley & Sons.

140. Sempere, L.F., Martinez, P., Cole, C., Baguñà, J. & Peterson, K.J. (2007). Phylogenetic distribution of microRNAs supports the basal position of acoel flatworms and the polyphyly of Platyhelminthes. *Evolut Develop*., 9: 409–415.

141. Sereno, P.C. (2007). Logical basis for morphological characters in phylogenetics. *Cladistics,* 23: 565–587.

142. Sereno, P.C. (2009). Comparative cladistics. *Cladistics*, 25: 624–659.

143. Smith, F.W., Bartels, P.J. & Goldstein, B. (2017). A Hypothesis for the Composition of the Tardigrade Brain and its Implications for Panarthropod Brain Evolution. *Integr. Comp. Biol.,* 57: 546-559.

144. Smith, F.W., Boothby, T.C., Giovannini, I., Rebecchi, L., Jockusch, E.L. & Goldstein, B. (2016). The Compact Body Plan of Tardigrades Evolved by the Loss of a Large Body Region. *Curr. Biol.,* 26, 224–229.

145. Smith, M.R. & Ortega-Hernández, J. (2014). *Hallucigenia's* onychophoran-like claws and the case for Tactopoda. *Nature*, 514: 363-366.

146. Snodgrass, R.E. (1960). Facts and theories concerning the insect head. *Smithson. Misc. Collect*., 142: 1-61.

147. Steinmetz, P.R.H., Kostyuchenko, R.P., Fischer, A. & Arendt, D. (2011). The segmental pattern of *otx, gbx*, and *Hox* genes in the annelid *Platynereis dumerilii*. *Evol. Dev*., 13: 72–79.

148. Stollewerk, A., Schoppmeier, M. & Damen, W.G. (2003). Involvement of *Notch* and *Delta* -genes in spider segmentation. *Nature*, 423: 863-865.

149. Strausfeld, N.J. & Hirth, F. (2013). Deep homology of arthropod central complex and vertebrate basal ganglia. *Science,* 340: 157-161.

150. Strausfeld, N.J. (2012). Reiterations, Appendages, and the Ancient Brain. In: *Arthropod Brains: Evolution, Functional Elegance, and Historical Significance.* (pp.401-454) London: The Belknap Press of Harvard University Press.

151. Strausfeld, N.J., Ma, X., Edgecombe, G.D., Fortey, R.A., Land, M.F., Liu, Y., Cong, P. & Xian-Guang, H. (2016). Arthropod eyes: The early Cambrian fossil record and divergent evolution of visual systems. *Arthropod Struct. Dev.,* 45: 152-172.

152. Turner-Evans, D.B. & Jayaraman, V. (2016). The insect central complex. *Curr. Biol.,* 26: R453-R457.

153. Urbach, R. & Technau, G.M. (2003). Molecular markers for identified neuroblasts in the developing brain of *Drosphila*. *Dev*., 130: 3621-3637.

154. Urbach, R. & Technau, G.M. (2004). Neuroblast formation and patterning during early brain development in *Drosophila. BioEssays*, 26: 739-751.

155. Valentine, J.W. & Hamilton, H. (1997). Body plans, phyla and arthropods. In: R.A. Fortey & R.H. Thomas (eds.) *Arthropod Relationships, Systematics Association Special Volume Series 55* (pp.1-9). London: Chapman & Hall.

156. Valentine, J.W., Jablonski, D. & Erwin, D.H. (1999). Fossils, molecules and embryos: new perspectives on the Cambrian explosion. *Development,* 126: 851–859.

157. Van Roy, P., Daley, A.C. & Briggs, D.E.G. (2015). Anomalocaridid trunk limb homology revealed by a giant filter-feeder with paired flaps. *Nature*, 522: 77-80.

158. Wägele, J.W., Eriksson, T., Lockhart, P. & Misof, G. (1999). The Ecdysozoa: artifact or monophylum? *J. Zool. Syst. Evol. Res*., 37: 211–223.

159. Waggoner, B.M. (1996). Phylogenetic hypotheses of the relationships of arthropods to Precambrian and Cambrian problematic fossil taxa. *Syst. Biol.,* 45: 190–222.

160. Walker, M.H. & Tait, N. (2004). Studies of embryonic development and the reproductive cycle in ovoviviparous Australian Onychophora (Peripatopsidae). *J. Zool., Lond.,* 264: 333–354.

161. Walossek, D. & Müller, K.J. (1998). Cambrian 'Orsten'-type arthropods and the phylogeny of Crustacea. In: R.A. Fortey & R.H. Thomas (eds.) *Arthropod Relationships, Systematics Association Special Volume Series 55* (pp. 139-153). London: Chapman & Hall.

162. Waloszek, D., Chen, J., Maas, A. & Wang, W. (2005). Early Cambrian arthropods – new insights into arthropod head and structural evolution. *Arthropod. Struct. Dev*., 34: 189-205.

163. Warren, R. & Carroll, S. (1995). Homeotic genes and diversification of the insect body plan. *Curr. Opin. Genet. Dev*. 5, 459-465.

164. Weygoldt, B.P. (1986). Arthropod interrelationships – the phylogenetic-systematic approach. *J. Zool. Syst. Evol. Res.,* 24: 19–35.

165. White, J.G., Southgate, E., Thomson, J.N. & Brenner, F.R.S. (1986). The structure of the nervous system of the nematode *Caenorhabditis elegans. Phil. Trans. R. Soc. Lond. B.,* 314: 1-340.

166. Whittington, H.B. (1978). The lobopod animal Aysheaia pedunculata Walcott, middle Cambrian, Burgess Shale, British Columbia. *Phil. Trans. R. Soc. Lond. B. Biol. Sci.,* 284: 165-197.

167. Wilmer, P. (1990). Morphological patterns and traditional divisions: Body cavities. In: *Invertebrate Relationships: Patterns in animal evolution.* (pp. 22-39). Cambridge: Cambridge University Press.

168. Wolff, T., Iyer, N. & Rubin, G. (2014). Neuroarchitecture and neuroanatomy of the *Drosophila* central complex: A GAL4-based dissection of protocerebral bridge neurons and circuits. *J. Comp. Neurol.*, 523: 997–1037.

169. Yang, J., Ortega-Hernández, J., Butterfield, N.J., Liu, Y., Boyan, G.S., Hou, J.-B., Lan, T. & Zhang, X.-G. (2016). Fuxianhuiid ventral nerve cord and early nervous system evolution in Panarthropoda. *PNAS,* 113: 2988-2993.

170. Zhang, X.-G., Smith, M.R., Yang, J. & Hou, J.-B. (2016) Onychophoran-like musculature in a phosphatized Cambrian lobopodian*. Biol. Lett*., 12: 20160492.

171. Zhang, Z.-Q. (2011). Animal biodiversity: an outline of higher-level classification and survey of taxonomic richness*. Zootaxa*, 3148: 1-237.

172. Zhang, Z.-Q. (2013). Animal biodiversity: an outline of higher-level classification and survey of taxonomic richness (Addenda 2013). *Zootaxa,* 3703: 1-82.

# ADDITIONAL REFERENCES

## ART & PHOTOGRAPHY

### PHOTOGRAPHY AND SCIENTIFIC ILLUSTRATION


I. Baer, A., Hansch, S., Mayer, G., Harrington, M.J. & Schmidt, S. (2018). Reversible supramolecular assembly of velvet worm adhesive fibers via electrostatic interactions of charged phosphoproteins. *Biomacromolecules*, 19: 4034–43.

II. Dowding, J. (n.d.). *Swallowtail caterpillar*. [online] Greenwings Wildlife Holidays. Available at: https://greenwings.co/our-holidays/butterfly-holidays/swallowtail-weekend-norfolk/swallowtail-caterpillar-by-julian-dowding/ [Accessed 17/10/2019].

III. Natural History Museum / Alamy Stock Photo (n.d.). Ranina ranina, *spanner crab* [image].

IV. Otto, J. (2015). *Peacock spider* Maratus caeruleus. [online] Flickr. Available at: https://www.flickr.com/photos/59431731@N05/20584033858/in/photostream [Accessed 17/10/2019].

V. Science Photo Library (n.d.). Water Bear, SEM [image].


### CHAPTER MARKERS

CHAPTER 1


Alternate Prehistory (2017). *Bubba gump*. [online] Deviantart. Available at: https://www.deviantart.com/alternateprehistory/art/Bubba-gump-701973034 [Accessed 17/10/2019].


CHAPTER 2


Cowpland (n.d.). *Microscope silhouette vector image*. [online] VectorStock. Available at: https://www.vectorstock.com/royalty-free-vector/microscope-silhouette-vector-15840206 [Accessed 18/10/2019].


CHAPTER 5


Wachsmuth, D. (n.d.). *Hallucigenia.* [online] Dirkwachsmuth.cgsociety.org. Available at: https://dirkwachsmuth.cgsociety.org/9pi8/hallucigenia [Accessed 30/09/2019].

## REFERENCES

Tchijova, N. (n.d.). *Black silhouette of open book.* [online] 123RF. Available at: https://www.123rf.com/photo_18843887_black-silhouette-of-open-book-.html [Accessed 31/10/2019].

## ADDITIONAL REFERENCES

Sound Experience. (n.d.). *Camera clipart.* [online] Available at: https://www.soundexp.org/party-for-adventuress/camera-clipart-camera-clipart-clipart-free-clipart-images-free-clipart-and/ [Accessed 31/10/2019].

## APPENDIX

Жуковецкая, Ю. (n.d.). *Human appendix black icon.* [online] 123RF. Available at: https://www.123rf.com/photo_61468887_stock-vector-human-appendix-black-icon.html [Accessed 31/10/2019].

# APPENDIX

## CHAPTER 1

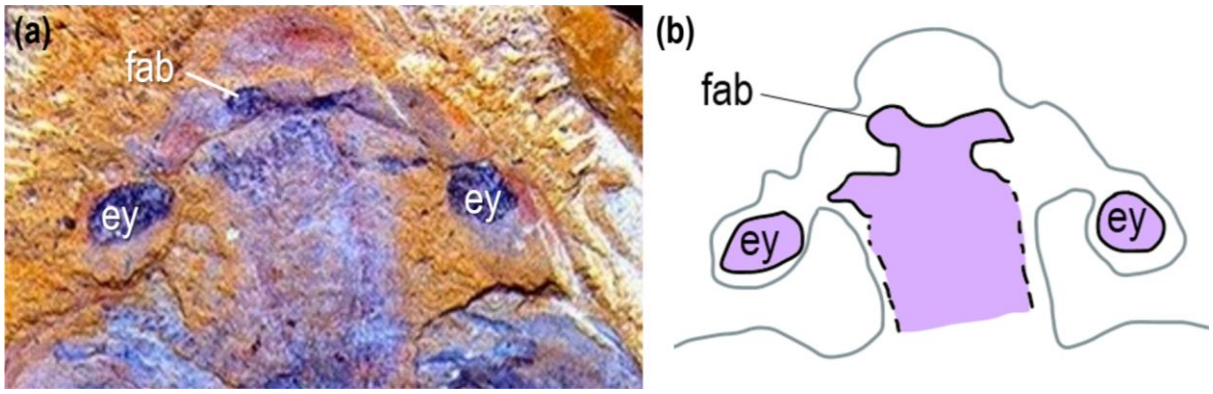


**APPENDIX 1.1.** *Anterior region of the stem-group Cambrian euarthropod* Lyrarapax unguispinus. (a) *Original fossil material. Modified from Cong et al. (2014).* (b) *Revised Illustration.*

***Abbreviations:*** *ey, eye; fab, frontal appendage base.*

## CHAPTER 2

**APPENDIX 2.1.** *Figshare links to scanning electron micrographs (SEM) and synchrotron x-ray computed tomography (sXCT) datasets. Files enabling a reconstruction of the 3D model and Avizo project are denoted by asterisks.*

| File name | Figshare link |
|---|---|
| Avizo project* | https://figshare.com/s/ddd663b4d3cf7254b016 |
| sXCT dataset* | https://figshare.com/s/c780af60a647116fb215 |
| All label fields* | https://figshare.com/s/d5168e671e6dc8b13630 |
| Label surfaces* | https://figshare.com/s/b202056975a94a95041e |
| Individual label fields | https://figshare.com/s/942be3f8584a7790b427 |
| SEM dataset | https://figshare.com/s/b8595986247d3a974fbf |

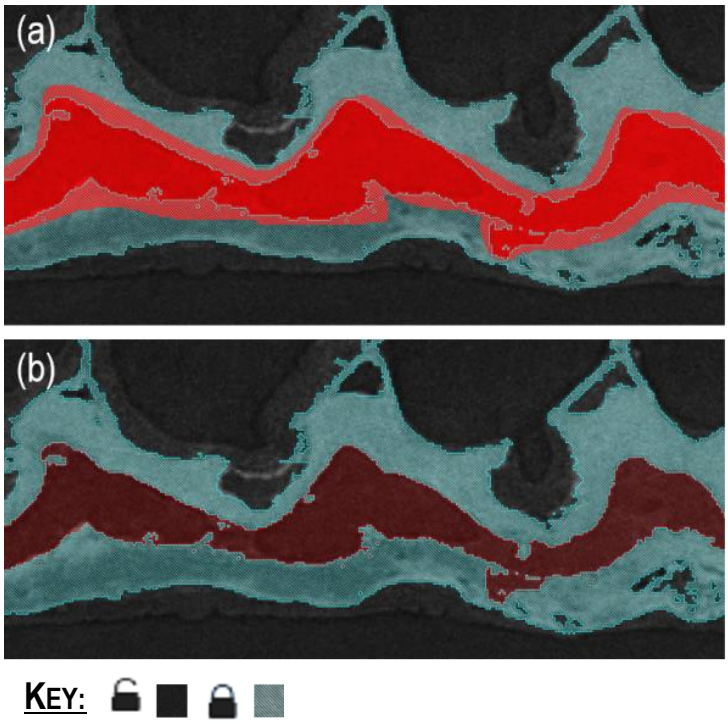


**APPENDIX 2.2.** *Where needed, individual internal chambers were segmented using the <brush> tool (show in red). By locking the tissue previously mapped by the <magic wand> (shown here in pale blue/grey), chambers could be traced roughly without editing the locked material. The rough tracing of the chamber is shown in bright red* (a), *whilst the resulting label is shown in dark red in* (b).

**APPENDIX 2.3.** *CODE USED TO GENERATE A MAXIMUM PARSIMONY TREE IN R*

Tree space was searched using Nearest Neighbour Interchanges with the parameters maxHits and maxIter set to 100. A more extensive search was conducted using Nixon's (1999) parsimony ratchet, where SearchHits= 40, SearchIter = 2000, RatchIter=10. An arbitrary Goloboff's (1993) concavity (k) constant of 6 and verbosity value of 2 were selected. Annotations are indicated in blue.

```
library(TreeSearch)

library(ape)

setwd(paste0( 'insert file destination here'))

matrix.data <-  'insert matrix file name here (i.e. supplementary material 1)'

dataset <- ReadAsPhyDat(matrix.data)

nj.tree <- NJTree(dataset)

outgroup <- "insert outgroup here (i.e. Tubiluchus_Priapulida)"
```

```
rooted.tree <- EnforceOutgroup(nj.tree, outgroup)

better.tree <- IWTreeSearch(tree=rooted.tree, concavity = 6, dataset=dataset,
EdgeSwapper=RootedNNISwap, verbosity=2)

better.tree <- IWTreeSearch(better.tree, dataset, concavity = 6, maxHits=100,
maxIter=100, EdgeSwapper=RootedTBRSwap, verbosity=2)

best.tree <- IWRatchet(better.tree, dataset, concavity = 6, verbosity=2,
ratchIter=10,

swappers=list(RootedTBRSwap, RootedSPRSwap, RootedNNISwap))

write.nexus(best.tree, file= path/to/file) #insert file destination to save tree
```

# CHAPTER 3

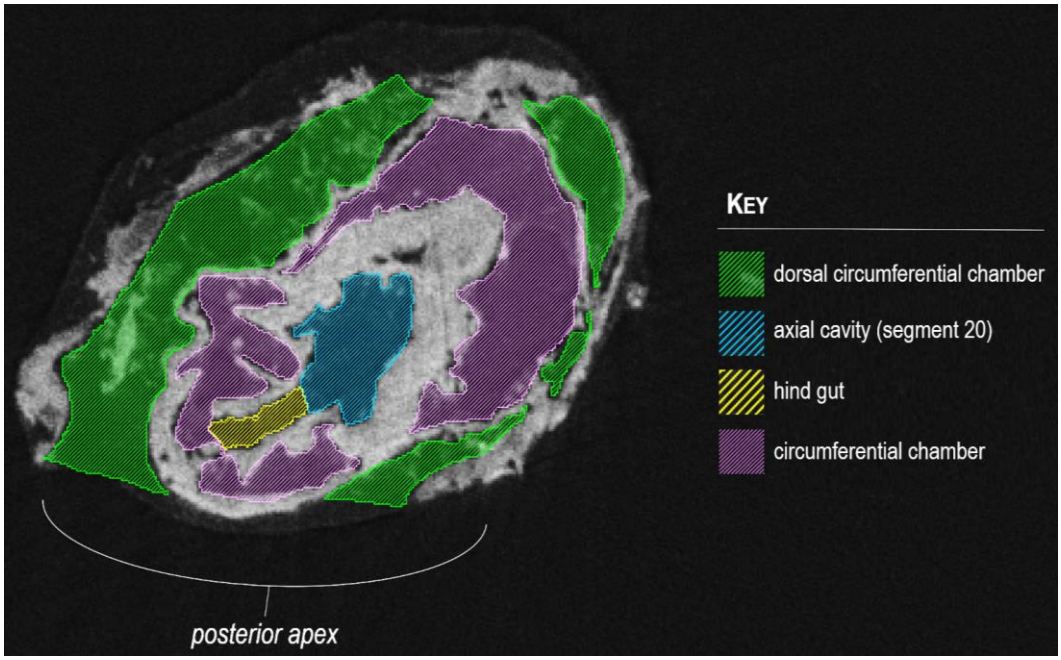


**APPENDIX 3.1.** *Lateral orthoslice of the sXCT data. Ventral is left. The anal tube (yellow), which projects from the axial cavity (blue) of the posteriormost segment, does not perforate the exterior to form an anus. It is instead capped by the circumferential chamber (pink), a layer of flesh, and the apical posterior cavity (green).*

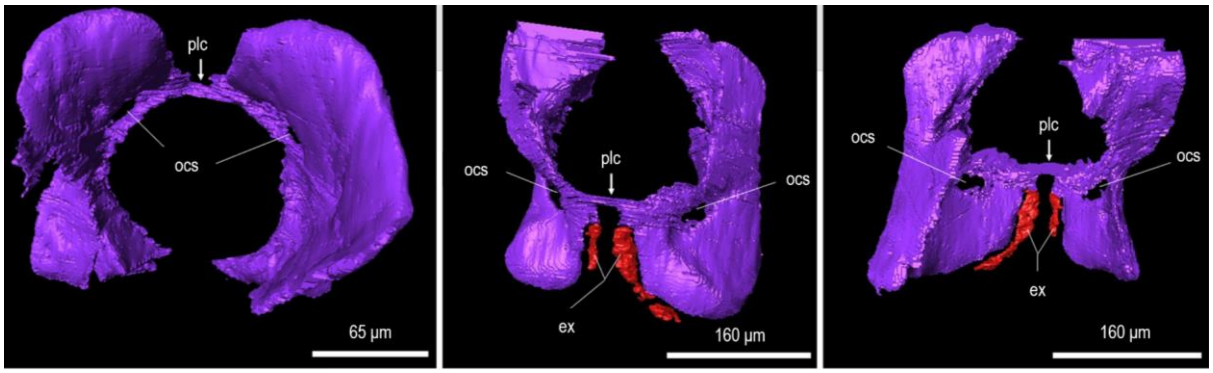


**APPENDIX 3.2.** *3D renders of the first axial cavity segment generated in Avizo. The first segment is modified into halves that flank the foregut.* (a) *Anterior view, ventral is up.* (b) *Posterior view, dorsal is up.* (c) *Tilted dorsal view. Posterior is up. Oblate cylindrical structures (ocs) puncture the ventral aspect of chamber. A pair of ventral extensions (ex), coloured red, are depicted in* (b) *and* (c)*. White arrows indicate a posterolateral connection between the two halves of the cavity.*

***Abbreviations:*** *ex, axial cavity paired extensions; ocs, oblate cylindrical structure; plc, posterolateral connective.*

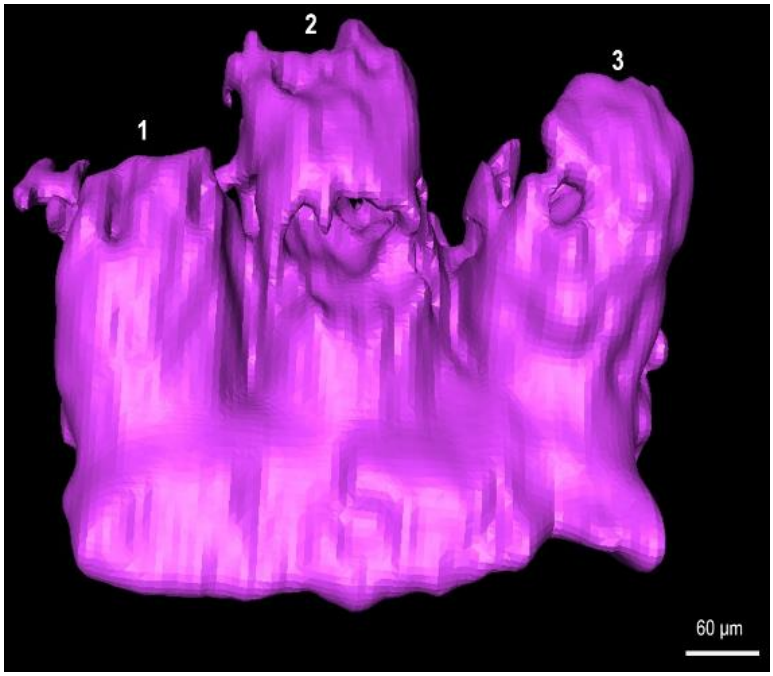


**APPENDIX 3.3.** *3D render of the trilobed chamber generated in Avizo. Dorsal is up.*

# CHAPTER 4

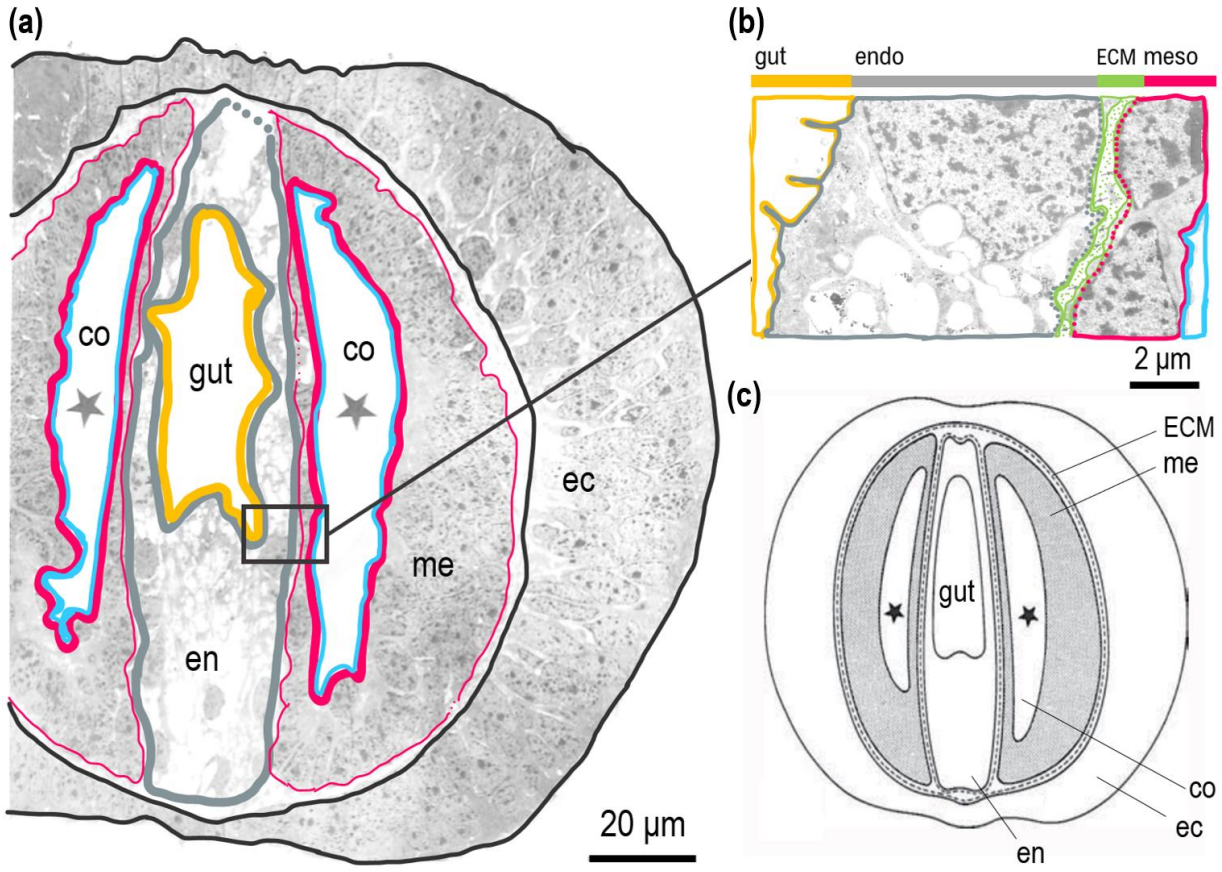


**APPENDIX 4.1.** *Cross section through the body of an* Epiperipatus biolleyi *onychophoran embryo.* (a) *The gut is enclosed by layers of endoderm (en / endo) and mesoderm (me / meso). The transitory embryonic coelom (co), indicated by stars, is situated within the mesoderm (me) to either side of the gut.* (b) *Close-up of* (a) *depicting part of the gut and coelom.* (c) *Illustration depicting transitory coelomic spaces during ontogeny. Modified from Bartolomaeus, & Ruhberg, 1999.*

***Abbreviations:*** *co, coelom; ec / ecto, ectoderm; ECM, extracellular matrix; en / endo, endoderm; me / meso, mesoderm.*

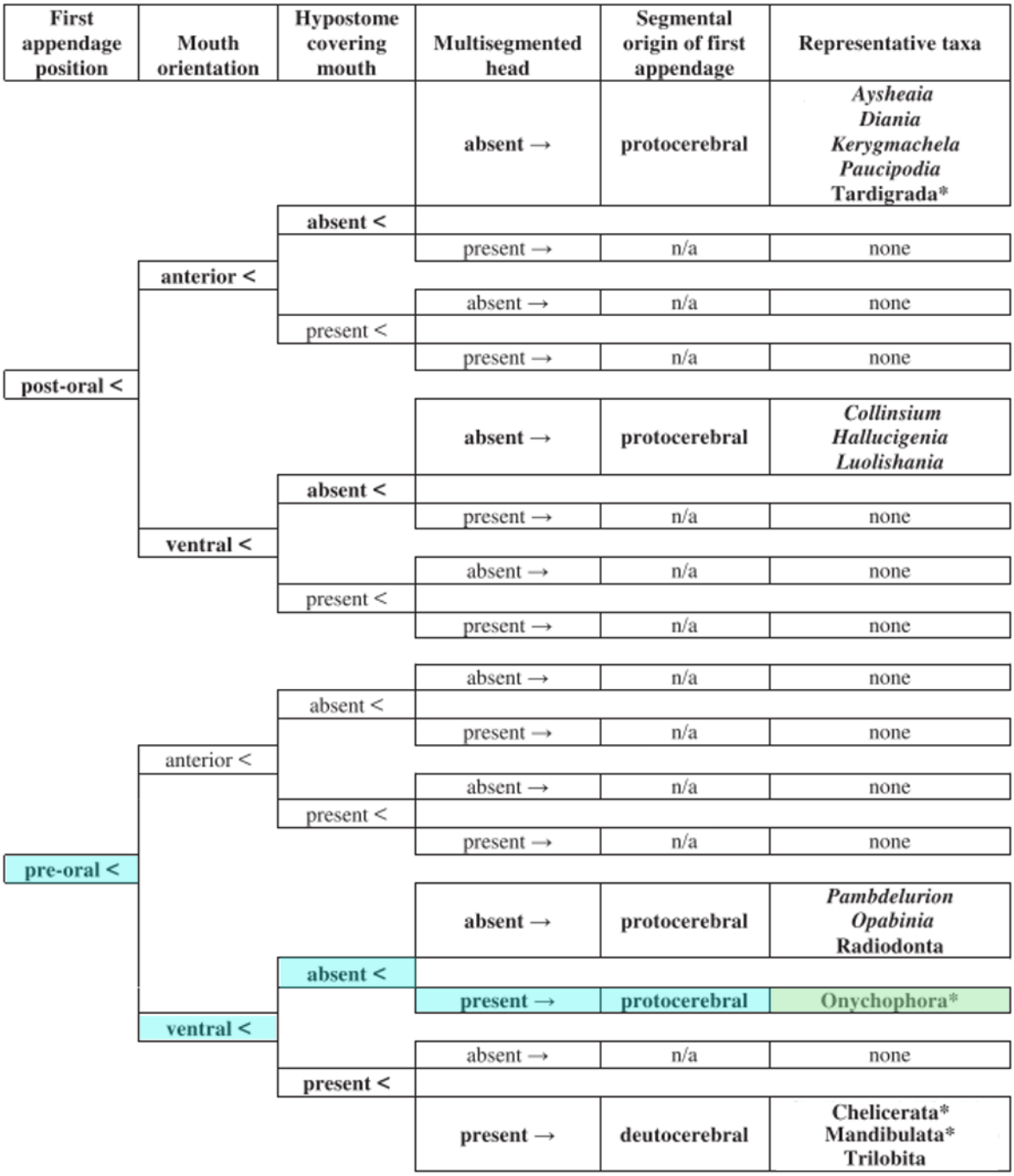


**APPENDIX 4.2.** *Key for determining segmental affinity of the anteriormost appendages in extant (*) and extinct panarthropods. YKLP 12357, the pathway for which is highlighted in green, is resolved here as an onychophoran. Pathways leading to known taxa are indicated in bold letters. Modified from Ortega-Hernández et al., 2017.*

# CHAPTER 5

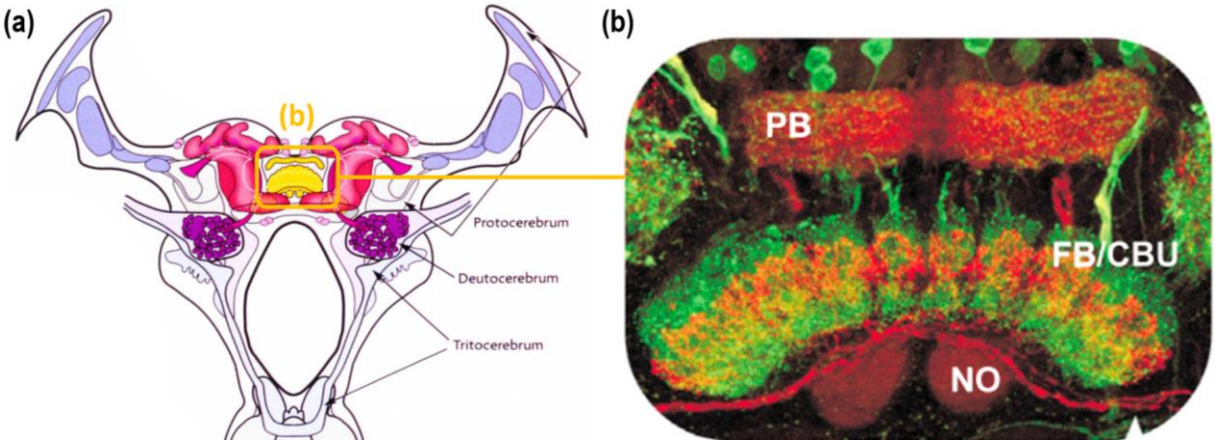


**APPENDIX 5.1.** *The central complex and support structures of an adult* Periplaneta americana *(American cockroach) brain. Anterior is up.* (a) *Illustration, frontal view. Arrows indicate the extent of the protocerebrum, deutocerebrum, and tritocerebrum. Mushroom bodies, shown in pink, dominate the protocerebral segment, and are positioned to either side of the central complex, which is shown in yellow. From Strausfeld, 2012.* (b) *Double immunolabelling. Close-up of the central complex and support structures. Allatostatin-like (AS) and tachykinin-related peptide (TRP) are coloured green and red respectively. From Turner-Evans & Jayaraman (2016), modified from Loesel et al. (2002).*

***Abbreviations**: CBU, central body upper; FB, fan-shaped body; NO, noduli; PB, protocerebral bridge.*

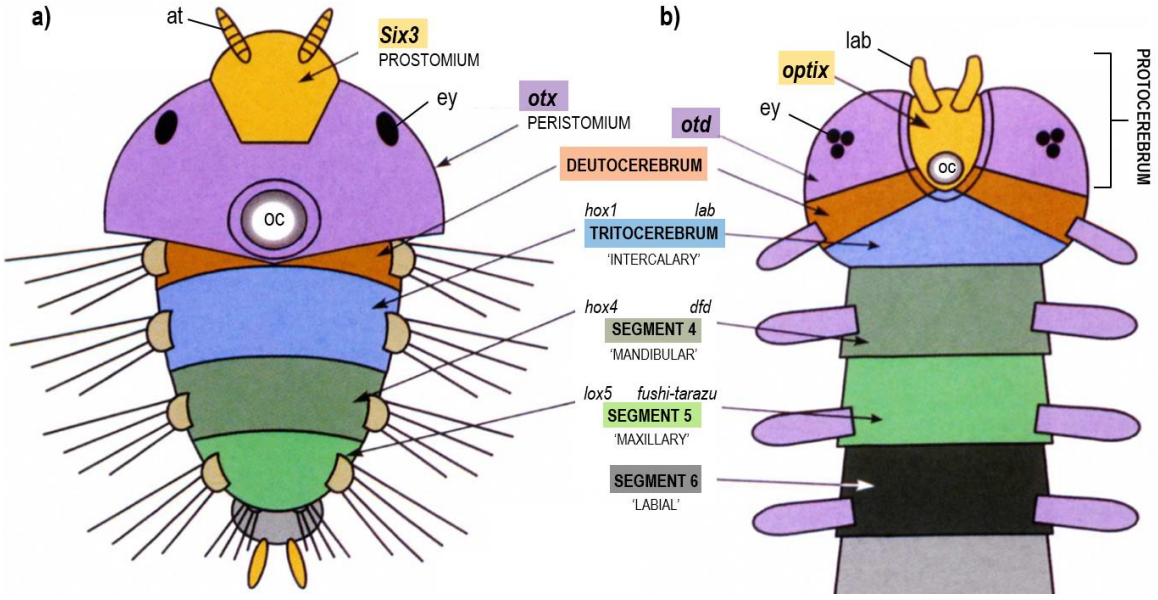

**APPENDIX 5.2.** *See previous page. Hypothesis for head segment alignment in* (a) Platynereis *(annelid) larvae, after Steinmetz et al. (2011), and* (b) *a* Triboleum *(euarthropod) embryo, after Urbach and Technau (2003). Ventral view, anterior is up. In both taxa, the six 3 / optix domain, which bears the annelid antennae and the euarthropod labrum, is considered asegmental. The succeeding domains are segmental. Figure adapted from Strausfeld (2012).*

***Abbreviations:*** *at, antenna; ey, eye; lab, labrum; oc, oral cavity; otd, orthodenticle.*

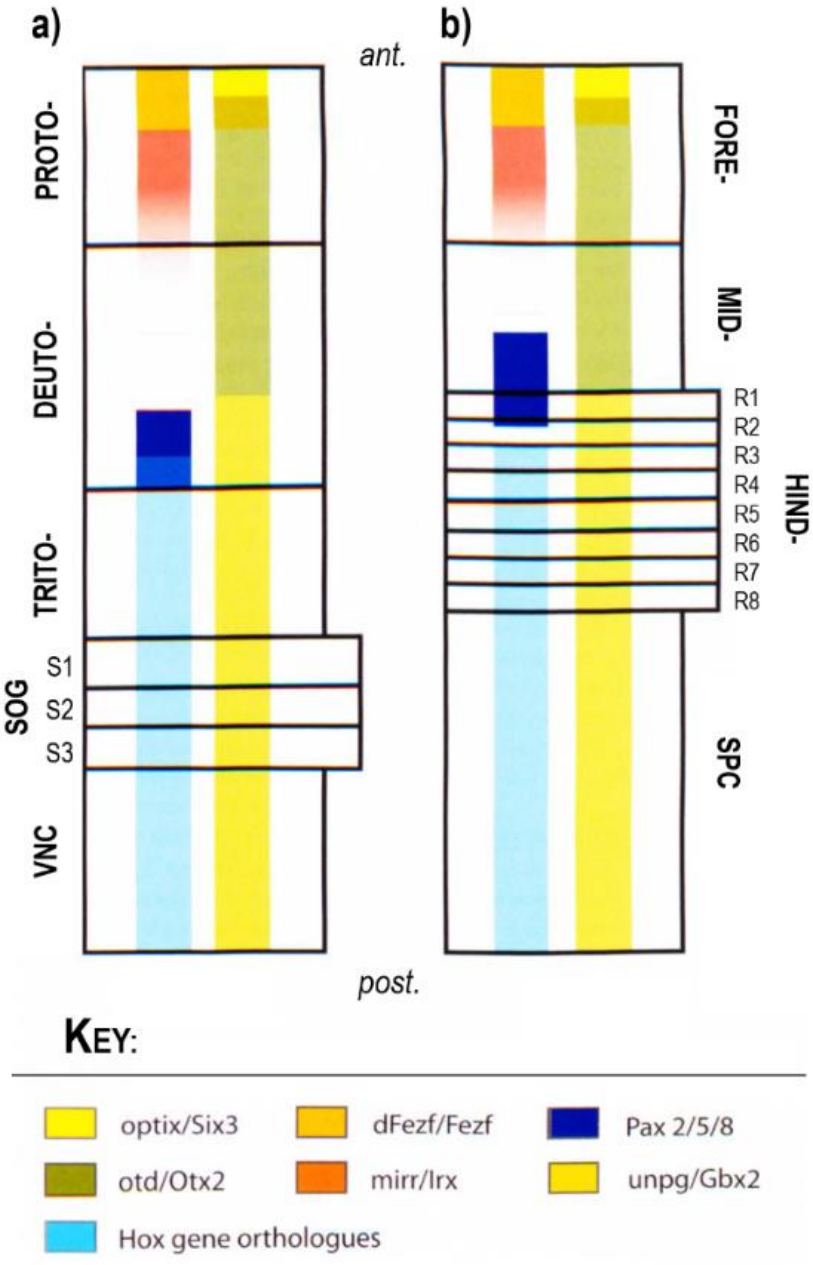


**APPENDIX 5.3**. *Expression of conserved developmental control genes along the anterior-posterior (ant. / post.) axis, schematically depicted as coloured domains, in the developing central nervous systems of bilaterians. Expression patterns are remarkably similar in both* (a) *mice and* (b) *Drosophila, indicating a shared common origin. Figure adapted from Riebli and Reichert (2016).*

***Abbreviations:*** *ant, anterior; deuto-, deutocerebrum; fore-, forebrain; hind-, hindbrain; post, posterior; mid-, midbrain; proto-, protocerebrum; r, rhombomere; s, segment; sog, suboesophageal ganglion; spc, spinal cord; trito-, tritocerebrum; vnc, ventral nerve cord.*

**PLATE 1.** ***Refer to supplementary material*** *for high resolution image. SEM micrographs depicting lateral views of* (a) *a Stage IV Euperipatoides rowelli (extant onychophoran) embryo and* (b) *YKLP 12387, a stage-3 Cambrian lobopodian embryo. Anterior is up, dorsal is right. Both animals exhibit a posteriad reduction in trunk appendage (t) length and a ventral oral cavity (oc).* (a) *Ventrolateral antennae (at) are succeeded by the jaws (jw), visible as developing lobopodous appendages, the slime papillae (sp), and the walking legs (t1-14). The head region is continuous with the trunk. Figure adapted from Walker & Tait (2004).* (b) *A constriction of the body distinguishes the trunk from an additional anterior module. The specimen's stunted anteriormost appendages (aa) are positioned laterally and are derived from the additional anterior region. Paraoral eyes (ey) are situated at the base of the anteriormost appendages in the first true body segment. The first stunted and uniquely lateral trunk appendage (t1) is succeeded by 16 ventrolateral trunk appendages (t2-17). The first nine appendages are rounded, whilst t13-17 are conical. The original morphologies of t10-12 are not preserved. Unlike E. rowelli, the fossil specimen does not possess an anus (an).*

***Abbreviations:*** *aa, asegmental appendages; an, anus; at, antennae; ey, eye; oc, oral canal; t, trunk appendage.*

**PLATE 2.** ***Refer to supplementary material*** *for high resolution image.* (a), (b)i), (c): *3D renders of YKLP 12387 generated in Avizo.* (b)ii) *Interpretative illustration.* (a) *Lateral view. The additional anterior module is demarcated by a constriction of the trunk (indicated by a dashed line). This region is distinguishable from the succeeding segments by the absence of the segmental organ systems, such as the longitudinal dorso- (ds) and ventrolateral sinuses, the intestinal system, and the axial cavity (ac). Paraoral eyes (ey) are situated in the first true body segment at the base of the anteriormost appendages, which are derived from the 'core' anterior cavity (cac) predominating the additional anterior module. The circumoral ring (cor) links the ventral aspect of the circumferential chamber (ccv) to this module. The lateral and dorsal aspects of the circumferential chamber are omitted for clarity, whilst the ventral component is only depicted in the first few segments. The intestinal opens anteroventrally, terminating in blind hindgut (hg).* (b) *Dorsal view. Both a dorsal extension of the core anterior cavity (cd) and the anterodorsal cavity (ad) run along the specimen's plane of bilateral symmetry. The core anterior cavity's lateral extensions (al) are adjacent to these voids. Both the lateral extensions and the asegmental dorsal chamber do not proceed beyond the third segment, whilst the dorsal extension is believed to extend along the entire trunk. (i) A poorly preserved region of the anterodorsal chamber extends into the additional anterior module. (ii) The presumed extent of the anterodorsal chamber, the core anterior cavity's dorsal extension, and the dorsolateral sinuses are illustrated.* (c) *Ventral view of the anterior, dorsolateral view of the posterior. The circumoral component of the circumferential cavity has been omitted for clarity. The trilobed chamber (tlc) corresponds to an oval-shaped ventral opening positioned just posterior to the oral cavity (oc). See caption for Plate 3 for abbreviations list.*

---

***Plates 2 & 3 – Abbreviations:*** *aa, anteriormost appendages; aac, anteriormost appendages lateral connective; ac, axial cavity; ad, anterodorsal dorsal cavity; ate, axial cavity trunk appendage extension; av, anteroventral cavity; cac, core anterior cavity; cc, circumferential chamber; ccv, circumferential chamber ventral component; cd, core anterior chamber (cac) dorsal extension; cl, core anterior chamber (cac) lateral extensions; cor, circumoral ring; ds, dorsolateral sinuses; dsc, dorsolateral sinus (ds) connective; dsp, dorsolateral sinus (ds) process; ey, eye; eyi, inner ocular structure; eyo, outer ocular structure; fg, foregut; hg, hindgut; i, inner; mg, midgut; o, outer; oc, oral cavity; s, segment; t, trunk appendage; tlc, trilobed chamber.*

**PLATE 3.** ***Refer to supplementary material*** *for high resolution image. 3D renders of YKLP 12387's anterior generated in Avizo. For clarity, the specimen's tissue is not depicted in* (a) *&* (b)*, and the circumoral ring of the circumferential chamber (cc) is omitted.* (a) *Lateral view. The swollen anterior region is demarcated by a constriction of the trunk. The additional anterior module is distinguishable from the succeeding segments by the absence of segmental systems, such as the axial cavity (ac). The additional anterior module's internal morphology is defined by a single fold, the axis of which is situated at the apex and demarcated by a dashed line. The anterior ventral cavity (av) is positioned just anterior to the fold. The circumferential chamber is rendered transparent.* (b) *Dorsal view.* (c) *Ventral view. The additional anterior region is dominated by the 'core' anterior cavity (cac), which bears the anteriormost pair of stunted appendages (aa). Ventrolaterally descending circumoral extensions (cov) of the core anterior cavity project towards to the ocular structures (ey). These are composed of inner and outer paraoral teardrop-shaped voids. The oral cavity (oc) is demarcated by a dashed line. The first segment (s1) of the axial cavity is a modified pelvis-shaped module that wraps around the foregut (fg), which has been omitted here for clarity. For abbreviations, see plate 2 caption.*